INTEGRATION OF LITHOFACIES AND GEOMECHANICAL CHARACTERIZTICS OF LOWER SILURIAN QUSAIBA SHALE, SAUDI ARABIA

BY

AYYAZ MUSTAFA

A Thesis Presented to the
DEANSHIP OF GRADUATE STUDIES

KING FAHD UNIVERSITY OF PETROLEUM & MINERALS

DHAHRAN, SAUDI ARABIA

In Partial Fulfillment of the
Requirements for the Degree of

MASTER OF SCIENCE

In

GEOLOGY

NOVEMBER, 2014

INTEGRATION OF LITHOFACIES AND GEOMECHANICAL CHARACTERISTICS OF LOWER SILURIAN QUSAIBA SHALE, SAUDI ARABIA

AYYAZ MUSTAFA

GEOLOGY

NOVEMBER, 2014

KING FAHD UNIVERSITY OF PETROLEUM & MINERALS

DHAHRAN- 31261, SAUDI ARABIA

DEANSHIP OF GRADUATE STUDIES

This thesis, written by **Ayyaz Mustafa** under the direction of his thesis advisor and approved by his thesis committee, has been presented and accepted by the Dean of Graduate Studies, in partial fulfillment of the requirements for the degree of **MASTER OF SCIENCE IN GEOLOGY.**

Dr. Mustafa M. Hariri
(Advisor)

Dr. Abdulaziz Al-Shaibani
Department Chairman

Dr. Ali Sahin
(Co-Advisor)

Dr. Salam A. Zummo
Dean of Graduate Studies

Dr. Abdulazeez Abdulraheem
(Member)

10/2/15
Date

Dr. Gabor Korvin
(Member)

Dr. M. Omar Abouelresh
(Member)

DEDICATION

I would like to dedicate this work to my Mother and Father, without their prayers, motivation and support I may not be able to complete MS successfully

To my brother Muhammad Aziz Naeem and sisters for their continuous encouragement and support

To my Teachers for their guidance and tutelage

To my beloved country ‘Pakistan’

ACKNOWLEDGEMENTS

"In the name of Allah, The Most Gracious and The Most Merciful"

All praise belongs to Almighty Allah (s.w.t.) for bestowing me with courage and perseverance to carry out this work sincerely. I thank Almighty Allah for giving me opportunity to do my M.S. successfully at King Fahd University of Petroleum and Minerals, Dhahran.

I would like to express my deepest gratitude to King Fahd University of Petroleum and Minerals for providing me good academic platform and financial support during my M.S.

My deepest gratitude and appreciation goes to my thesis advisors and mentors Dr. Mustafa M. Hariri and Dr. Ali Sahin for their constant guidance, motivation and support during the course of my studies. Their valuable suggestions broadened my horizon in the field of unconventional hydrocarbon resources, made this work interesting and challenging for me. I also wish to express my deep gratitude and appreciation to Dr. Abdulaziz Abdulraheem, Prof. Gabor Korvin and Dr. M. Omar Abouelresh for their reviews, guidance, and efforts serving on my thesis committee.

I am very grateful to Ministry of Petroleum and Minerals, Saudi Arabia for providing valuable data for this study and Mr. Abdulaziz Al-Dagal for his administrative assistance and cooperation.

I would like to thank several individuals for their technical support; Dr. Mohammad A. Mohiuddin and Dr. Safdar khan for their guidance and assistance in geomechanics part of thesis, Dr. Lamidi Babalola for his assistance with thin section study, Dr. Hazim Abass for providing his expert views and guidance.

I also wish to express my deep gratitude and appreciation to Mr. Azizullah Khan and Mr. Hector Gonzalez for their assistance with sample preparation, Mr. Syed Shujath for his cooperation in laboratory testing.

I would also like to express my deep gratitude to my uncle Mr. Muhammad Javed Khan and family for their encouragement and support during my study at KFUPM.

I am very thankful to Mohamed Abdel Gadir Yasin, Muhammad Haroon Tayyab, Waleed Ejaz, Muhammad Hammad Malik, Asif Abbas, Saad Khan, Ammar Jumma and Muhammad Jabir for their help and encouragement during my Masters. Also special thanks to Mohammad Najam, Ahmer Ali Buzdar, Waqas Ahmed khan for their camaraderie and good spirits. I would also like to acknowledge all the Earth Sciences faculty members with whom I took courses during my M.S., who helped me a lot during my coursework. I also owe thanks to all the students and faculty with whom I interacted during my Master's program.

TABLE OF CONTENTS

LIST OF TABLES

LIST OF FIGURES

LIST OF ABBREVIATIONS

1-D MEM	:	One Dimensional Mechanical Earth Model
TCF	:	Trillion Cubic Feet
GPa	:	Giga Pascal
MPa	:	Mega Pascal
YM	:	Young's Modulus
PR	:	Poisson's Ratio
UCS	:	Uniaxial Compressive Strength
ASTM	:	American Standard for Testing Materials
PSI	:	Pound per Square Inch
QFM	:	Quartz Feldspar Mica
Britt_YM	:	Brittleness Index based on Young's Modulus
Britt_PR	:	Brittleness Index based on Poisson's ratio
BI	:	Brittleness Index
TIV	:	Transversely Isotropic Vertical
TIH	:	Transversely Isotropic Horizontal

ABSTRACT

FULL NAME : AYYAZ MUSTAFA

THESIS TITLE : INTEGRATION OF LITHOFACIES AND GEOMECHANICAL CHARACTERISTICS OF LOWER SILURIAN QUSAIBA SHALE, SAUDI ARABIA

MAJOR FIELD : GEOLOGY

DATE OF DEGREE : NOVEMBER, 2014

This study integrated the three different aspects of research on the unconventional shale gas reservoir: Geological characteristics, fracture study, and geomechanical characteristics. Qusaiba Shale in the Rub' Al-Khali Basin has been taken as a case study to investigate its geological characteristics (lithofacies, natural fractures, primary sedimentary structures, microscopic characteristics, porosity, mineralogy, and elemental composition) and geomechanical characteristics (Young's modulus, Poisson's ratio, Cohesion and Friction). Determination of the geological and geomechanical characteristics are two main folds of objective that enable us to better understand the reservoir heterogeneity and variability and allow us to improve the potential for the development and production of these resources in Saudi Arabia and elsewhere.

The study was conducted on sixty feet continuous subsurface core samples representing Qusaiba Shale and Mid-Qusaiba Sandstone from Rub Al-Khali basin southeast Saudi Arabia. It includes lithofacies identification, fracture identification, preparation of mechanical earth model, brittleness and anisotropy analysis. Lithofacies were identified through core, thin sections examination, mineralogy and elemental composition, and

micro-images analysis. Fractures were identified in cores and thin sections study. Geomechanical analysis includes establishing the empirical relations, development of mechanical earth model, and brittleness and anisotropy analysis.

The geological characterization categorized the Qusaiba Shale into three lithofacies: (1) Micaceous laminated organic-rich mudstone facies (Lithofacies-I), (2) Laminate clay-rich mudstone facies (Lithofacies-II), and (3) Massive siliceous mudstone facies (Lithofacies-III) and Mid-Qusaiba Sandstone into two lithofacies: (1) Quartz Arenite and (2) Quartz Wacke. All lithofacies have different geomechanical characteristics and provide the basis to identify the brittle layer within entire shale interval and to analyze the anisotropy of Qusaiba Shale.

ملخص الرسالة

الاسم الكامل: آياز مصطفى

عنوان الرسالة: تكامل السحنات الصخرية والمميزات الجيوميكانيكية لطفل قصيبة من السيلوري الأسفل, المملكة العربية السعودية.

التخصص: جيولوجيا

تاريخ الدرجة العلمية: نوفمبر 2014

هذه الدراسة تشتمل على ثلاثة ملامح للبحث في مكامن الغاز غير التقليدية: الخواص الجيولوجية, دراسة الشقوق, والخواص الجيوميكانيكية. طفل قصيبة في حوض الربع الخالي أخذ كدراسة حالة لقحص خصائصه الجيولوجية (السحنات الصخرية, الشقوق الطبيعية, والتراكيب الرسوبية الأولية, الخواص المجهرية, المسامية, التركيب المعدني, والعناصر المكونة) و الخواص الجيوميكانيكية (معامل يونق, نسبة بويسن, معامل الاحتكاك والتماسك) استخراج الخواص الجيوميكانيكية والجيولوجية يمثلان هدفين يمكنان من فهم عدم التجانس. والتغيرات التي تسمح بتحسين القدرة للانتاج والتطوير لهذه الموارد في المملكة العربية السعودية والمناطق الاخرى.

تم تنفيذ الدراسة على ستين قدم مستمرة لعينات أساسية تمثل طين قصيبة و رمل وسط قصيبة من حوض الربع الخالي جنوب شرق السعودية. وهي تتضمن التعرف على السحنات الصخرية و الكسور, وتحضير النموذج الأرضي الميكانيكي, تحاليل عدم التجانس والهشاشة. السحنات الصخرية تم التعرف عليها من خلال العينات الأساسية , اختبارات الشرائح الرقيقة, التركيب المعادن والعناصر, وتحاليل الصور المجهرية. الكسور تم التعرف عليها من خلال العينات الاساسية و دراسة الشرائح الرقيقة. التحاليل الجيوميكانيكية تتضمن تأسيس علاقات تجريبية و تطوير نموذج أرضي ميكانيكي, وتحاليل عدم التجانس والهشاشة.

المميزات الجيولوجية قسمت طفل قصيبة الى ثلاثة سحنات صخرية: (1) السحنات الطينية العضوية المترققة الغنية بالمايكا (سحنة 1), (2) السحنات الطينية الغنية بالطين المترقق (سحنة 2). (3) السحنة الطينية السيلكية الكتلية (سحنة 3). وسحنات رمل وسط قصيبة : (1) اريناية الكوارتز و (2) واكي الكوارتز. كل السحنات الصخرية لديها

مميزات جيوميكانيكية وتمد بالاساسيات اللازمة للتعرف على الطبقة الهشة داخل الاجزاء الطينية ولتحليل عدم التجانس في طفل قصيبة.

CHAPTER 1

INTRODUCTION

This thesis presents integration of three different aspects of research on the unconventional shale gas reservoir: Geological characteristics, mineralogical and elemental composition and geomechanical characteristics. These characteristics are essential to understand the full reservoir lifecycle (Josh et al., 2012). Qusaiba Shale in the Rub' Al-Khali Basin has been taken as a case study to investigate its geological characteristics (lithofacies, sedimentary structures, microscopic characteristics, porosity, mineralogy, and elemental composition) and geomechanical characteristics (Young's modulus, Poisson's ratio, Cohesion and Friction).

The objectives of this study are twofold: first, to evaluate the geological characteristics of the Qusaiba Shale, second, to determine the geomechanical characteristics in order to have clear understanding of heterogeneity and mechanical parameters variability. The study intends to highlight the sweet spots (that have good reservoir and completion quality) in terms of brittleness for hydraulic fracture optimization. As for the mineralogy, rock fabrics, and geomechanics are interrelated and have influence on production, an integrated approach to understand the relation between these factors, is needed to achieve the optimum hydraulic fracture design (Britt and Schoeffler, 2009). Using the integrated results, exploration, development and production will be cost effective with improved recovery. This study aims to provide a better understanding of shale gas reservoirs in

terms of geological and geomechanical characteristics and allow us to improve the potential for the development and production of these resources in Saudi Arabia and elsewhere.

Identification of lithofacies, macro to micro primary sedimentary structures, and visual porosity by core examination and thin section study are important for this type of researh. Lithofacies identification is essential and provides the basic framework for the mineralogy and elemental analysis. Core examination and thin section study reveal mineralogy, texture, cements, matrix, pore spaces, micro-laminations, provenance, diagenesis, and environment of deposition. Different kinds of sedimentary structures (soft sediment deformation, bioturbation, lamination pattern and fractures) provide the information about the events at the time of deposition and post-deposition (Slatt et al., 2008).

X-Ray Diffraction (XRD) provides bulk mineralogy, relative abundance of clay species, and elemental composition. Mineralogy is the main factor that controls the brittleness of shale. Brittle zones and fractures are mainly associated with high quartz and other brittle minerals (pyrite, calcite, dolomite etc.) contents rather than clay content (Young et al., 1984). Mineral morphology that relates to mineral origin, relationship of clay minerals with pore system, pore geometry and elemental composition are determined using Scanning Electron Microscopy attached with energy dispersive spectroscope (SEM-EDS).

Geomechanics has been recognized as an essential tool for the exploration, development and production from unconventional resources (Gao et al., 2013). Geomechanical tests

include acoustic velocity measurements, uniaxial compressive strength and empirical relations in order to have elastic and failure mechanical parameters. Geomechanical analysis provides information about the mechanical behavior in terms of anisotropy, elastic and failure/strength parameters. These geomechanical parameters can be obtained from experimental laboratory work and/or log based measurements to generate the one dimensional mechanical earth model (1-D MEM). The 1-D MEM can be used in the design of the hydraulic fracturing stimulation treatments in deciding the multi-lateral drilling pad location and direction (Britt and Schoeffler, 2009).

1.1 Unconventional Resources

There are two types of natural energy resources: conventional and unconventional. The conventional resources are those having significant porosity and permeability for oil/gas storage and flow. Mainly traditional methods are used to produce from such resources. In conventional resource hydrocarbons are found in discrete fields but in unconventional cases, they are found over a wider area that has low exploration risks. Low porosity (less than 10%) and low permeability (micro to nanodarcy range) are main characteristics of these unconventional plays (Williams 2002). In spite of the difficulties in production, unconventional resources are the main focus of industry due to the tremendously increasing demand for energy (EIA, 2014). Therefore, special techniques need to be designed for successful exploration, development and production of these unconventional plays.

There are several types of unconventional natural gas resources. They include coal bed methane, shale gas, tight gas, and methane hydrates. Among these, shale gas, tight sand and coal bed methane are major sources of unconventional gas (Schmoker, 2002).

1.2 Shale Gas

Shale gas is the source of natural gas found in shale formations (Schmoker, 2002). Shale gas is extensively distributed in sedimentary basins as shale is the most common organic-rich sedimentary rocks. For the conventional gas/oil, shale has been recognized as source rock where hydrocarbons are generated from organic matter and then migrated to reservoir rocks; however, some hydrocarbon is left behind in shale due to the very low permeability. We need to apply integrated technologies for the successful exploration, development and production of shale gas sources. For successful application of these technologies, it is very important to have complete understanding of shale under consideration.

Major developments have been taken place in USA and Canada on the unconventional natural gas resources during the last three decades, especially on the shale gas and tight sand gas (Holditch, 2003; Holditch, 2006). Various authors reported about 22 major shale plays, distributed in different regions of USA. Other parts of the world also have extensive shale resources, especially Middle East, China, Latin America, and Russia (Sahin 2013). According to recently released figures, the USA produced 58% of its natural gas from unconventional resources (mainly shale and tight sand) and more production is expected in the future (Warlick, 2006).

The major constituents of shale are very fine (clay size) particles (< 2 μm) with varying proportion of silt (2-60 μm) and fine sand (> 60 μm). The principle components are shown in Figure 1.1. Porosity of shale is ranging from close to zero to 6% having pore size from 2 to 50 nm which are normally filled with organic matter (Eseme et al., 2007).

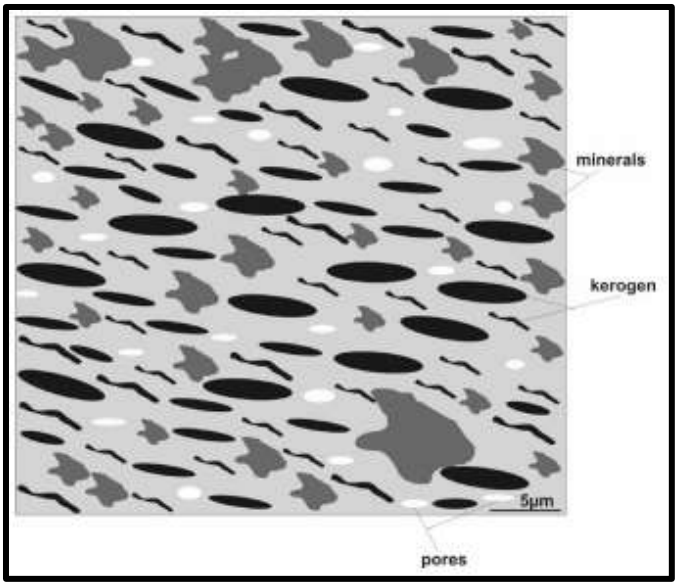

Figure 1.1: Principle components in shale (Eseme et al., 2007)

In shale, organic matter and minerals are present in micro-lamination; however, laminations on macro level are also observed in cores and wireline logs (Fertl, 1976).

1.3 Shale Gas in Saudi Arabia

The Middle East and North Africa is the third largest region (with about 2547 Tcf) after North America and China in terms of the estimated unconventional shale gas resources as shown in Table 1.1 (Kawata and Fujita, 2001). Despite of its favorable geology, Saudi Arabia possesses only 4% (282.6 Tcf) of natural gas reserves of the world in its conventional reservoirs. Considering the overall geological conditions, this figure appears to be far below the expectations (Sahin, 2013).

Table 1.1: Distribution of unconventional natural gas resources (Coal bed methane (CBM), Shale gas (SG), Tight gas (TG)) (after Kawata and Fujita, 2001)

REGION	TYPES OF GAS (Tcf)			
	CBM	SG	TG	TOTAL
North America	3,017	3,840	1,371	8,228
Latin America	39	2,116	1,293	3,448
W. Europe	157	509	353	1,019
Central and E. Europe	118	39	78	235
Former Soviet Union	3,957	627	901	5,485
M. East & N. Africa	0	2,547	823	3,370
Sub-Saharan Africa	39	274	784	1,097
Asia (including China)	1,215	3,526	353	5,094
Pacific (OECD)	470	2,312	705	3,487
Other Asia Pacific	0	313	549	862
South Asia	39	0	196	235
World	9,051	16,103	7,406	32,560

Conventional and unconventional resources are commonly distinguished on the basis of permeability cut-off value (0.1 milli-darcy). Statistical analysis, using this cut-off, revealed that proportion of low permeability resources is several times higher than high permeability resources since permeability is log-normally distributed (Sahin, 2013) (Figure 1.2).

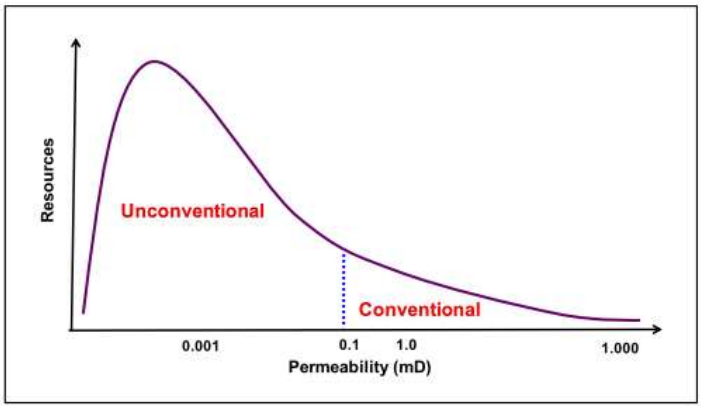

Figure 1.2: Lognormal distribution of natural gas resources (Sahin, 2013)

1.4 Role of Fractures in Production

In most shale gas reservoirs, natural fractures play vital role in production due to their interaction with hydraulic fractures. Natural fractures in Barnett Shale (USA) play significant role through the enhancement of hydraulic fracture stimulation treatments. Hydraulic fracture stimulation causes the tensile failure at these weak planes and results in reactivation of natural fractures that tend to generate a complex network of fractures and stimulate the large volume of rock. Prospective shale gas reservoirs contain natural fractures and have good production potential (Gale et al. 2014).

The fracture study in the Mishref Formation (Kuwait) using borehole images, electrical logs and production data revealed that fracture permeability does not only depend on faulting and deformation, but also on fracture-prone mechanical layers (Ozkaya and Lewandoswki, 2007). Due to intense faulting within the Mishref Formation, fracture permeability is significant within brittle layers (2-5 feet thick) due to well fracture network.

1.5 Geological Setting of the Study Area

The Paleozoic rocks in Saudi Arabia represented in a sequence of lithological formations in the Precambrian rocks of the Arabian Shield. They dip gently to north-east, east and south-east from Arabian Shield and cover an enormous area in subsurface. In the Rub' Al-Khali Basin, these units are intersected at 14,000 ft to 18,000 ft depth range. Based on their low porosity (< 10%) and very low permeability (< 0.1 mD), they are considered as tight formations (Sahin, 2013).

Paleogeographic map indicates that the Arabian Plate was present at about 45^0-60^0 South during the Silurian period as shown in Figure 1.3 (Konert et al., 2001). In Saudi Arabia, the Early Silurian (Llandovery) time represents the most important regional marine transgression following the de-glaciation phase of the Late Ordovician (Late Ashgill) Zarqa/Sarah Gondwanaland glaciation (Le Heron. and Craig, 2008).

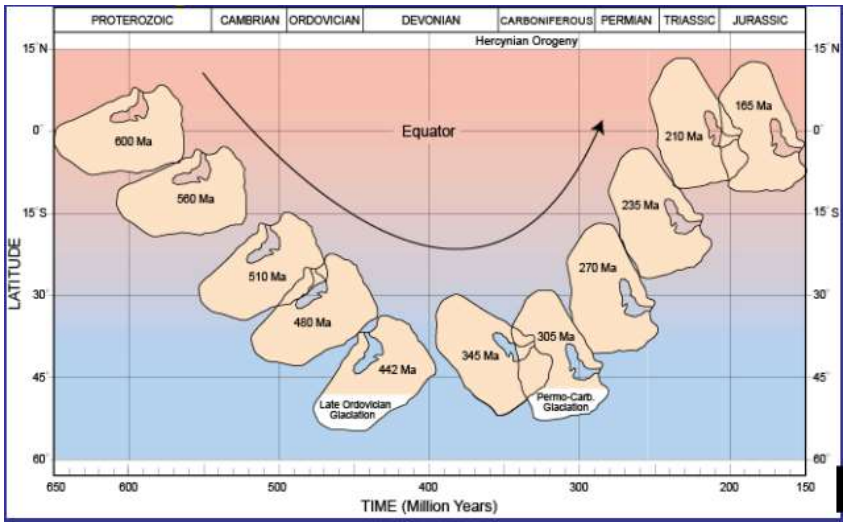

Figure 1.3: Paleogeographic change of the Arabian Plate during the Paleozoic time (Konert et al., 2001)

After this transgression, anoxic water bottom condition in sediment-starved basin prevailed providing the favorite depositional condition for organic-rich shale at the base of the Silurian transgression (Jones and Stump 1999). The Lower Silurian Qusaiba Shale is the main source rock in the Paleozoic petroleum system in Saudi Arabia and is also known as Qusaiba hot shale (Cole, 1994; Abu-Ali et al., 1991) It is considered to be one of the main targets for unconventional shale gas resources in Saudi Arabia (Sahin, 2013).

Stratigraphically, the Qusaiba Member is subdivided in two units, the upper and lower. The lower Qusaiba Member is characterized by progradational series, whereas the upper

member is exhibiting a fining-upward series (Jones and Stump, 1999). The upper Qusaiba shale is prodeltaic and the basal hot shale is formed by regional marine transgression, which is characterized by organic matter of the type-II of marine environment (Luning et al., 2000). The generalized stratigraphic column representing Paleozoic in Al-Qasim area is shown below (Figure 1.4).

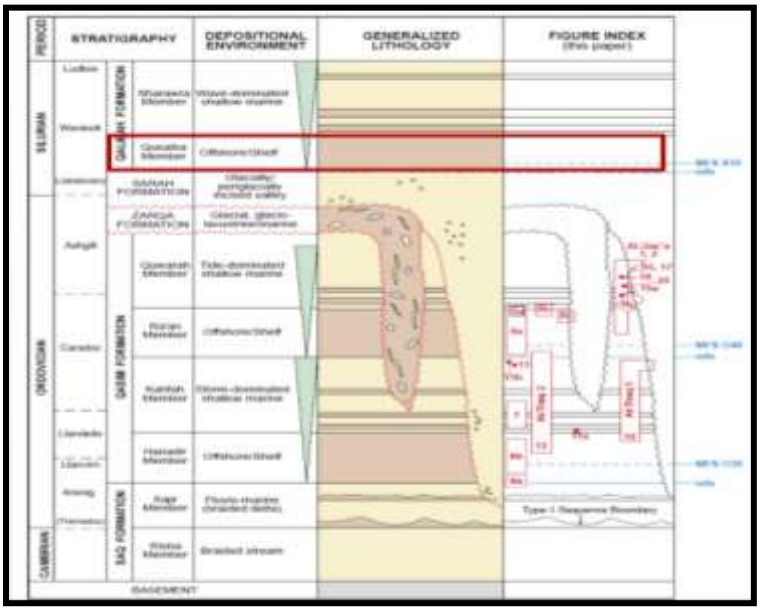

Figure 1.4: Generalized stratigraphy of Qusaiba Member of Qalibah Formation (Senalp and Al-Duaiji, 2001)

The type locality and type sections of Qusaiba Shale are located in Northwestern part of Saudi Arabia (Cole, 1994). The Qusaiba Shale is also encountered in the Rub Al-Khali basin over the range of depths. The data of this work, including subsurface core samples and well logs, are obtained from two wells located in the north-eastern part of the Rub Al-Khali Basin (Figure 1.5).

Figure 1.5: Location map for the study area (Google Maps)

1.6 Motivation and Objectives

The objective of this study is to characterize the Qusaiba Shale from geological and geomechanical perspectives. The mechanical and geological characteristics provide better understanding of shale behavior within a reservoir under different stress conditions. Anisotropy, determined from laboratory experiments is key factor for hydraulic fracture orientation. Geology and geomechanics of shale gas have been studied by various researchers; therefore, their integration is the main essence of this study. The one-Dimensional Mechanical Earth Model (1-D MEM) developed during the course of study can be used to highlight the brittle layers/zones within whole shale interval and optimize the hydraulic fractures treatment.

In summary, this study addressed the three key areas: (1) understand heterogeneity within the Qusaiba Shale in study area, (2) integrate the factors controlling the production from shale reservoirs through lithofacies, mineralogy and geomechanical analysis, and (3) predict the mechanical behavior of Qusaiba Shale lithofacies.

1.7 Problem Statement

Shale gas reservoirs have several challenges since gas is stored in very low permeability (micro- to nanodarcy range) rock matrix (Williams, 2002). Production of shale gas totally depends on fracture permeability. Natural fractures and induced fractures have the main contribution towards the total gas production (Montgomery et al., 2005). Identification and characterization of natural fractures are essential to predict the flow potential of shale gas. To produce gas on commercial scale, it is necessary to develop integrated hydraulic fracture stimulation. Obviously, success of these techniques is mainly dependent on the geological and geomechanical characteristics of the shale.

In the light of the above statements, the geological and geomechanical characteristics of Qusaiba Shale must be well understood. Geological characteristics include lithofacies, lamination pattern, primary sedimentary structures (macro and micro scale), total organic content, mineralogical and elemental composition. These characteristics will allow to delineate the brittle zone within the shale formation (Young et al., 1984).

In order to deal with aforementioned problems, Geomechanics has been recognized as a powerful tool for development and production from shale gas (Gao et al., 2013). Mechanical parameters including Young's modulus, Poisson's ratio, and rock strength under different confining pressures, failure parameters (cohesion and angle of friction)

provide the clear picture for rock deformational behavior (Rickman et al. 2008). The magnitudes and directions of in-situ stresses are important to optimize the hydraulic fracturing design. Using mechanical parameters, the 1-D MEM is generated to define the most brittle zones within the entire formation. To sum up exploration, development and production from shale gas reservoirs are not possible without taking geomechanics into consideration.

1.8 Methodology

Diverse and integrated techniques have been adopted for this study. The results from different disciplines have been integrated to provide complete description of the Lower Qusaiba Shale. Integration of lithofacies, mineralogy and rock mechanical properties enables us to construct a complete geomechanical model to delineate the brittle zones within Qusaiba Shale. The integrated model can resolve many problems related to drilling, fracturing and production from the shale reservoir.

The core objectives of the study are achieved through the following steps:

- Core examination, thin sections study, mineralogy, micro-imaging and elemental analysis for lithofacies identification.
- Fracture identification (natural and induced) through core examination and thin section study
- Measurement of the geomechanical parameters (elastic and failure)
- Determine the fractures type and their distribution within lithofacies
- Integrating the lithofacies and geomechanical characteristics

Sixty feet (60ft) of subsurface cores from two wells representing Qusaiba Shale and Sandstone within the north-eastern Rub Al-Khali Basin, have been used for the study. Cores have been fully described in terms of color, size, mineralogy, and primary structures. Geological characteristics of shale on macro-scale were studied using binocular microscope to identify lithofacies, their variation, and sedimentary structures. Fifty nine thin sections were examined micro-scale geological features under microscope.

Mineralogical compositions and their relative abundances were determined using the XRD technique. Surface morphology visualization including identification of various types of minerals especially clay minerals and the study of the micro-pores and porosity network were performed using the SEM. Furthermore, the SEM-EDS was used to conduct elemental analysis with relative abundances.

Geomechanical properties such as uniaxial compressive strength, Young's modulus, Poisson's ratio, cohesion, friction, ultrasonic velocities were determined in both horizontal and vertical directions in order to take sample-scale anisotropy into account. Ultrasonic velocity (primary and secondary waves) measurements were carried out to attain the stiffness in terms of dynamic Young's modulus and Poisson's ratio using Autolab 500. Various confining pressures were applied during measurements to simulate the reservoir conditions.

The compression test equipment was used to determine the uniaxial compressive strength (UCS). The static Young's modulus and Poisson's ratio were determined from the stress strain results obtained from UCS test. The test was performed using both vertical and horizontal samples.

CHAPTER 2

LITHOFACIES ANALYSIS

This chapter deals with geological features resulting from core examination and petrographic analysis. Core examination and petrography are of utmost importance for lithofacies analysis which is highlighted in the following sections.

Core examination and petrography of the tight formations like shales provide information to define the reservoir heterogeneity and production potential of shale play by analyzing its texture, mineralogy, sedimentary features. The formation and maturation process in tight reservoirs are controlled by various geological factors including source rock quality, sedimentary environment, structural elements, and reservoir heterogeneity (Huang et al., 2013). The results from thin sections and core examination indicated that TOC, brittleness, porosity, and fracture density are the four main shale characteristics that define the shale productivity (Ouenes, 2013).

2.1 Petrography

Petrographic study was conducted using thin section microscopy, the XRD, and the SEM-EDS.

Pore type, size and arrangement are very important in fine-grained reservoir rocks and can be evaluated by micro-pore analysis through petrography (Milner et al., 2010).

Thin section microscopy is based on mineralogy, organic matter distribution, and diagenetic features which are the main factors that provide the basis for the lithofacies

identification and classification (Huang et al., 2013). Mineralogy is the key parameter that indicates the brittleness/fracability of the reservoir (Wang et al., 2008).

Shale is investigated precisely using the SEM. This technique provides sufficient information about the microstructures in terms of morphology, concentration and pore size and geometry (Grunewald and Pingel, 2014). Micro analysis techniques (SEM and BSEM) were applied to carbonaceous mudstone, Western Canada, to determine the fabric characteristics of intrinsic and secondary porosity providing sufficient information on depositional environment and burial processes (Jiang and Cheadle, 2013). The SEM provided the insight of rock fabric, arrangement of grains in shale such as Devonian Shales, USA (Davies et al., 1990). Minerals with same chemical composition can be distinguished on the basis of their crystal systems under the SEM. Hence, SEM yields three-dimensional view of microstructures, fabrics and pore geometry (Bryant, 1990).

2.2 Qusaiba Shale Lithofacies

Lithofacies in Qusaiba Shale, on both macro and micro scales, were identified from core and thin sections study (CPM Reports, 2009). Thirty feet (30ft) of subsurface core was available from one well representing Qusaiba Shale within the Rub Al-Khali Basin. The cores were examined using binocular lens and fully described in terms of color, size, primary sedimentary structures and vertical lithofacies variation. Detailed description of core is presented in Appendix-A.

In addition to core examination, thirty thin sections were used for thin section microscopy to examine the different components of shale, mineralogy, natural microfractures,

porosity type as well as other micro-scale geological features. Thin section results are provided in Appendices B.

Mineralogical and elemental compositions were determined using ten representative samples (Appendix-D). Micro-analysis of Qusaiba Shale was conducted in order to focus on the micro-pores network, pore geometry, and mineral morphology. To see the complete SEM-EDS results, please refer to Appendix-E. On the basis of core description and petrography (Mustafa et al., 2014), this study categorized Qusaiba Shale in three different lithofacies as below.

1) Micaceous laminated organic-rich mudstone facies (Lithofacies-I)
2) Laminate clay-rich mudstone facies (Lithofacies-II)
3) Massive siliceous mudstone facies (Lithofacies-III)

2.2.1 Micaceous laminated organic-rich mudstone facies (Lithofacies-I)

This lithofacies covers approximately 18% (4.84 Ft) of total length of the examined core. The Lithofacies-I is black in colour with horizontal and parallel laminae of 1-3 mm thickness (Figure 2.1). Both sharp and gradational contacts have been observed. The low-calcite content in the Qusaiba Shale was indicated by very low effervescence with 10% HCl solution.

Lithofacies-I is composed mainly of detrital mineral grains (quartz, micas). Clay minerals represent the groundmass in which these grains are embedded. The clay minerals preferentially deposited in horizontal laminations (Tucker, 2001). Organic matter ranges from light brown to dark brown to black reflecting different levels of maturity (Kleineidam et al., 1999) and it is present in both disseminated and laminated form. Mica

flakes (2-10 %) are aligned with the lamination planes. Interparticle porosity is very low (< 1%), however, fractures and lamination planes enhance porosity (visual assessment using chart by Terry and Chillinger, 1955) to about 5-6% in some cases. Scattered euhedral pyrite crystals are also encountered throughout the whole lithofacies (Figure 2.2).

XRD analysis shows that this lithofacies composed of quartz, muscovite, kaolinite, and albite (Table 2.1). The SEM results high organic matter content (about 12-15% of the total lithofacies volume, Figure 2.2). This has been confirmed by elemental composition analysis by EDS: Al, Si, K, O and Na (Figure 2.3).

On the basis of above discussed features (high organic matter, pyrite, lamination pattern, scarcity of bioturbation and soft sediment deformation) in cores and thin sections, Lithofacies-I has been interpreted to be deposited in low energy environment with anoxic conditions (Abouelresh and Slatt, 2011). Clay dominated mudstone with high organic matter was possibly deposited in moderate to high water depth (Hulsey, 2011). Presence of pyrite (FeS_2) indicate anoxic (reducing) environment of deposition for Qusaiba Shale (Cole, 1994).

The results from core examination, thin sections, mineralogy, and elemental analysis for Lithofacies-I are shown below.

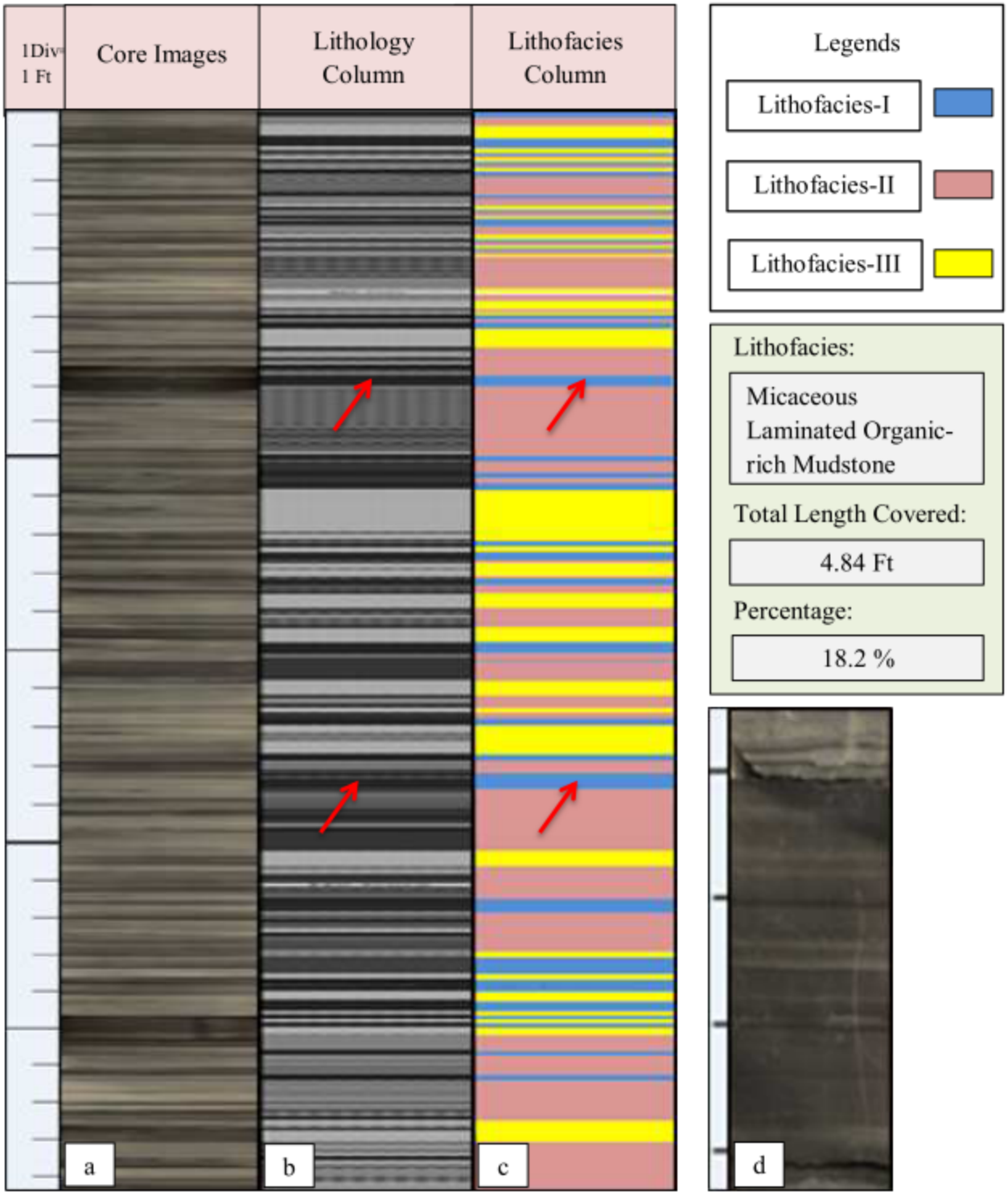

Figure 2.1: (a) Total Core Image, (b) Lithology Column, (c) Lithofacies Column (red arrows are pointing to Lithofacies-I) (d) Representative Image of Lithofacies-I (1 Div. = 1 inch)

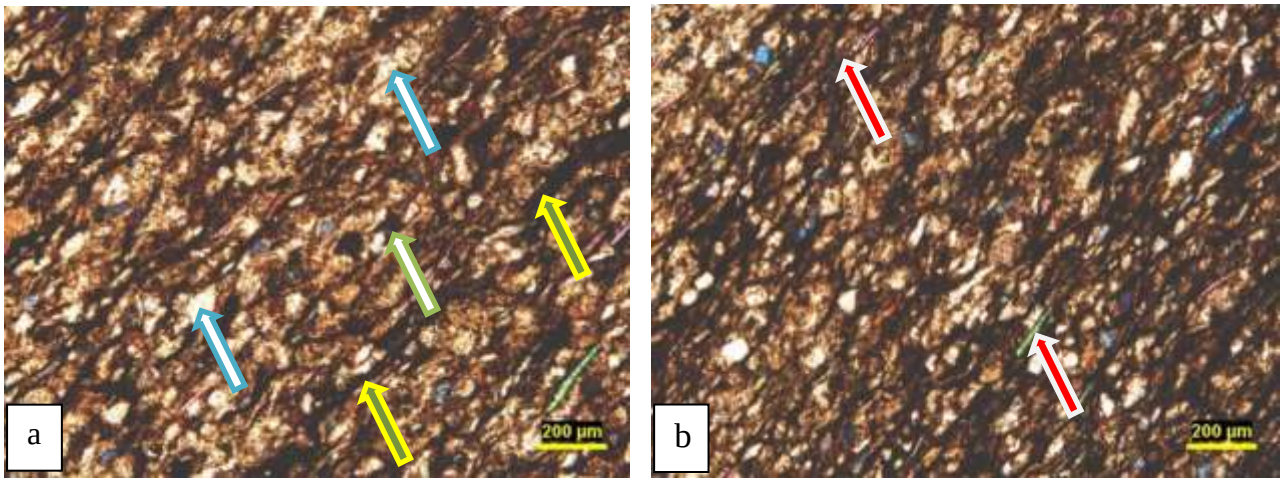

Figure 2.2: Field of view under plane polarized light showing (a) Micaceous laminated organic-rich mudstone facies. Yellow arrows point lamination plane filled with organic matter, blue arrows point to silica grains. Green points to pyrite (b) Micaceous laminated organic-rich mudstone facies. Red arrows point to mica flakes.

Table 2.1: Mineralogy of Lithofacies-I

Minerals	Percentage (%)
Quartz	39.9
Muscovite	23.7
Kaolinite	27.8
Albite	8.6

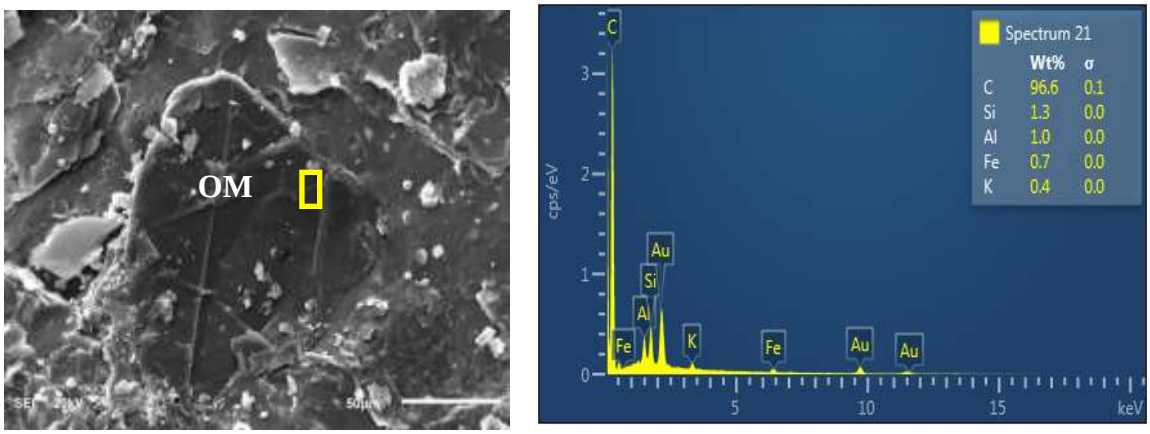

Figure 2.3: SEM image and elemental composition of Organic matter 'OM' contaminated in Lithofacies-I.

2.2.2 Laminated clay-rich mudstone facies (Lithofacies-II)

Laminated clay-rich mudstone facies (Lithofacies-II) is the dominant lithofacies in Qusaiba Shale with occurrence of 55.87 %. This lithofacies is present in lamination pattern with varying thickness of about 5-15 mm. Based on visual colour with light and dark grey laminae, probably the Lithofacies-II is composed of alternating argillaceous and siliceous laminae (Figure 2.4).

Lithofacies-II is composed mainly of clay minerals (groundmass) embedded with detrital mineral grains (quartz and micas). High silica mudstone is present alternately. Mica occurs in the form of elongated flakes representing about 2-5 %. Interparticle porosity is very low (< 1%), however, natural fractures and lamination planes enhance porosity to about 2-3% in some cases (Terry and Chillinger, 1955). The organic matter represents about 1-5 % of the total lithofacies volume (Figure 2.5). The minerals identified quartz, muscovite, kaolinite, and albite as main minerals in this lithofacies (Table 2.2). Quartz percentage is relatively higher than that of Lithofacies-I. The elemental composition of Lithofacies-II indicates Al, Si, K, O and Na as major elements (Figure 2.6).

Primary sedimentary structures include lamination pattern, bioturbation and soft sediment deformation (Figure 2.7). On the basis of observed features, the depositional environment has been interpreted as cyclic high and low energy environment (Hulsey, 2011). Hypopycnal (low density flow) and hyperpycnal (higher density flow) are interpreted as depositional processes (Abouelresh and Slatt, 2011).

The results from core examination, thin sections, mineralogy, and elemental analysis of Lithofacies-II are shown below.

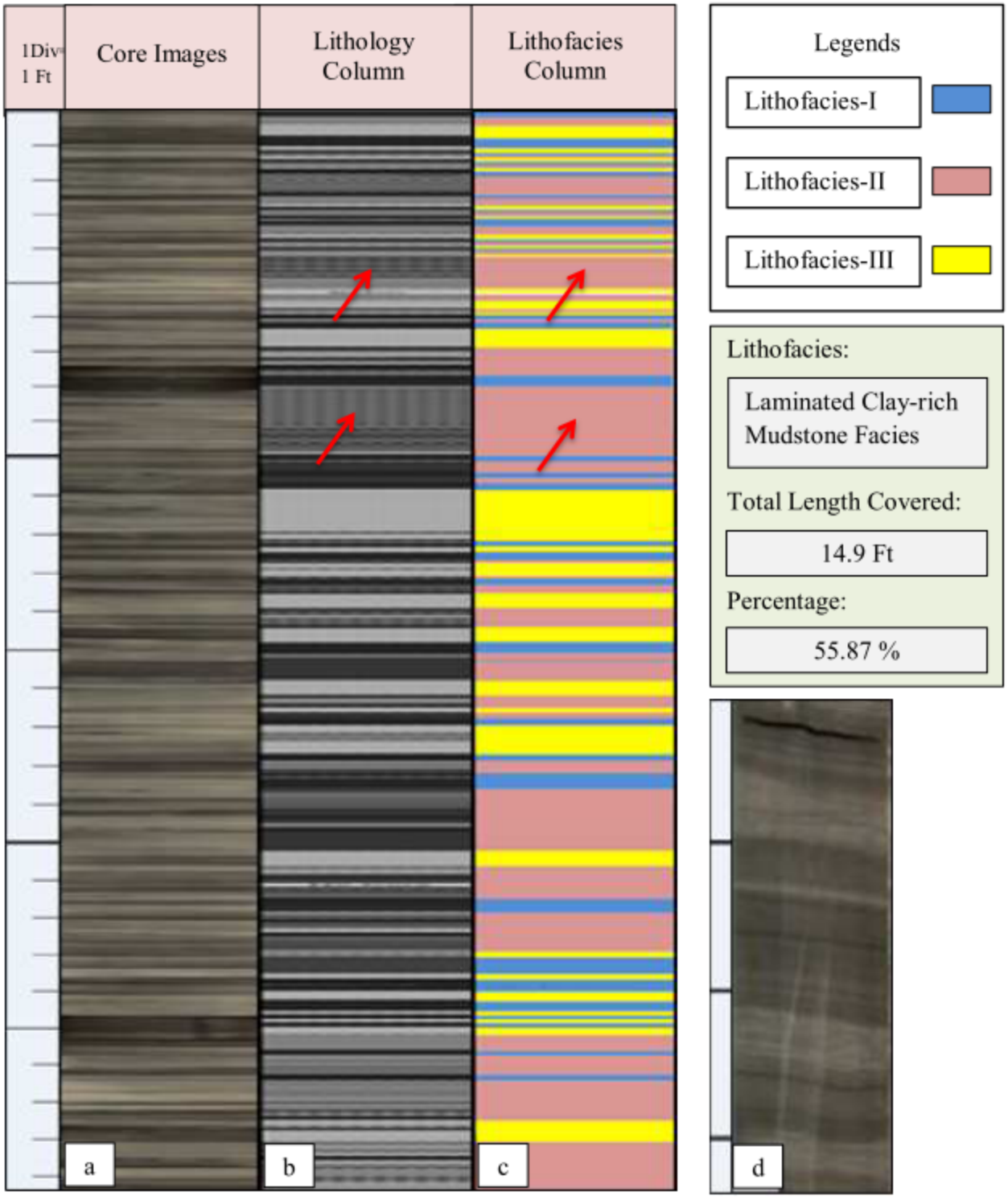

Figure 2.4: (a) Total Core Image, (b) Lithology Column, (c) Lithofacies Column (red arrows are pointing to Lithofacies-II) (d) Representative image of Lithofacies-II (1 Div. = 1 inch)

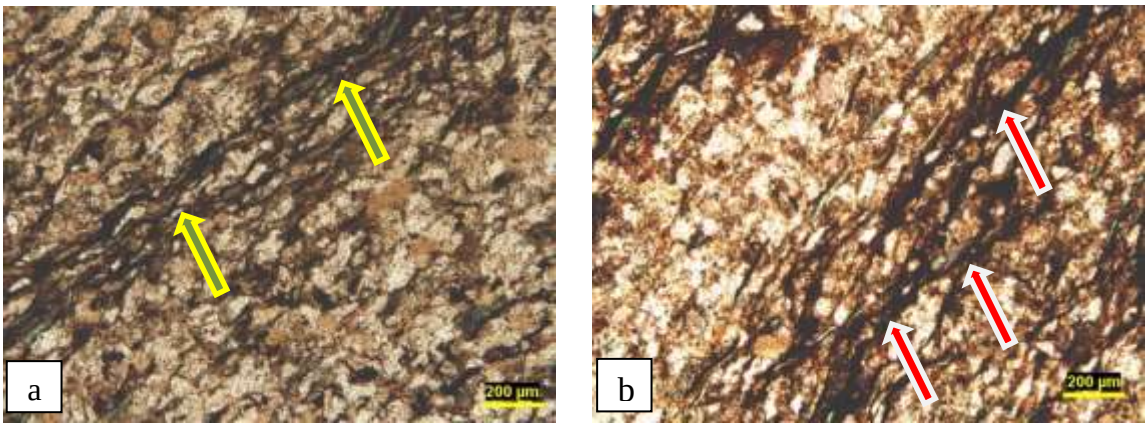

Figure 2.5: Field of view in plane polarized light showing (a) Laminated clay-rich mudstone facies (yellow arrows point to lamination planes), (b) Laminated clay-rich mudstone facies (Red arrows point to lamination planes filled with organic matter).

Table 2.2: Mineralogy of Lithofacies-II

Minerals	Percentage (%)
Quartz	49.3
Muscovite	13.3
Kaolinite	8.7
Albite	28.7

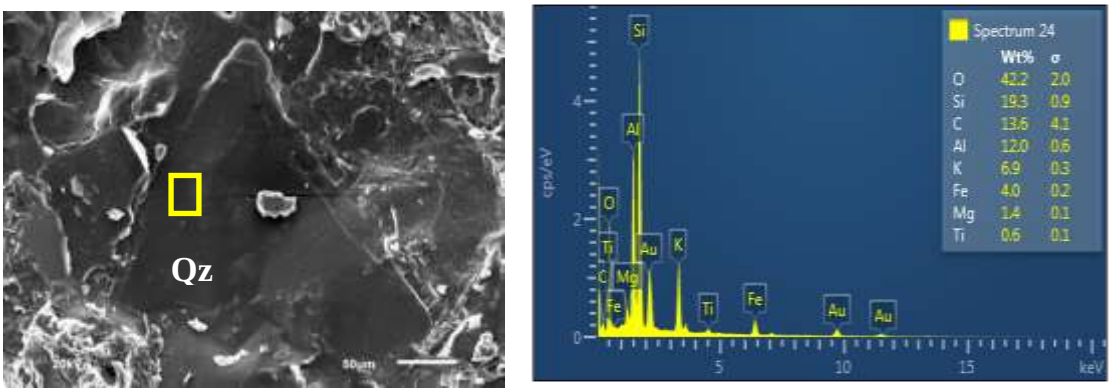

Figure 2.6: SEM Image of Quartz grain with its elemental composition

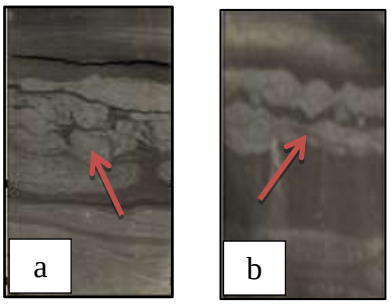

Figure 2.7: Core images showing (a) Bioturbation, (b) Soft sedimentary deformation

2.2.3 Massive siliceous mudstone facies (Lithofacies-III)

This lithofacies is observed as light grey to grey with high silica content. It represents approximately 26% of total core (Figure 2.8). It occurs in a relatively thick massive laminae (>15 mm). No prominent sedimentary structure has been observed in this lithofacies.

Lithofacies-III is mainly composed of detrital mineral grains (quartz, micas) with high silica contents embedded in clay groundmass. Interparticle porosity is very low (< 1%). No prominent micro-scale bedding fractures have been observed in this facies. The organic matter is about 1- 3 % of the total lithofacies volume (Figure 2.9 (a) & (b)).

The mineralogy of Lithofacies-III comprises quartz, illite, feldspar (albite), and chlorite (Table 2.3). This lithofacies tends to be more brittle due to high concentration of quartz (78.1%) as it is reflected also by SEM images and elemental composition (Figure 2.10). The elements, found in this lithofacies, are Si, Al, O, K, Na, Mg, and Fe.

Massive silica rich mudstones are interpreted to be deposited in low energy environment. The possible processes involved are suspension settling and hemipelagic plumes (Hulsey, 2011). The results obtained from core examination, thin sections, mineralogy, and elemental analyses for Lithofacies-III are illustrated in Figure 2.8.

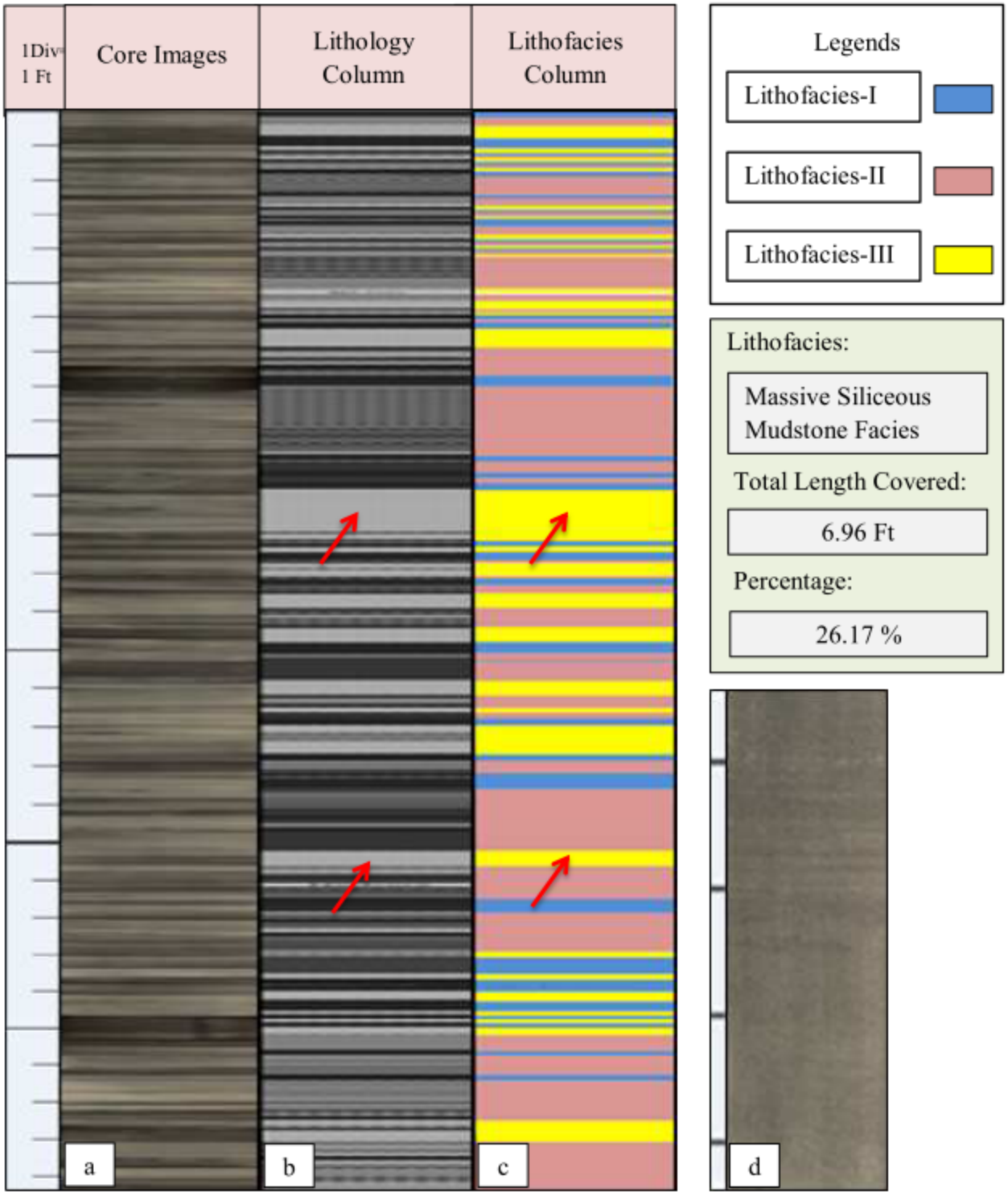

Figure 2.8: (a) Total Core Image, (b) Lithology Column, (c) Lithofacies Column (red arrows are pointing to Lithofacies-III), (d) Representative Image of Lithofacies-III (1 Div. = 1 inch)

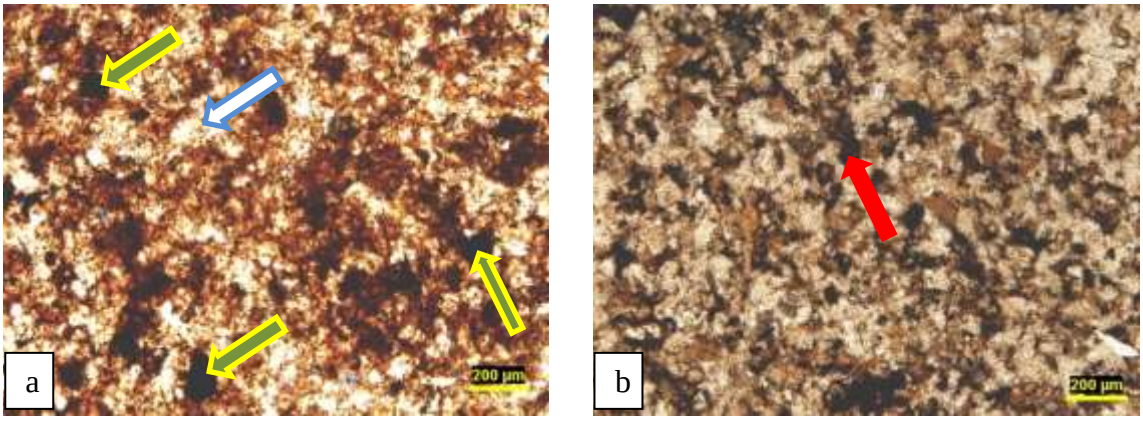

Figure 2.9: Field of view in plane polarized light (a), massive siliceous mudstone facies, blue arrow points silica and yellow arrow points organic matter (b) Massive siliceous mudstone with disseminated organic matter (red arrow).

Table 2.3: Mineralogy of Lithofacies-III

Minerals	Percentage (%)
Quartz	78.1
Chlorite	13.4
Illite	5.8
Albite	2.7

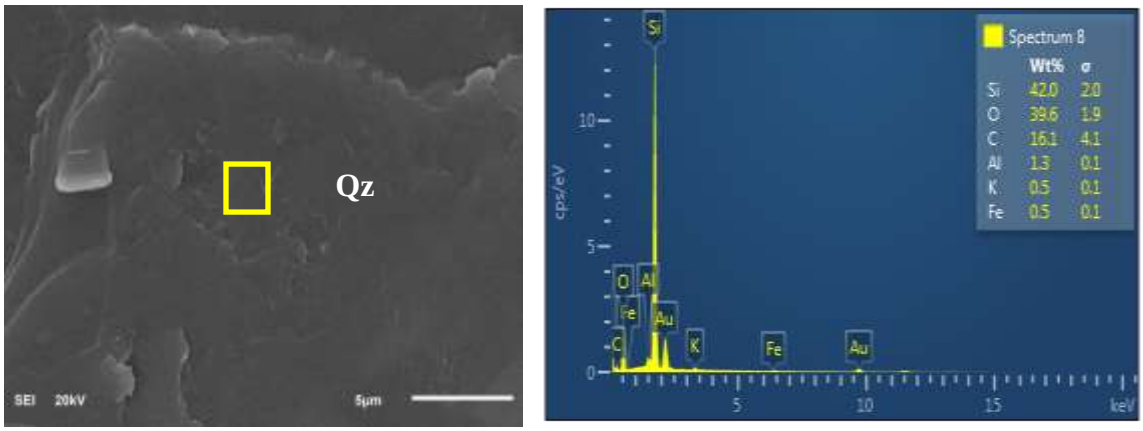

Figure 2.10: Quartz grain under SEM-EDS with elemental composition

2.3 Mid-Qusaiba Sandstone Lithofacies

Mid-Qusaiba Sandstone has been categorized in two lithofacies: Quartz Arenite Facies (Lithofacies-IV), and Quartz Wacke Facies (Lithofacies-V). These lithofacies are discussed below.

2.3.1 Quartz Arenite Facies (Lithofacies-IV)

The core of the Mid-Qusaiba Sandstone has revealed an intercalation of massive light grey and dark (brownish) grey fine to medium grained sandstone. It is featured with intense fractures including horizontal, vertical and inclined which will be discussed in details in Chapter 3. Very few primary sedimentary structures like bioturbation, soft sediment deformation, and concretion were observed as shown in Figure 2.11. Gradual to sharp contacts have been observed between light and dark grey sandstone (Figure 2.12).

The quartz arenites are light grey with bimodal grains, fine to medium (125 – 250 microns for fine and 250 to 500 microns for medium) with few disseminated coarse grains (Figure 2.13 (a) and (b)). They are poorly to moderately sorted and generally sub-rounded to rounded (Figure 2.13 (a) and (b)). The quartz is ranging from 75 to 90% in this lithofacies. Quartz is mainly of monocrystalline type ranging from 93 to 97%, while the polycrystalline quartz ranges from 1-3%. Feldspars range from 1-2%. Other mineral constituents include rock fragments and heavy minerals (<1% or =1%). Micas are observed locally in some samples being less than 1%. Clay coating is present around the grains (Figure 2.13). Vacuoles are observed within quartz grains. Many grains have sutured grain contacts resulting in local partial dissolution of silica due to high compaction between grains (Barclay, 2006). Micro fractures and fractured grains are also observed in this lithofacies (Figure 2.13 (a)).

The clay and fine quartz minerals form the matrix (1% to 15%). The porosity in the quartz arenite lithofacies is mainly intergranular. It ranges from 5-15% with an average of about 9% (visual assessment using chart by Terry and Chilingar, 1955). Porosity is partially reduced by ferroan calcite cementation and clays. In addition to the tightly packed fabric observed in the samples, other main diagenetic features include silica cementation by quartz overgrowths (Figure 2.13). For complete thin sections descriptions, please refer to Appendix-C.

The major minerals are quartz, illite and feldspar (microcline) (Appendix-D). The elemental composition is Si, O and C as major elements along with Al, K, Mg and Fe indicating clay and fine quartz matrix present in Lithofacies-IV (Figure 2.14).

Based on features (fine to medium grained and bioturbation) discussed above, quartz arenite has been interpreted from middle shoreface to upper shoreface environment (Mahmoud et al. 1992).

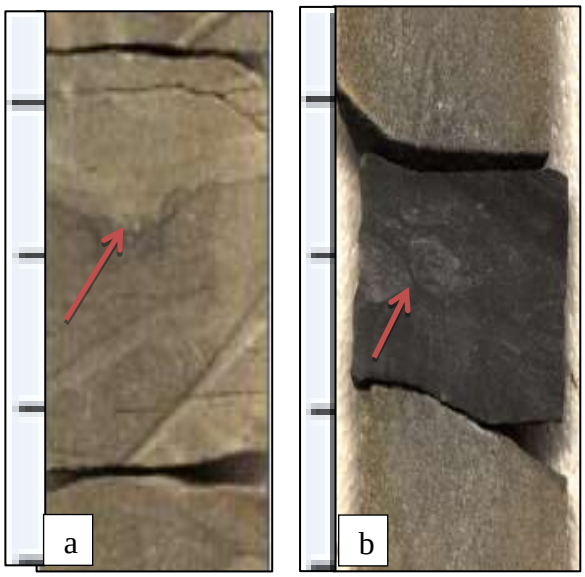

Figure 2.11: Sedimentary structures (a) Soft sediment deformation (b) Concretion

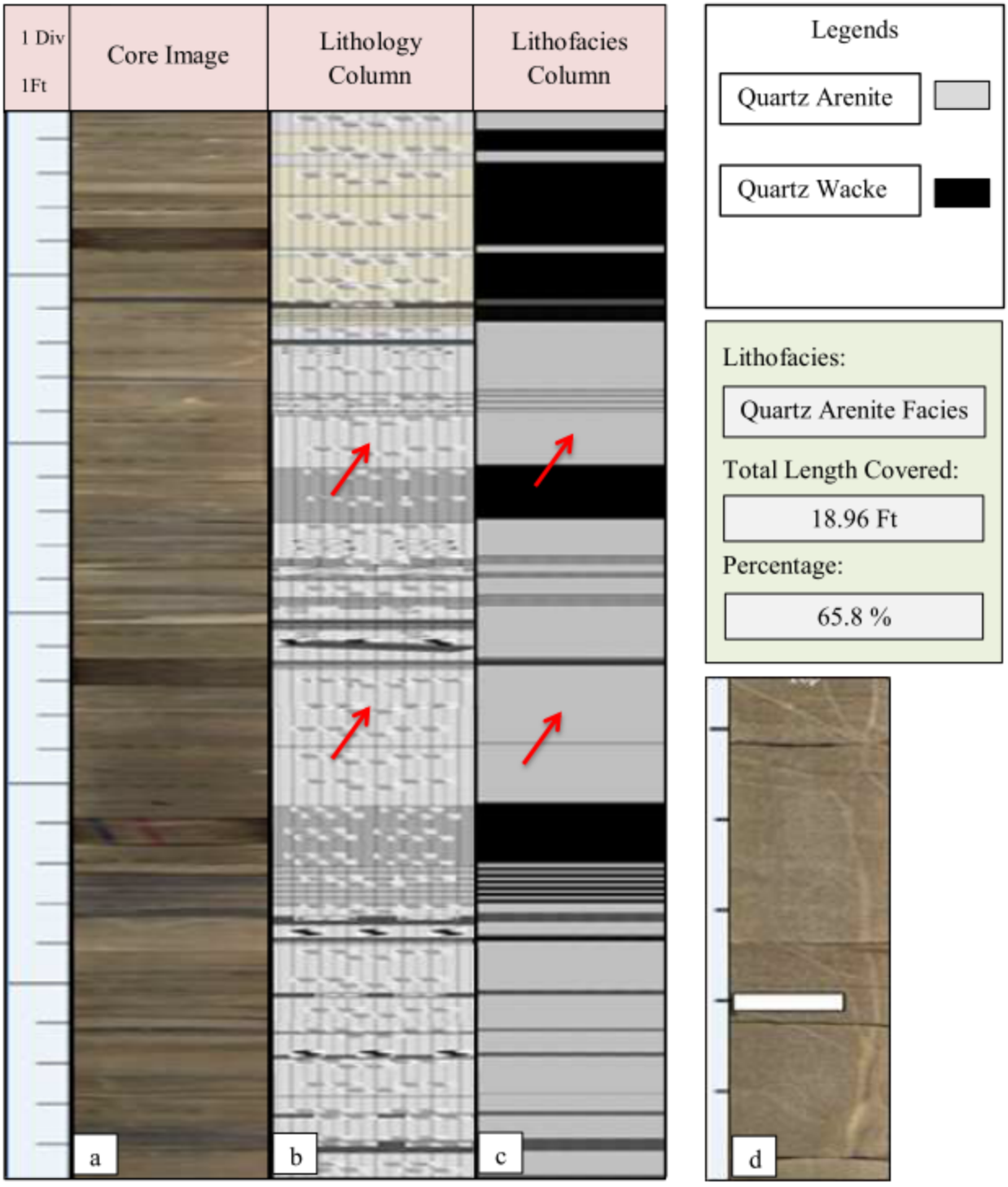

Figure 2.12: (a) Total Core Image, (b) Lithology Column, (c) Lithofacies Column (red arrows are pointing to Lithofacies-IV), (d) Representative Image of Lithofacies-IV (1 Div = 1 inch)

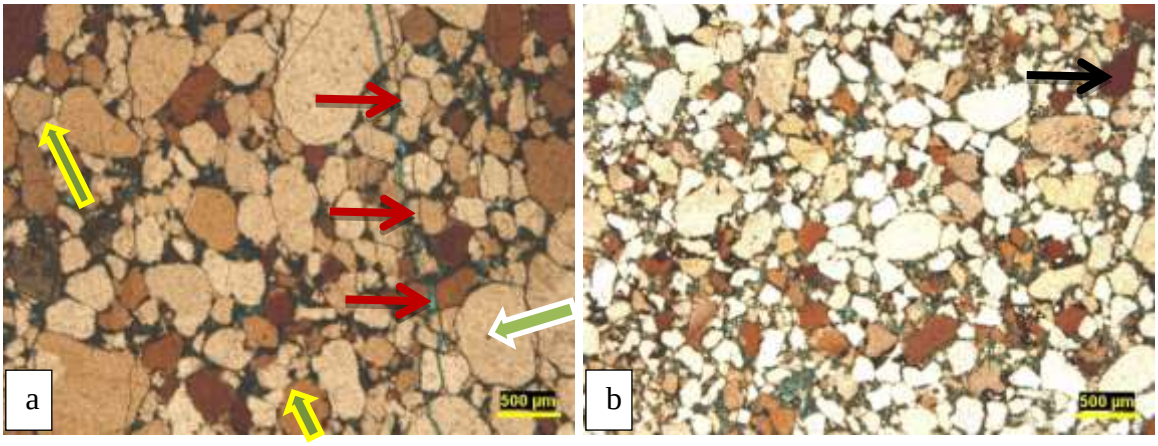

Figure 2.13: (a) Quartz Arenite lithofacies showing fractured quartz grains (red arrows) with sutured contact (yellow arrow), vacuole (green arrow) and matrix, (b) Quartz Arenite having 13-15% matrix, black arrow points lithic fragment.

Table 2.4: Mineralogy of Quartz Arenite

Minerals	Percentage (%)
Quartz	81.1
Illite	15
Feldspar	3.8

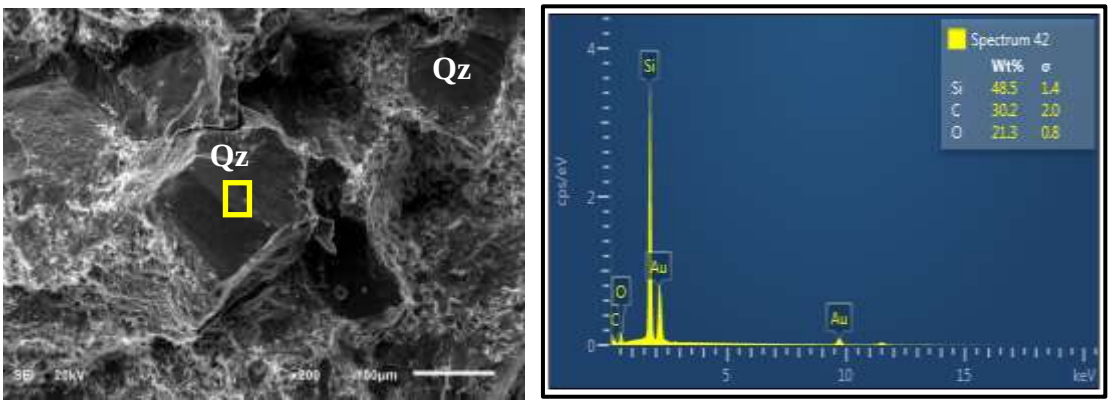

Figure 2.14: SEM Image of quartz grain embedded in clay matrix. Elemental composition of quartz grain.

2.3.2 Quartz Wacke Facies (Lithofacies-V)

The core examination has revealed an intercalation of dark (brownish) grey fine to medium grained sandstone and laminated silty shale with sharp contacts between them (Figure 2.15) (CPM reports, 2009). Primary sedimentary structures include bioturbation, soft sediment deformation.

The quartz wacke lithofacies are light grey with bimodal grains ranging from fine to medium (125 - 250 microns and 250 to 500 microns) grain size. They are poorly to moderately sorted and generally sub-rounded to rounded grains. The quartz is ranging from 65 to 80% by visual assessment. The quartz grains in quartz wacke lithofacies consist mainly of monocrystalline quartz (90 to 95%), while the polycrystalline variety ranges from 3 to 5%. Feldspars range from 1-2% and rock fragments are present about 1%. Quartz grains are coated with clay (Figure 2.16). Micro fractures are also observed in quartz grains (Figure 2.16).

Visual porosity assessment indicates 2 to 8% porosity with an average of about 5%. Porosity is mainly primary intergranular of micro pore type. The main diagenetic features observed include silica cementation by quartz overgrowths (Figure 2.16). Quartz is the main mineral found in this lithofacies with microcline and albite (Table 2.5). The major elements include Si, O, Al, K, Mg, Fe, indicating quartz mineral with clay matrix (Figure 2.17).

Based on the above features (fine to medium grained sandstone, bioturbation and laminated silty shale), quartz wacke lithofacies has been interpreted from middle shoreface to upper shoreface environment (Mahmoud et al., 1992).

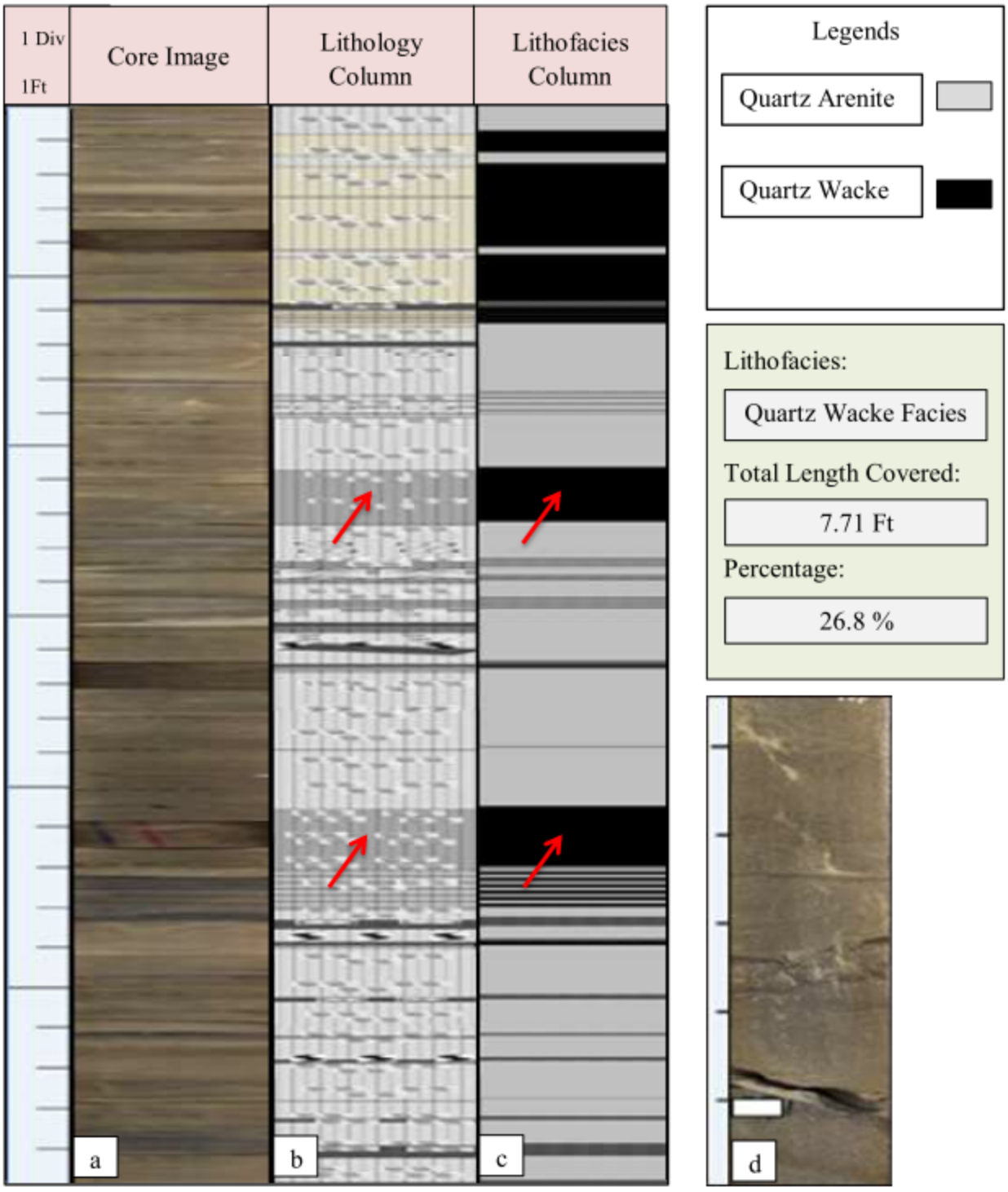

Figure 2. 15: (a) Total Core Image, (b) Lithology Column, (c) Lithofacies Column (red arrows are pointing to Lithofacies-V) (d) Representative Image of Lithofacies-V (Scale 1 Div. = 1 inch)

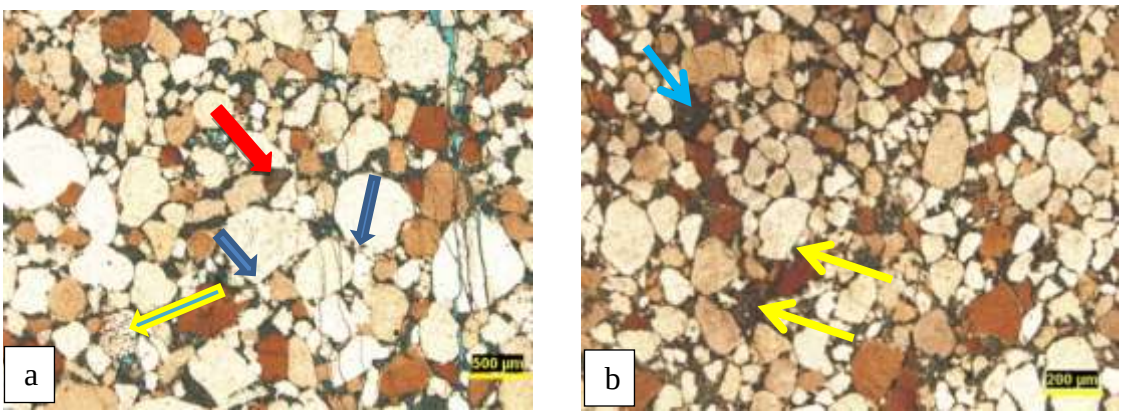

Figure 2.16: Quartz Wacke Lithofacies (a) quartz grains embedded in matrix, feldspar (yellow arrow), rock fragments (red arrow) and quartz overgrowth (blue arrows). (b) fracture plane within quartz grains (yellow arrows) and lithic fragments (blue arrow).

Table 2.5: Mineralogy of Quartz Arenite

Minerals	Percentage (%)
Quartz	66
Feldspar (Microcline)	16
Feldspar (Albite)	17

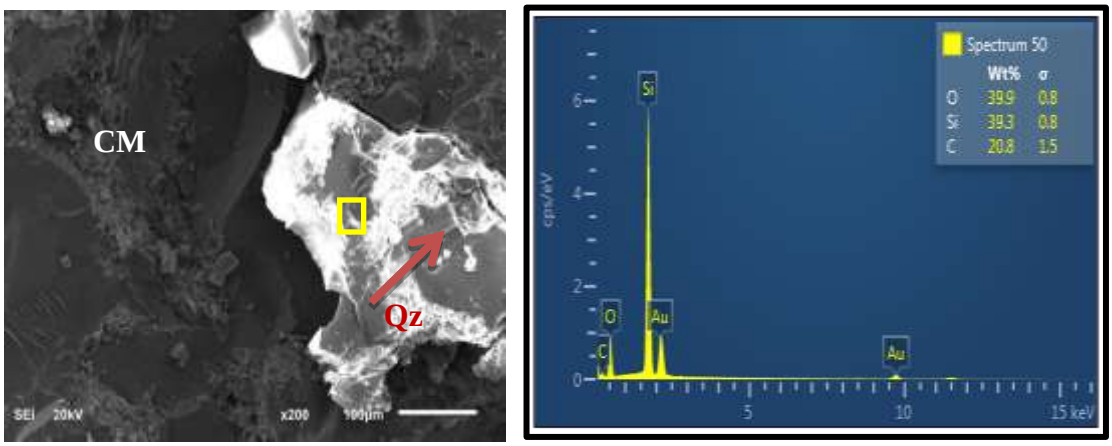

Figure 2.17: SEM Image for Quartz Wacke; quartz (Qz) grain embedded in clay matrix (CM). Elemental composition Quartz Wacke (yellow spot)

Table 2.6: Lithofacies and their main characteristics

	Lithofacies	Occurrence (%)	Description	Main Minerals	Quartz (%)	Main Elements	Interpreted Depositonal Environment
Qusaiba Shale	Micaceous laminated organic-rich mudstone facies	18.2	Horizontal and parallel laminae of 1-3 mm. Organic matter 12-15% by volume	quartz, illite muscovite, kaolinite, and albite	39.9	Si, Al, K, O, Na	Low energy, deep marine environment
	Laminated clay-rich mudstone facies	55.87	5-15 mm thick of lamination pattern. Organic matter is 1-5% by volume.	quartz, illite muscovite, kaolinite, and albite	49.3	Si, Al, K, O, Na	Cyclic high and low energy environment
	Massive siliceous mudstone facies	26.1	>15 mm thick laminae. 1-3% organic matter.	quartz illite, feldspar and chlorite	78.1	Si, Al, O, K, Mg, and Fe	Low energy environment, from suspension fallout.
Mid-Qusaiba Sandstone	Quartz Arenite	65.8	Massive light grey. Highly fractured	quartz, illite and feldspar	75-90	Al, K, Mg, and Fe	Middle to upper shoreface
	Quartz Wacke	26.8	Massive grey sandstone. Highly fractured.	quartz, microcline and albite	65-80	Si, O, Al, K, Mg, and Fe	Middle to upper shoreface

CHAPTER 3

FRACTURES SYSTEMS

In this chapter, the fracture systems in Qusaiba Shale and Mid-Qusaiba Sandstone will be addressed. Density, aperture, persistence and extent of fractures are main parameters for fractures description. Fractures are good indicators for the brittle zones and considered as essential for production from tight formations like shale. These natural fractures provide conductive flow paths for the hydrocarbon to the wellbore and also play significant role after being enhanced using hydraulic fracture stimulation treatments. However, in some cases intensely fractured zones do not significantly contribute to production depending upon the filling material of fractures (Gale et al., 2014).

Montgomery et al., (2005) studied fractures in Barnett Shale, USA to define the process of generation and fracture network within the reservoir through coupling the natural fractures with hydraulically induced fractures that contribute to total gas production. An intense fracture system does not always mean high permeability; sometimes fracture permeability is very low due to their filling with impermeable material. An example is that highly intense fractured zones of Barnett Shale have low production, as compared to zones with low intensity fractures (Montgomery et al., 2005, Bowker, 2007). The brittleness is of utmost importance to explain fracture initiation and propagation (Britt and Schoeffler, 2009).

Various kinds of fractures are commonly developed in shale including tectonic, bedding, diagenetic contraction, and stylolite fractures. Tectonic fractures are developed due to the local or regional tectonic stress release and concentration. Fractures are also developed along lamination/bedding planes and are termed as bedding fractures/cracks (Figure 3.1) (Ding et al., 2013). Reservoir permeability is strongly dependent on these bedding fractures which may be found in visibly non-fractured zones (He et al., 2011).

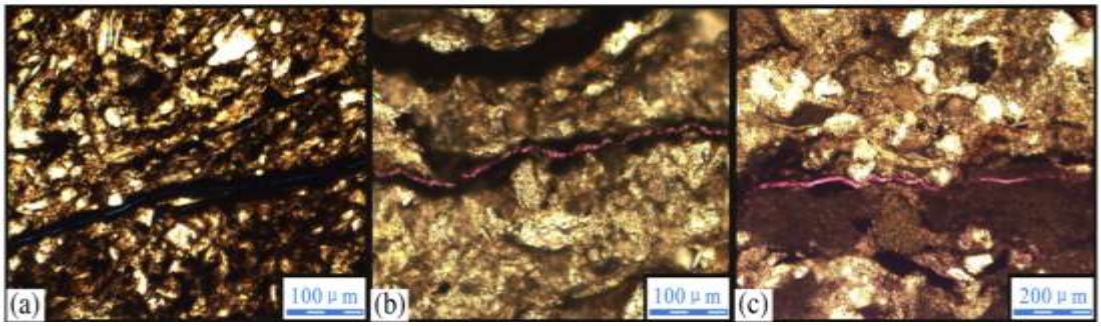

Figure 3.1: Micro-fractures from black shale reservoirs of Lower Permian Shanxi Formation (Ding et al., 2013)

Tectonic and bedding fractures are very important for development of shale reservoirs. They enhance the effective porosity and permeability as well as provide the main pathways for the migration of gas. In addition, the presence of micro fractures increases the free and absorbed gas content within shale reservoirs through enhancing the pore space and specific surface area (Ding et al., 2013).

3.1 Fractures in Qusaiba Shale

Fractures have been observed on the both macro (cores) and micro (thin sections) scale in the Qusaiba Shale. Based on their scale, they are described in two groups in the following paragraphs.

3.1.1 Macro-scale Fractures

Various tectonic and bedding fractures were identified in core samples and thin sections with fracture planes being horizontal, vertical and irregular. However, most of them show fresh surfaces and are considered as induced fractures (Figure 3.2) (Bowker, 2007). Most of those fractures are open and few fractures are filled (Figure 3.3 (f) and (j)). Majority of the fractures are irregular, horizontal and vertical and are extensional fractures (Mode-I) with no considerable displacement along fracture planes (Figure 3.2 and 3.3). Some shear fractures (Mode-II) have also been observed with minor displacement along fracture plane (Figure 3.3 (f)).

Fracture density varies with lithofacies in Qusaiba Shale. The intensity of fractures (Mode-I and Mode-II) is higher in Lithofacies-III (contain relatively higher silica content). Fractures are also observed at the sharp contacts between Lithofacies-I and II. There is a periodic repetition in horizontally oriented natural and induced fractures after approximately every foot resulting in a specific pattern with horizontal planes as shown in Figures 3.2 and 3.3. Very few macro-scale fractures are observed in Lithofacies-I which contains relatively smaller amount of quartz (39%).

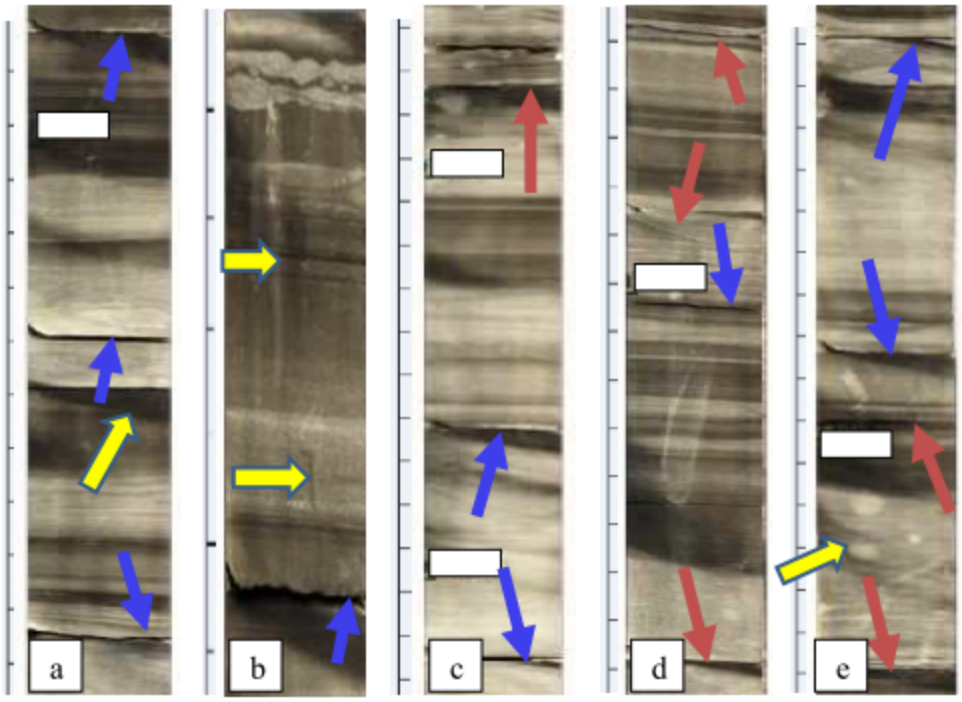

Figure 3.2: Core Images: (a) to (f), show induced (blue arrows) and natural (red and yellow arrows) fractures observed in Qusaiba Shale. (Scale 1 Div. = 1 inch)

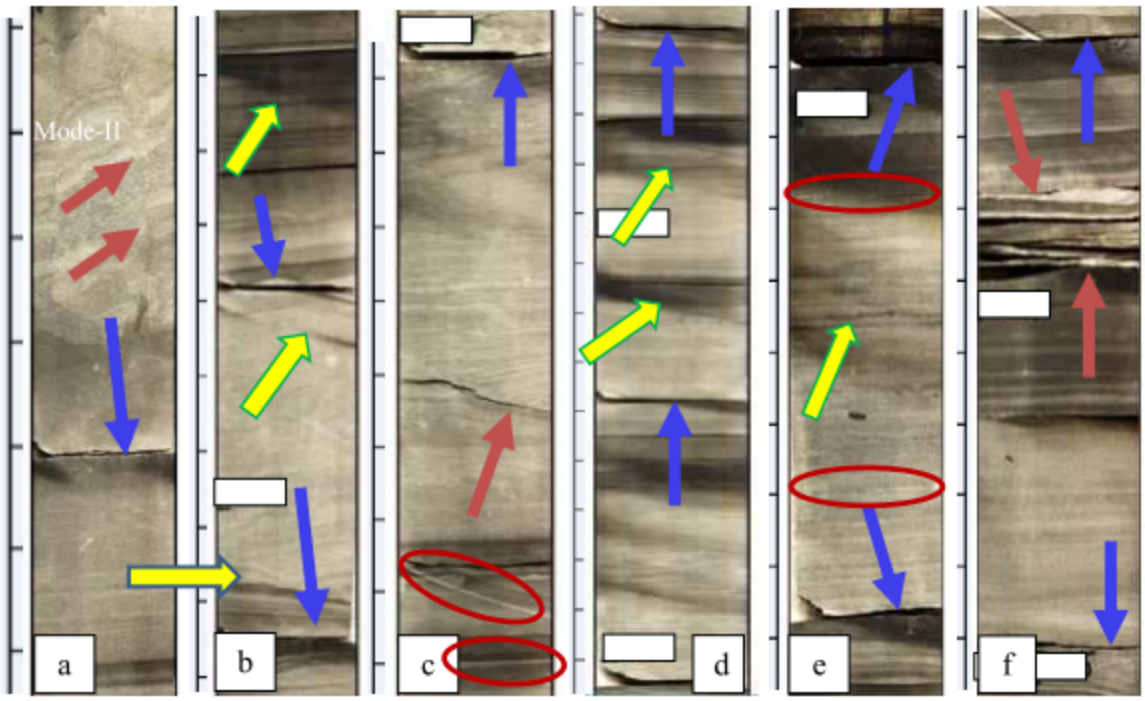

Figure 3.3: Core Images: (a) to (f) Natural fractures (red and yellow arrows and circles) observed in Qusaiba Shale. Some fractures are induced (blue arrows) during coring and handling. Most of the fractures are located in Lithofacies-II and III (light color). (Scale 1Div = 1 inch)

Similar kinds of horizontal fractures were also reported in Barnett Shale cores as shown in Figure 3.4 (Faraj and Brown, 2010).

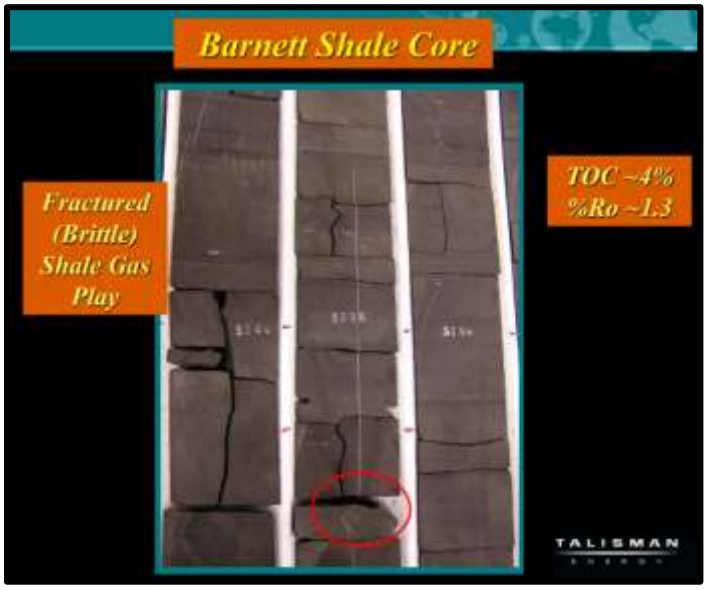

Figure 3.4: Fractures observed in Barnett Shale (Faraj and Brown, 2010)

3.1.2 Micro-Scale Fractures

Fractures which have length less than 10 mm and width less than 100 μm are referred to as micro-fractures (Ding et al., 2013). These fractures may be observed visibly non-fractured zones (He et al., 2011).

Micro scale bedding fractures (parallel to lamination planes) have been observed in thin sections images of Qusaiba Shale that are filled with organic matter (Figure 3.5 (a) and Figure 3.6). Micro-scale fractures are oriented along lamination planes and have relatively higher intensity in Lithofacies-I and II (Figure 3.5 (b), and 3.7 (b)).

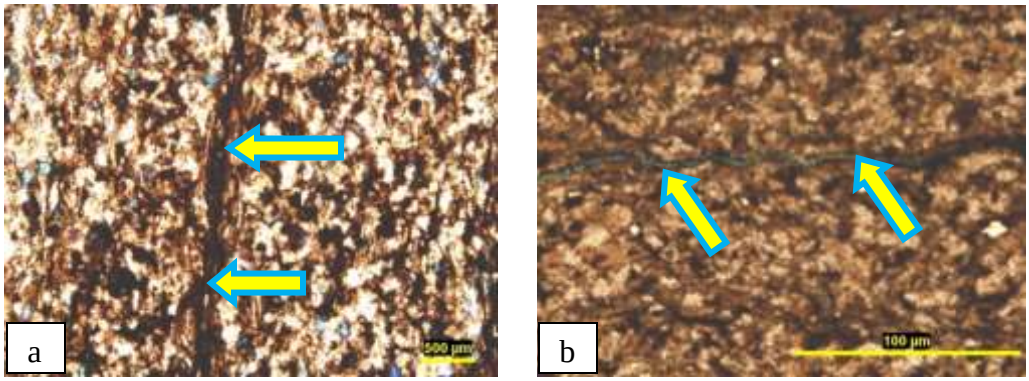

Figure 3.5: Thin sections, (a) Natural fracture filled with organic matter (b) Probably induced fracture in Lithofacies-II

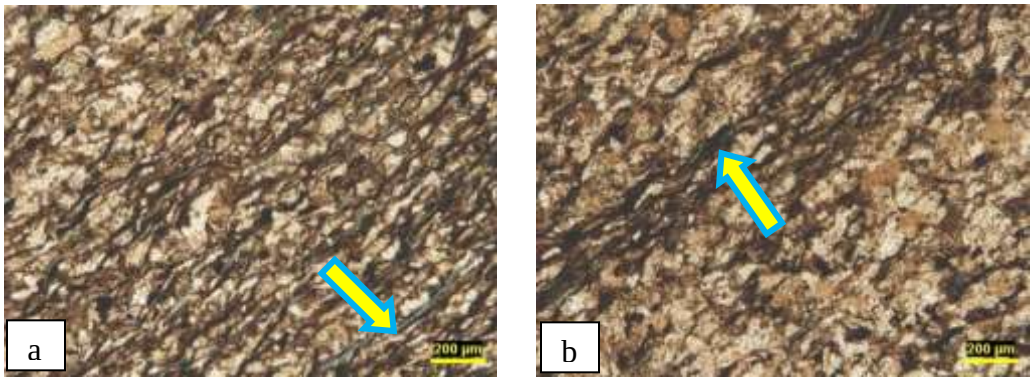

Figure 3.6: Thin sections images showing (a) fractures along lamination planes of Lithofacies-II (b) lamination planes filled with organic matter (Lithofacies-II)

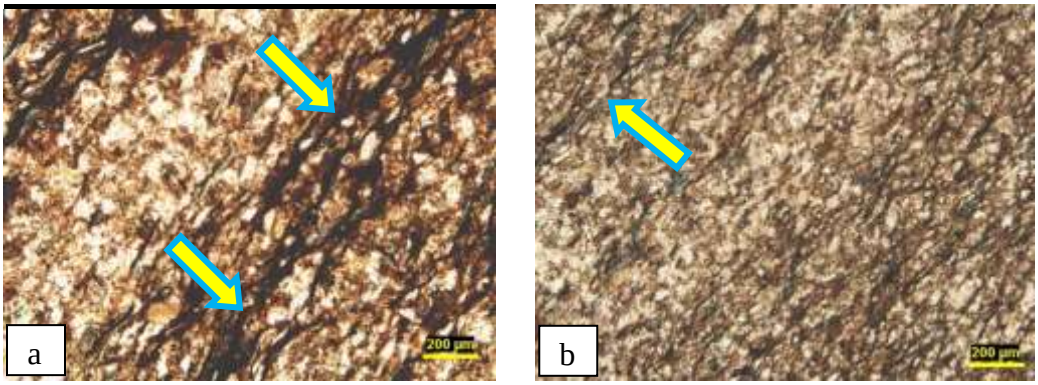

Figure 3.7: Thin section images show (a) lamination in Lithofacies-II filled with organic matter (b) fracture along lamination

3.2 Fractures in Mid-Qusaiba Sandstone

Highly intense fractures were observed in Mid-Qusaiba Sandstone in both macro and micro scales. Number of fractures with horizontal, vertical and irregular fracture (open and open) planes was observed in core samples. They reflected high tectonic stresses in the study area.

3.2.1 Macro-scale Fractures

The core samples of Mid-Qusaiba Sandstone exhibit macro-scale fractures with both open and filled types. Most of the filled fractures are oriented at 20^0 to 40^0 degrees. Most of the observed fractures are of extensional fractures (Mode-I) (Figure 3.8 and 3.9) and few of them as shear fractures (Mode-II) (Figure 3.9 (b)). Fracture density is relatively high compared to Qusaiba Shale. Mode-I fractures form the systematic pattern with horizontal oriented fracture planes as shown in figure 3.9 (c), (d), and (e)). The inclined fractures were developed under stress along particular direction, however, exact orientation of tectonic stresses (major and minor principle stresses) is not possible to determine from available data.

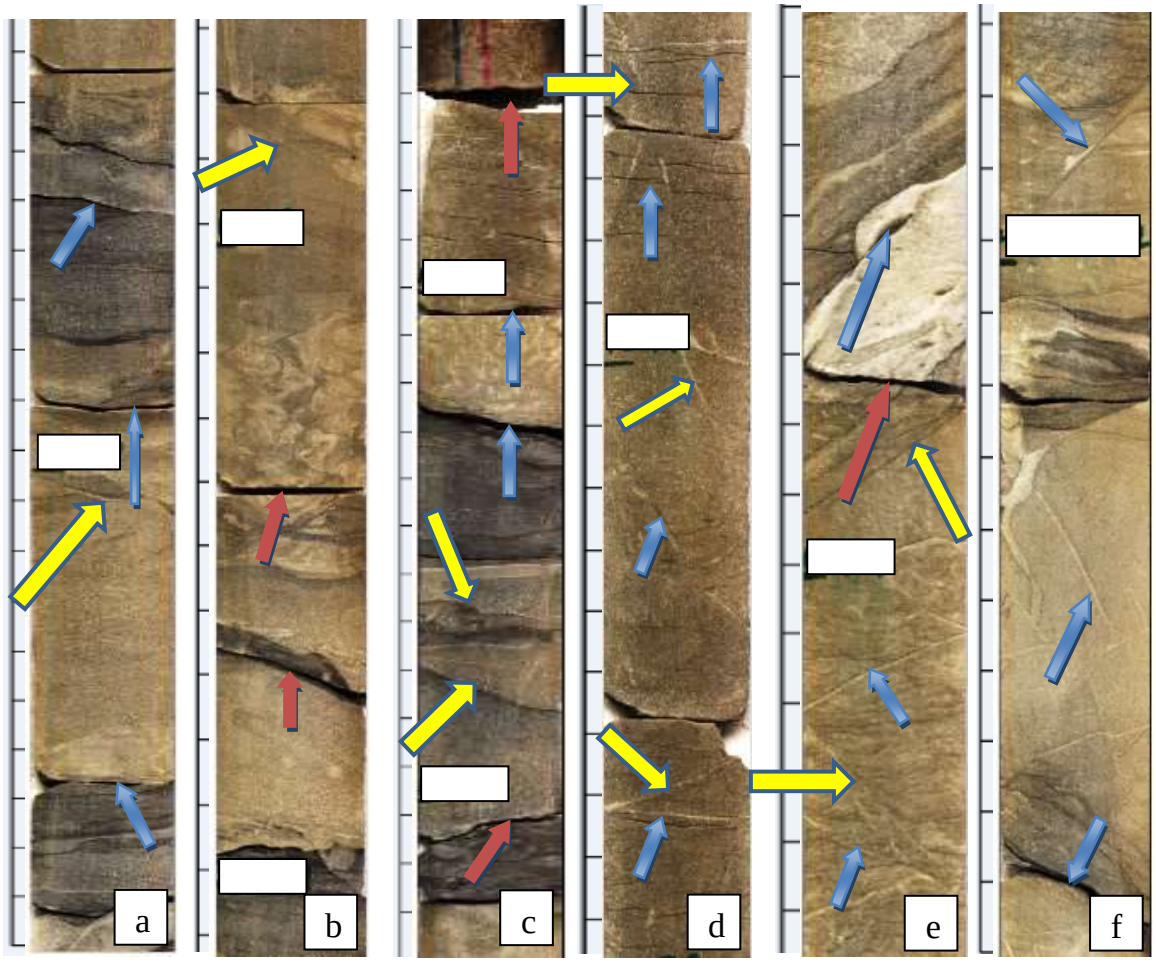

Figure 3.8: Core images (a) to (f) showing number of horizontally oriented and inclined fractures (yellow arrows): natural (blue arrows) and induced (red arrows).

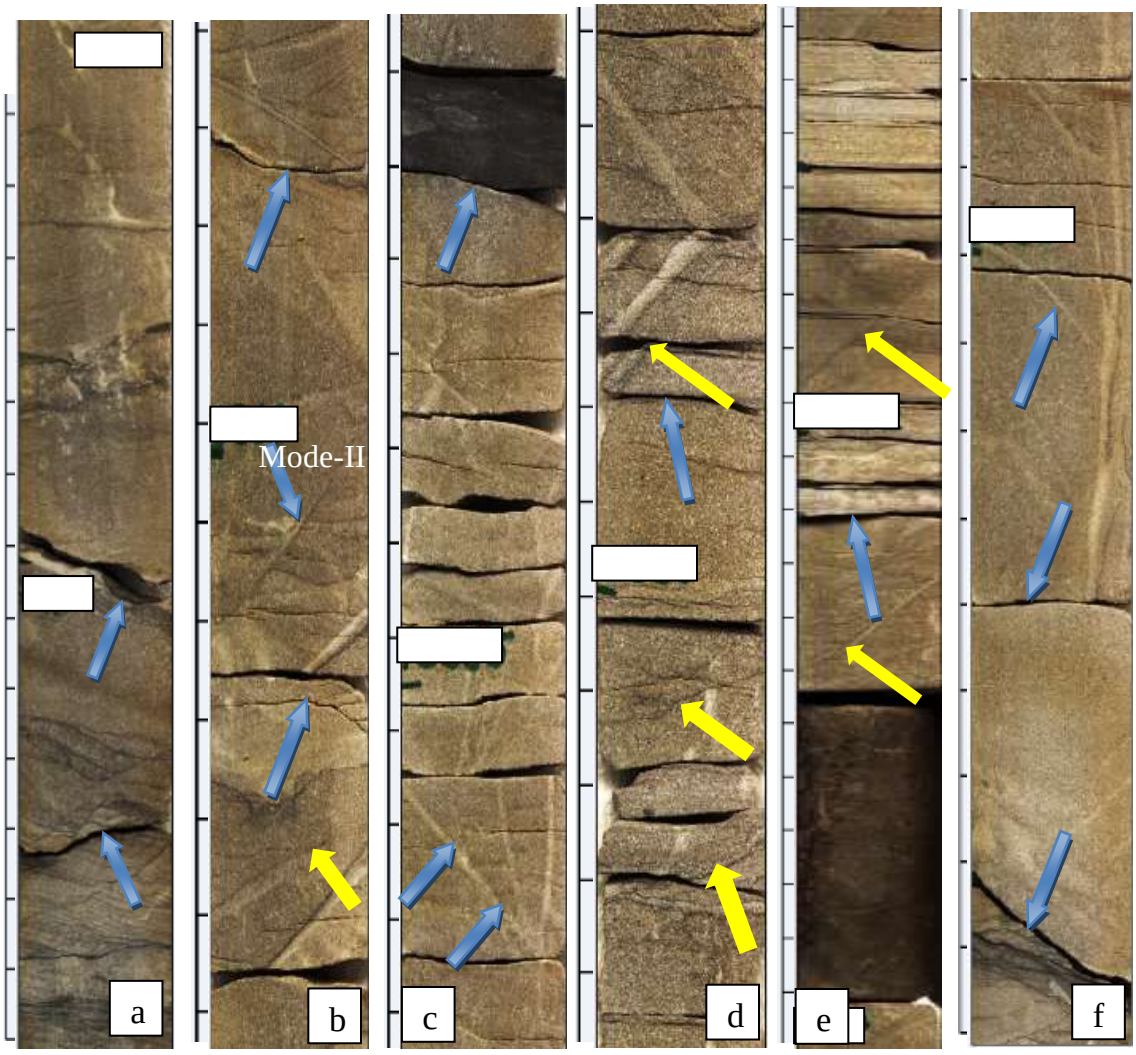

Figure 3.9: Core images (a to f) showing number of horizontal oriented and inclined fractures (yellow arrows). Mode-I and II (open and filled) fractures (blue arrows). Images c, d and e are showing systematic joint sets with fracture planes horizontally oriented.

3.2.2 Micro-scale Fractures

Micro-scale fractures were observed under thin sections. They are oriented randomly. They can be open or filled. These micro fractures may be associated with high in-situ stresses or tectonic activity (Ding et al., 2013). Due to high stresses, broken quartz grains have also been observed in thin sections (Figure 3.10 and 3.11). High intensity of fractures in sandstone reflects its brittle nature.

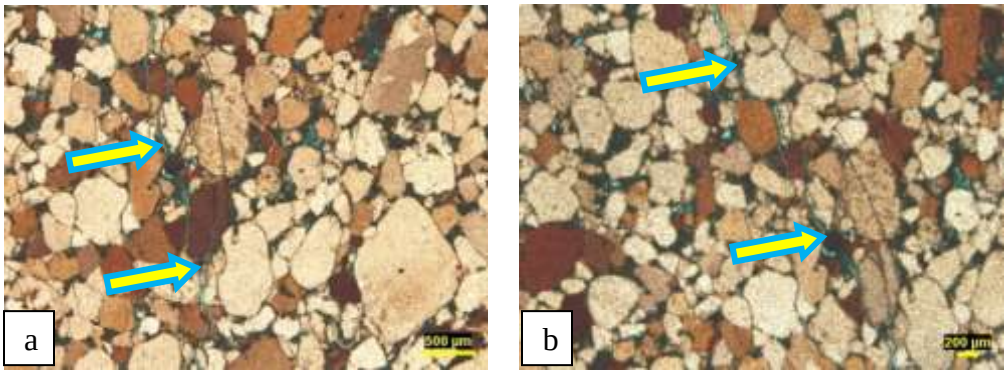

Figure 3.10: Thin sections images show (a) and (b) micro-scale fractures (Mode-I) with broken quartz grains

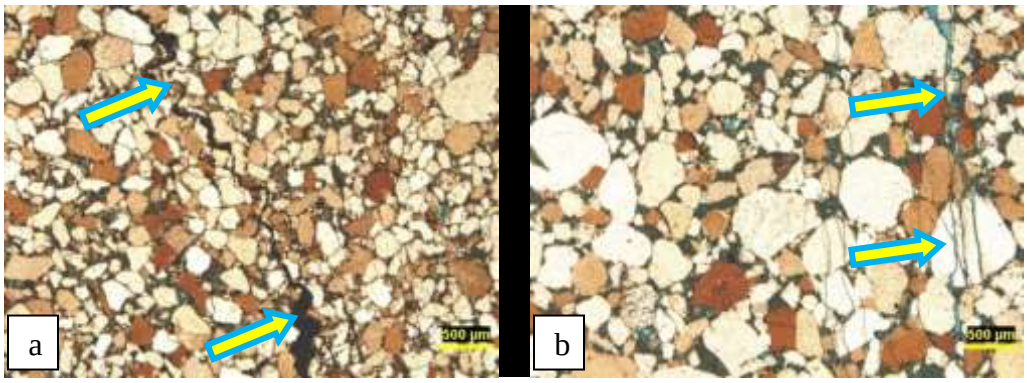

Figure 3.11: Thin section images show (a) natural fracture in quartz arenite filled with organic matter (b) fractured quartz grains

3.3 Fracture Analysis from Logs

Fractures were also identified in both the Qusaiba Shale and Mid-Qusaiba Sandstone using well log data. Micro spherically focused log (MSFL), porosity and density logs were used for the identification of fractures. Qusaiba Shale and Mid-Qusaiba Sandstone intervals were selected on the basis of gamma ray response, clay contents, and quartz, feldspar, mica (QFM) contents (Figure 3.12 and 3.15). Shallow resistivity measurement tools (microlog 'ML' and 'MSFL') exhibit low resistivity at open fracture locations and relatively higher values where healed fractures are present (Laongsakul and Dürrast, 2011). The highly fluctuated resistivity values with spikes in sandstone and shale

intervals indicate open fractures (Figure 3.12). Within sandstone interval, decreasing density with spikes also gives indication of fractures (Crain 2010). Shear wave energy is significantly attenuated and its travel time increases due to presence of fracture. Acoustic signals are attenuated and depict abrupt increase in travel transit time. The high variability in formation bulk density (Figure 3.13) indicates high fracture intensity with low resistivity and solid formation with high resistivity values. Low density values are observed at open fracture locations and slightly higher at filled/mineralized fracture locations (Laongsakul and Dürrast, 2011).

The MSFL (Figure 3.12) exhibited low values at fracture locations due to the conductive formation fluid and resistivity spikes with higher values indicating mineralized fractures (Laongsakul and Dürrast, 2011). Decrease in density has been observed at fractured zones with sharp spikes in Qusaiba Shale density log (Figure 3.13 and 3.16). Neutron porosity log may not be the good indicator for fracture identification (Crain, 2010), since neutron porosity is based on hydrogen concentration within formation which may overestimate porosity in hydrocarbon rich formations. S-wave travel time variation exhibited increase due the presence of fractures as shown in Figure 3.14. Diameter of borehole increases due to fracture resulting in increased caliper log measurements (Laongsakul and Dürrast, 2011). The increase in caliper log values at fractured interval has been observed in Figure 3.14.

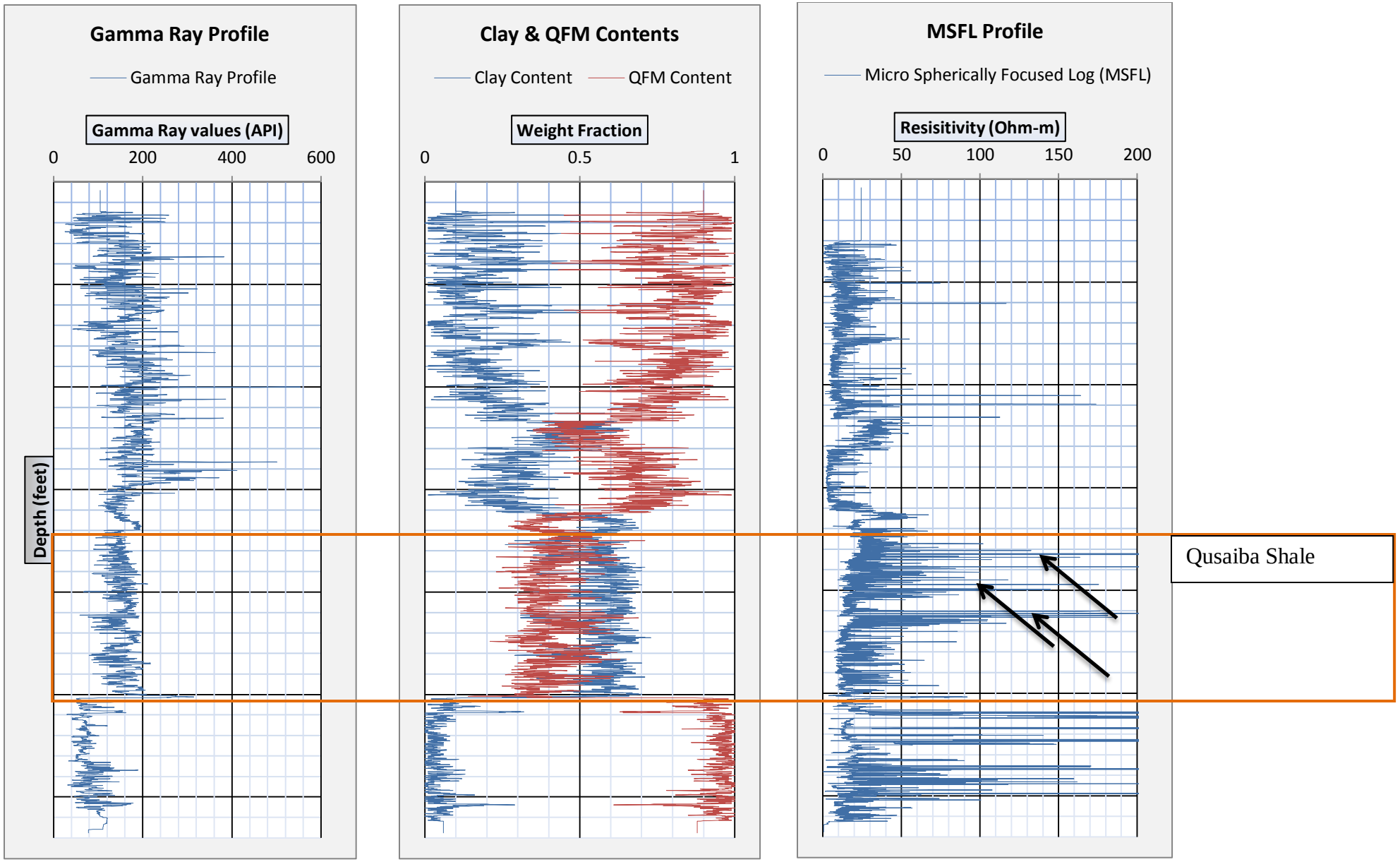

Figure 3.12: Gamma ray, clay content, and MSFL correlation (Depth Scale: 1 small division = 100 Ft)

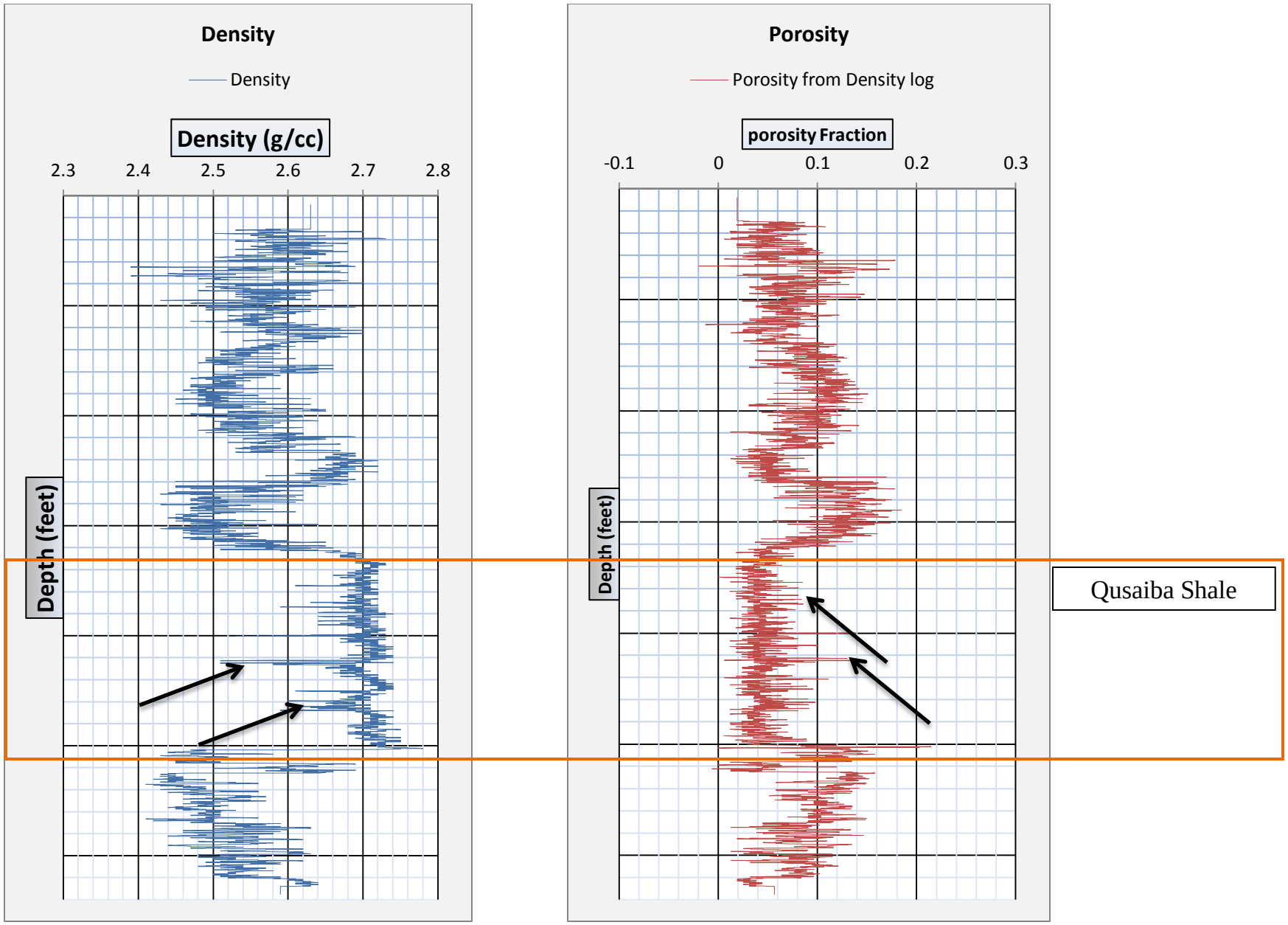

Figure 3.13: Density and porosity logs for Qusaiba Shale (Depth Scale: 1 small division = 100 Ft)

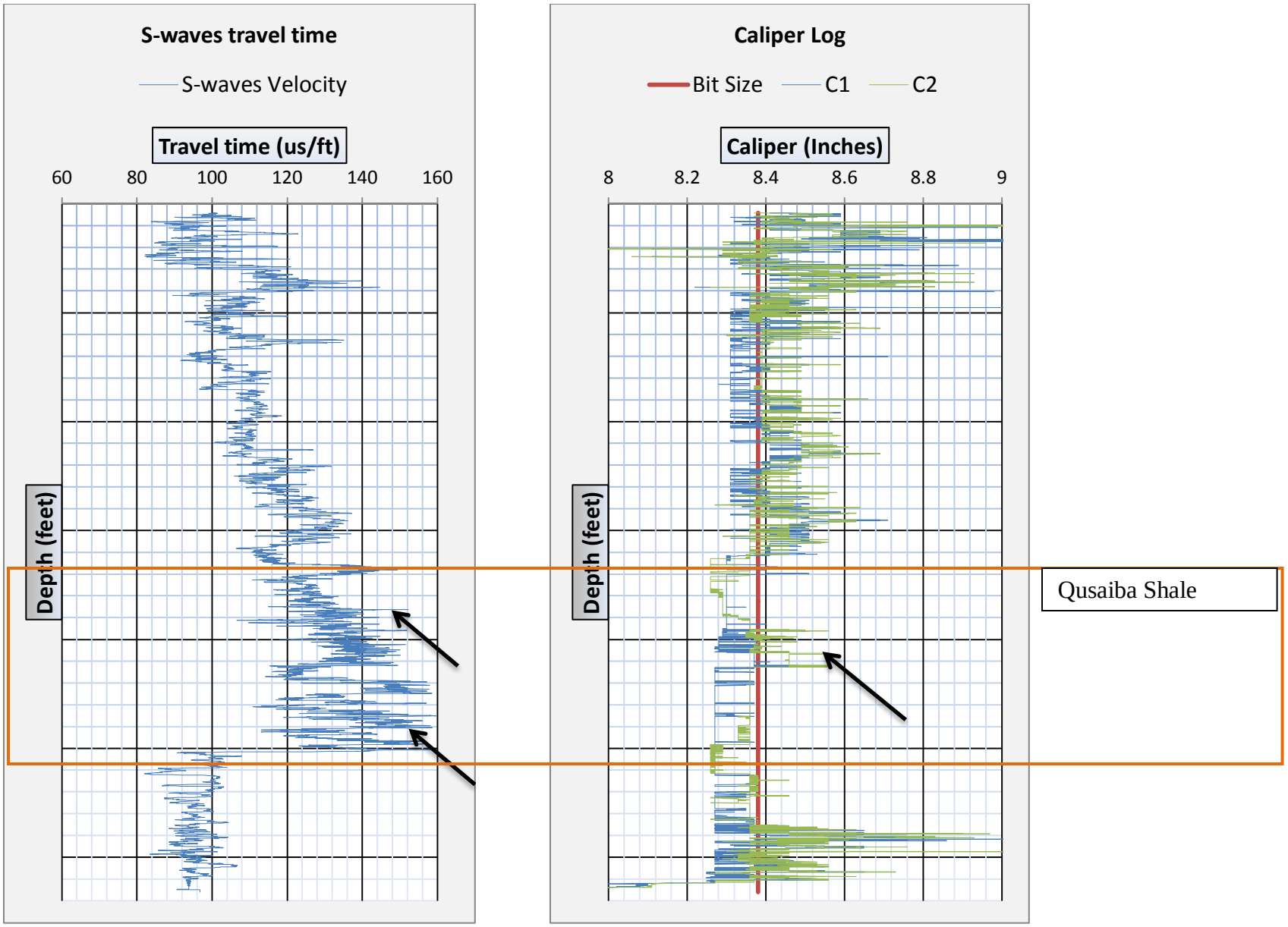

Figure 3.14: S-wave travel time and Caliper log variation with depth (Depth Scale: 1 small division = 100 Ft)

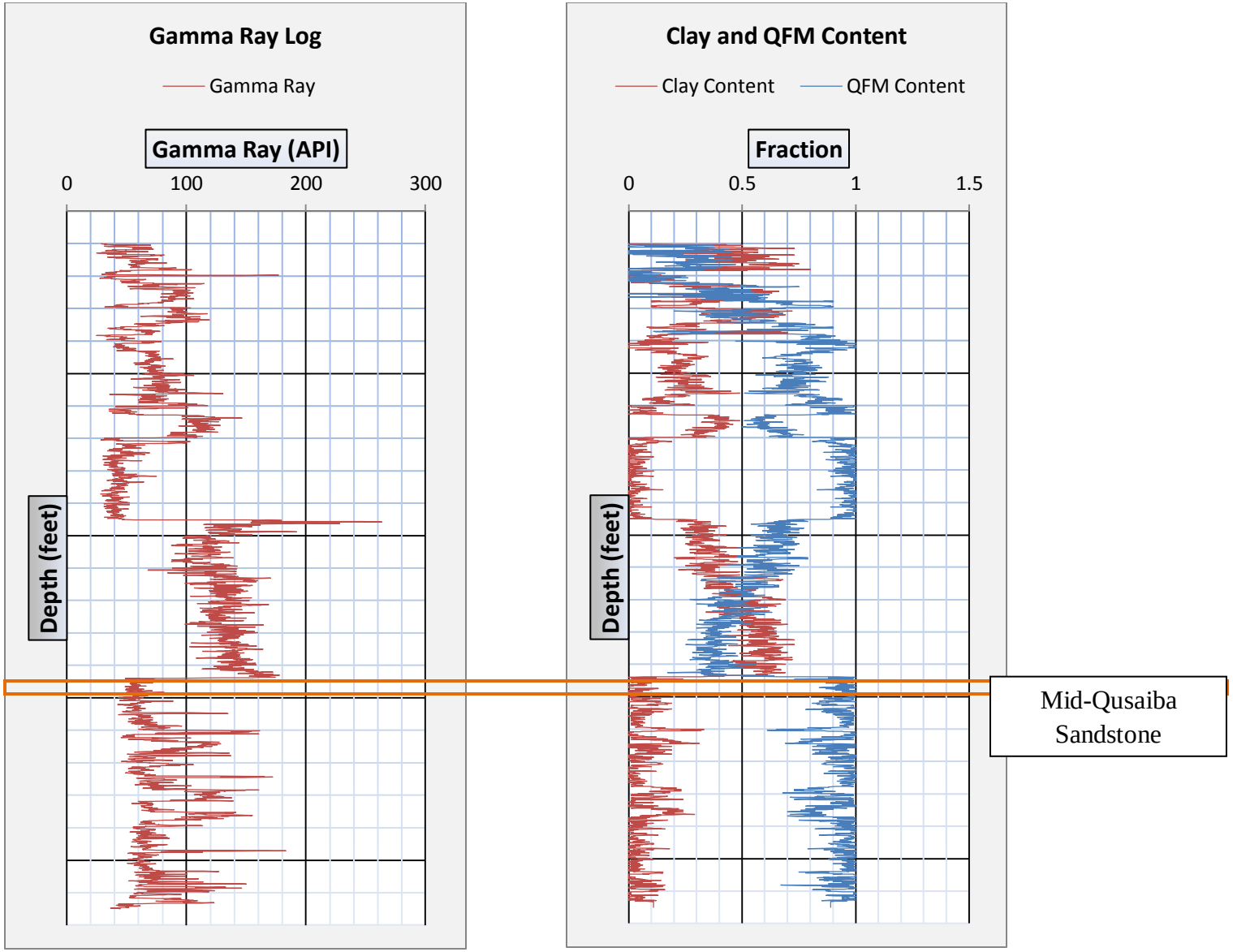

Figure 3.15: Gamma ray and Clay and Quartz Feldspar Mica (QFM) Contents (Depth Scale: 1 small division = 100 Ft)

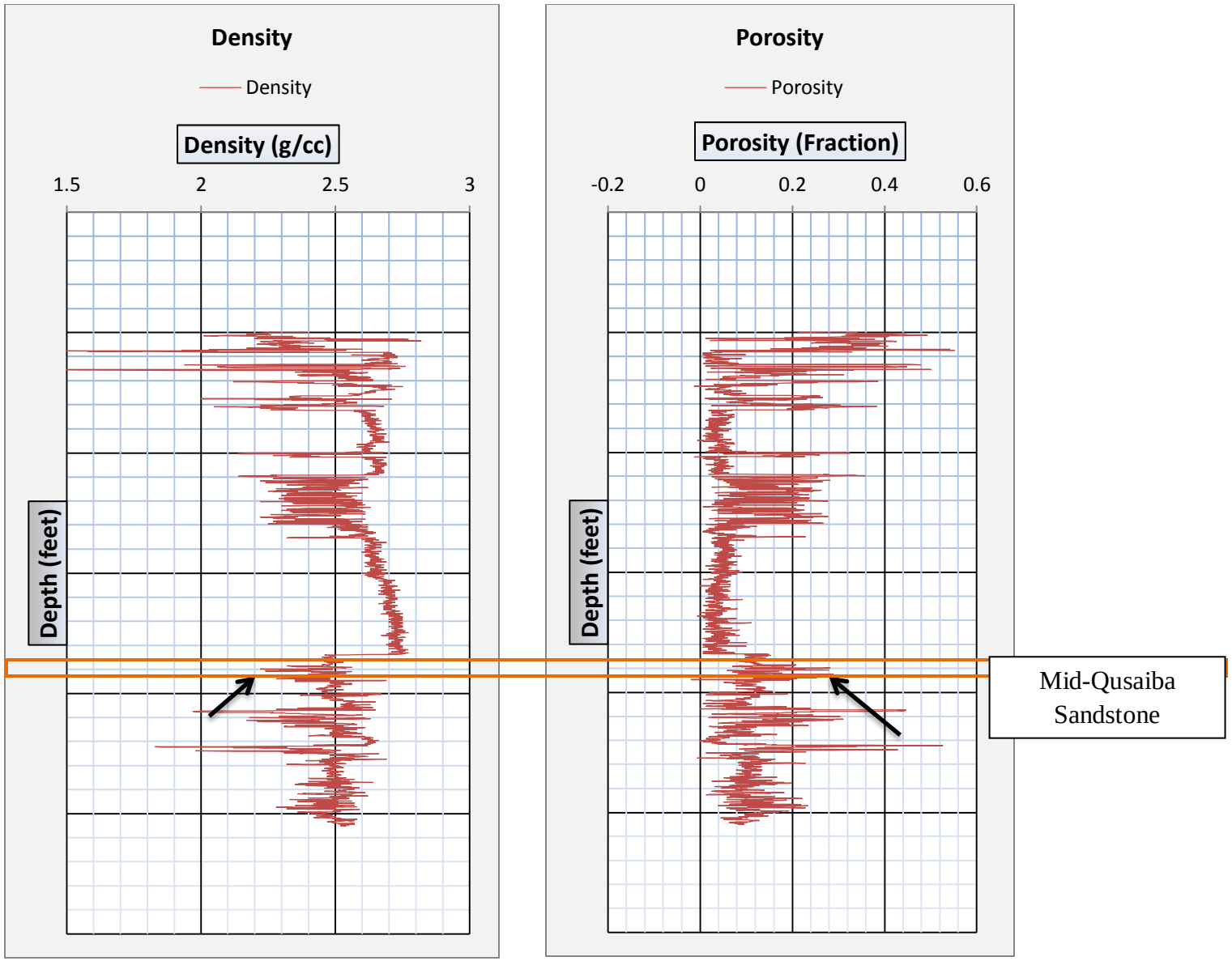

Figure 3.16: Density and porosity variation with depth (Depth Scale: 1 small division = 100 Ft)

Fractures with relatively lower density have been identified in Qusaiba Shale. Fracture identification with sharp decrease in density (spikes) in shale interval has been supported with porosity, sonic and caliper logs. On the other hand, Mid-Qusaiba Sandstone is highly fractured as indicated by sharp peaks in the porosity and density log values. Intense fractures indicate brittle nature of sandstone which is also revealed by mechanical parameters having high Young's Modulus (33 GPa) and low Poisson's ratio (0.2).

The fractures can play significant role in production from the Qusaiba Shale by developing a complex fracture network within reservoir with application of hydraulic fracture stimulation. As discussed earlier, the Lithofacies-III with high quartz content (60-78%) may be the probable cause for fracturing in shale interval. Lithofacies-III also exhibited higher Young's Modulus (32 GPa) and lower Poisson's ratio (0.25) as compared to Lithofacies-I and II (Table 3.1) exhibiting brittle behavior. These silica rich facies add brittleness to Qusaiba Shale, enhancing its' fracability.

Table 3.1: Fractures association with Lithofacies and Mechanical Parameters

	Lithofacies	Occurrence (%)	Mechanical Parameters		Fractures Density	
			Young's Modulus (Avg) (GPa)	Poisson's ratio (Avg)	Macro-scale	Micro-scale
Qusaiba Shale	Micaceous laminated organic rich mudstone facies	18.2	26	0.34	Low (Tectonic and bedding)	High (Bedding)
	Laminated clay rich mudstone facies	55.87	31	0.32	Higher than Lithofacies-I (Tectonic and bedding)	High (Bedding)
	Massive siliceous mudstone facies	26.1	32	0.25	Higher than Lithofacies-I & II (Tectonic and bedding)	Low (Bedding)
Qusaiba Sandstone	Quartz Arenite	65.8	33	0.2	High (Tectonic)	High (Irregular)
	Quartz Wacke	26.8	32	0.2	High (Tectonic)	High (Irregular)

CHAPTER 4

GEOMECHANICAL CHARACTERISTICS

In this study, geomechanical analysis was conducted in order to determine mechanical parameters using experimental as well as field (log) data. Mechanical properties are of utmost importance for shale characterization as will be discussed in the following sections.

4.1 Importance of Geomechanics

Geomechanics is of vital importance for the exploration, development and production of unconventional resources (Abousleiman et al., 2007). The key mechanical parameters (Poisson's ratio and Young's modulus) define the deformational behavior. Poisson's ratio explains the failure under stress while the Young's modulus determines the ability for fractures containment. Rocks tend to behave as brittle material with low Poisson's ratio (< 0.3) and high Young's modulus (>25 GPa) and give good response to hydraulic fracturing stimulation treatments. On the contrary, high Poisson's ratio and low Young's Modulus show ductile behavior and act as barrier to fracture propagation (Rickman et al., 2008). For the prospectivity evaluation and successful development of shale gas plays, mineralogy and rock mechanical parameters are essential. Shale with high silica and carbonate minerals and low clay constituents is prospective. Prospective shale responds

as a brittle material to applied stress, exhibits high Young's Modulus and low Poisson's ratio.

The integration of geomechanics with mineralogy, lithology leads to designing the optimum hydraulic fracture simulation treatment. The potential costs for hydraulic fracture treatment can be reduced significantly by identifying and categorizing the lithofacies in terms of mineralogy, organic matter and geomechanical properties (Jacobi et al., 2008). The geomechanical model is of key importance to optimize hydraulic fracture stimulation, tackle stability problems during drilling with minimum mud weight.

Anisotropy must be taken into account in stress modeling for unconventional shale reservoirs because static and dynamic elastic moduli of shale show remarkable variation in horizontal and vertical directions. Taking into account anisotropy in stress profile estimations result in better and cost effective completion decisions (Higgins et al., 2008). The reservoir simulation and geomechanical model revealed that stress anisotropy has significant influence on well productivity and on the permeability anisotropy for hydraulically fractured horizontal and non-fractured wells.

4.2 Material and Method

This study determined the mechanical properties such as Poisson's ratio, Young's modulus and unconfined compressive strength, cohesion, friction, and ultrasonic velocities in both horizontal and vertical directions in order to highlight the anisotropy in Qusaiba Shale and Mid-Qusaiba Sandstone samples. Samples were selected from each lithofacies and tested to determine their mechanical parameters using various techniques. Ultrasonic velocity (primary and secondary waves) measurements were carried out to

determine stiffness in terms of dynamic Poisson's ratio and Young's modulus using Autolab 500 testing equipment. Ultrasonic velocity measurements were performed at different confining pressures in order to simulate true reservoir conditions. The uniaxial compression test equipment was used in this study to determine the uniaxial compressive strength along with static Young's modulus and Poisson's ratio. The test was performed on both vertical and horizontal samples in order to take anisotropy into account.

Samples were selected from 30 feet of Qusaiba Shale and 30 feet of Mid-Qusaiba Sandstone, on the basis of variation in lithofacies. All five lithofacies, as discussed earlier in chapter 2, were considered for sampling.

However, depth correction is essential before sampling to attain the log depth calibration with core data. Depth corrections were performed by comparing the core gamma rays with the log values (Sahin and Abouelresh, 2014). For depth corrections, please refer to Appendix-F.

4.3 Sampling

Plugs were taken from each lithofacies as shown below (Table 4.1).

Table 4.1: Samples for Geomechanics Testing

Plug No.	Depth (ft)	Orientation	Lithofacies
1	XX	Vertical	L-II
2	XX	Horizontal	L-III
3	XX	Vertical	L-I
4	XX	Vertical	L-III
5	XX	Horizontal	L-II
6	XX	Vertical	L-III
7	XX	Vertical	L-II
8	XX	Vertical	L-II
9	XX	Horizontal	L-III
10	XX	Vertical	L-III
11	XX	Horizontal	L-II
12	XX	Vertical	L-II
13	XX	Vertical	L-III
14	XX	Vertical	L-I
15	XX	Horizontal	L-I

Samples locations are shown below in Figures 4.1 to 4.3.

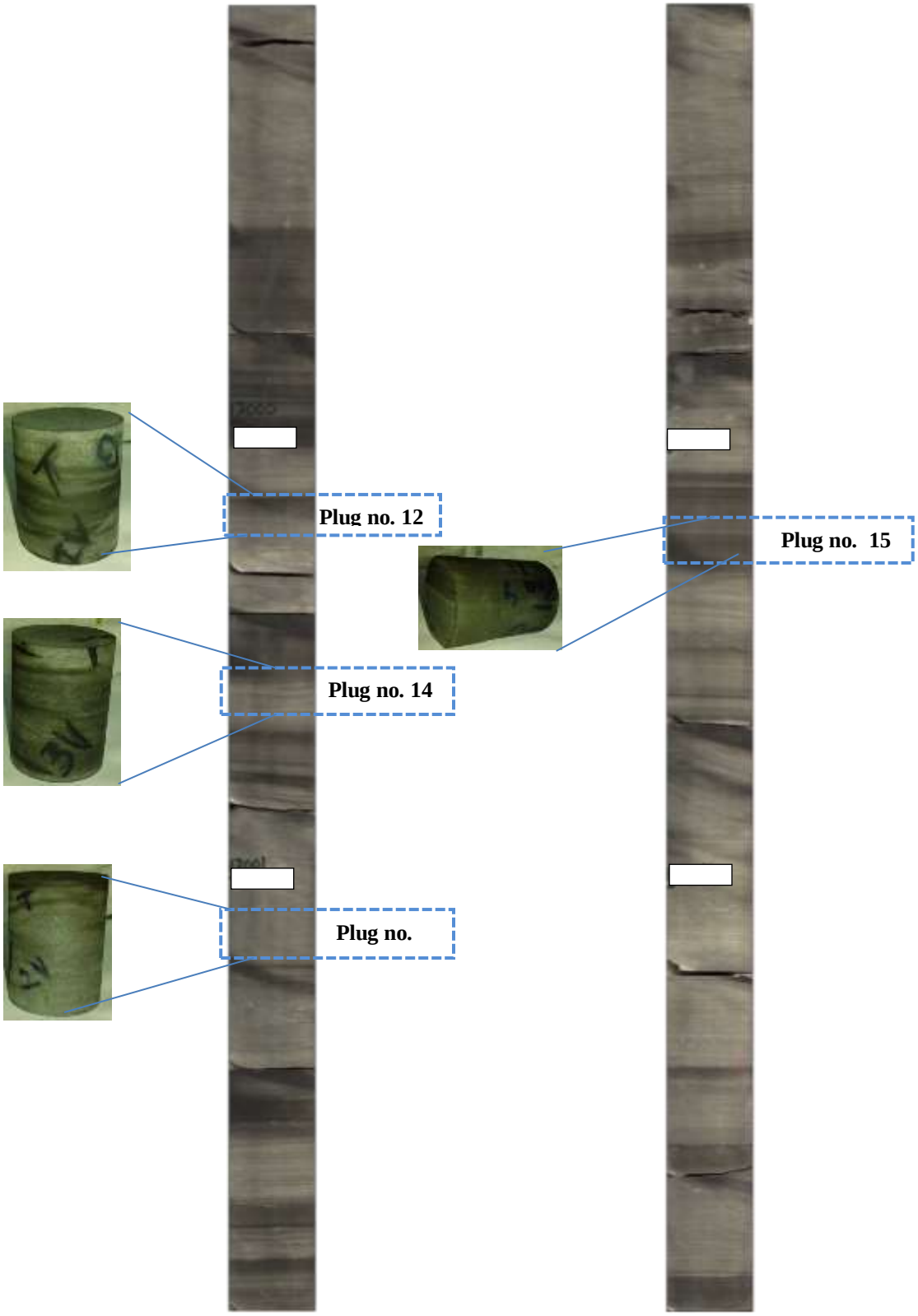

Figure 4.1: Core Plugs Locations (Qusaiba Shale, Upper Section)

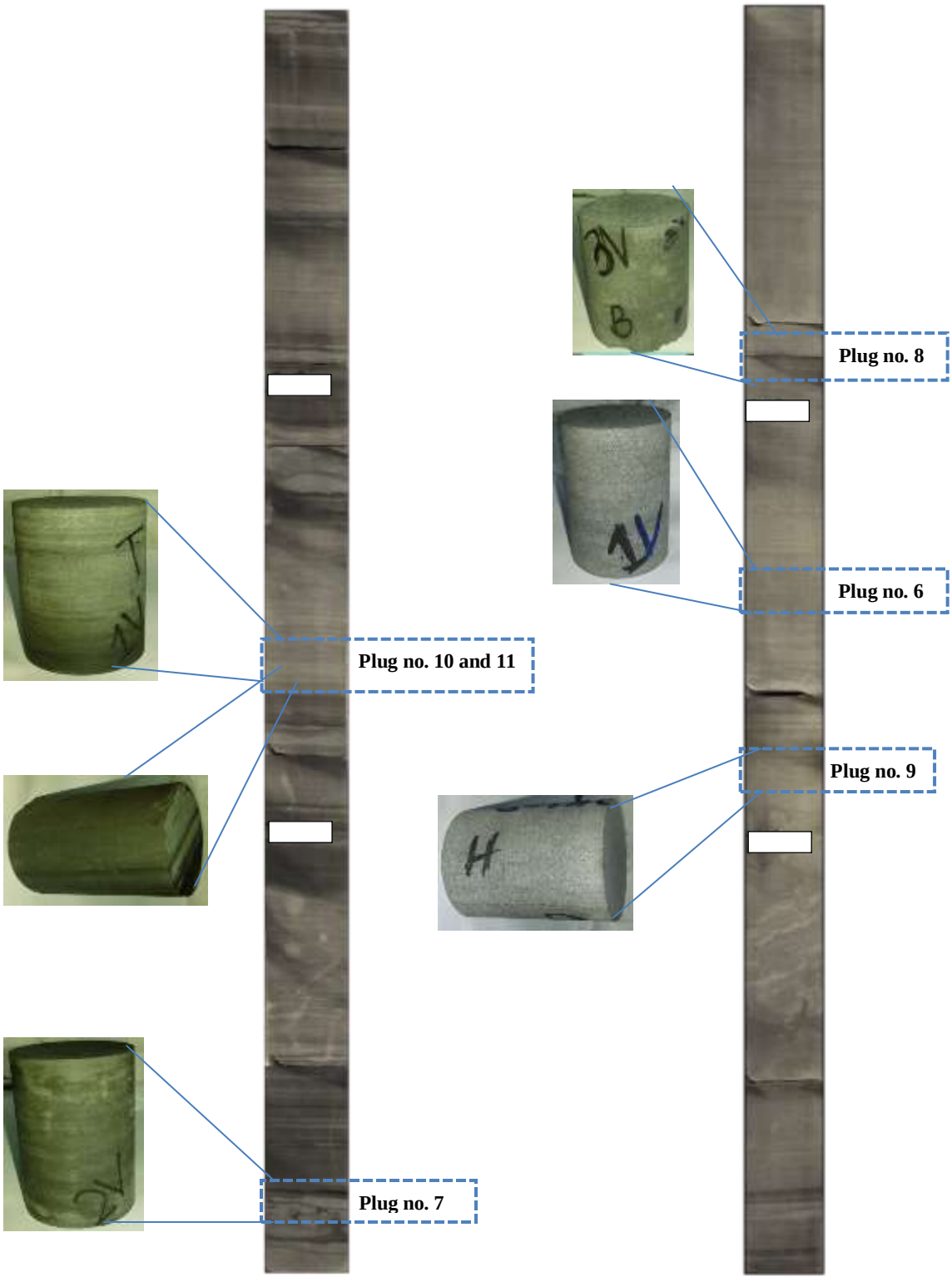

Figure 4.2: Core Plugs Locations (Qusaiba Shale, Middle Section)

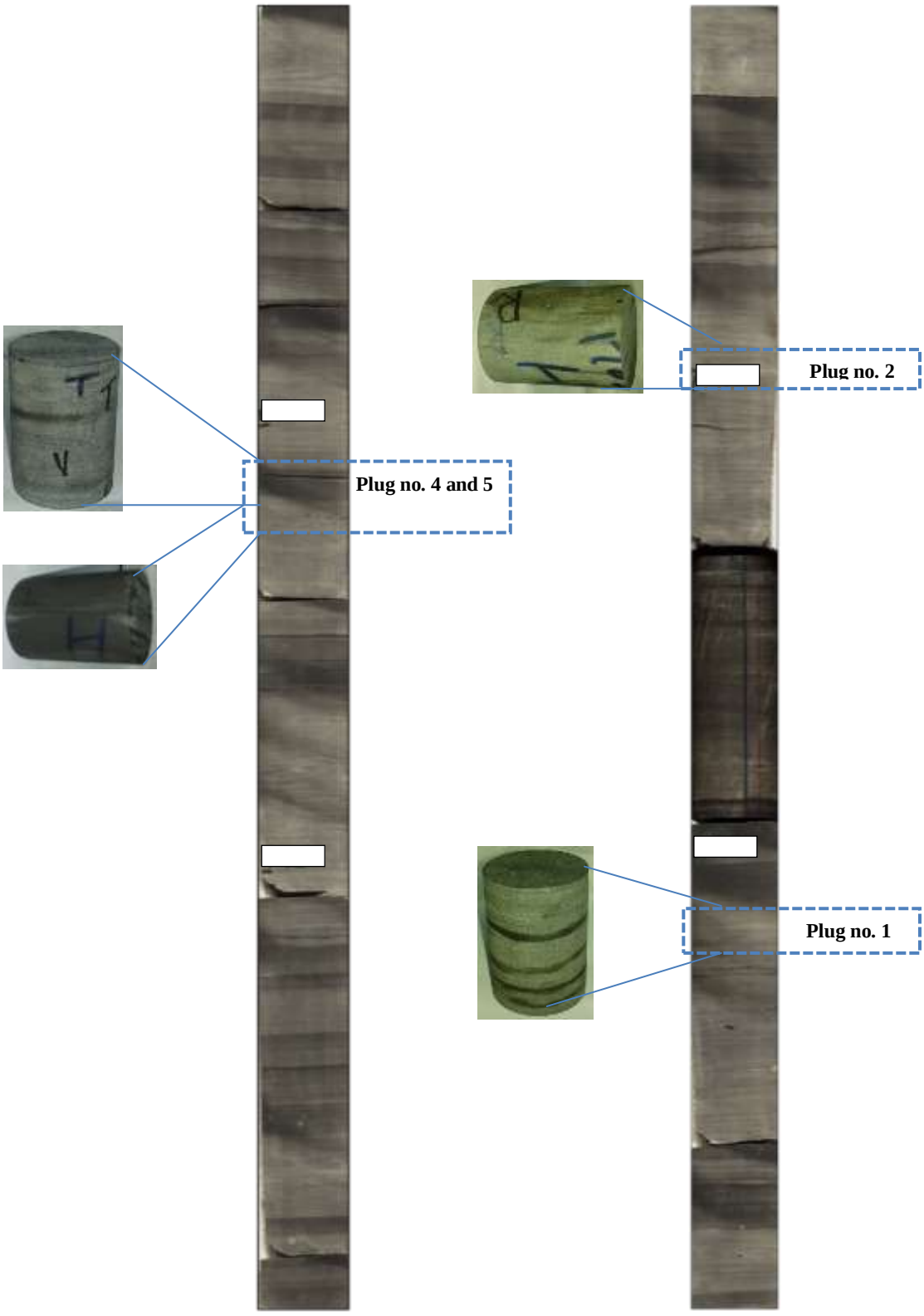

Figure 4.3: Core Plugs Locations (Qusaiba Shale, Lower Section)

4.4 Acoustic Wave Velocity Measurements

The acoustic measurements on rock samples were performed in this study to determine the compressional (P-wave) and shear (S-wave) wave velocities using the ASTM D 2845. They yield the dynamic elastic moduli i.e. Poisson's ratio and Young's modulus. Acoustic measurements were made on 19 shale samples using Autolab 500 equipment. The method and procedure adopted has already been discussed in Chapter 1. The measurements were performed under different confining pressures to simulate reservoir conditions.

The ultrasonic velocity measurement system yields velocities of compressional and shear wave and their variation with changes in confining pressures. Before conducting acoustic test, some pretest measurements (dimensions and density) were performed. These measurements (density and dimensions) (Table 4.2) are necessary to calculate the dynamic elastic parameters from measured acoustic velocity.

Table 4.2: Pre-test values for acoustic measurements

Plug No.	Length (mm)	Diameter (mm)	Average Length (mm)	Average Diameter (mm)	Volume (cc)	Weight (gms)	Density (gms/cc)
1	51.91	37.82	51.922	37.832	58.3364	156.82	2.6882
	51.91	37.83					
	51.92	37.83					
	51.93	37.83					
	51.94	37.85					
2	52.27	37.83	52.292	37.852	58.814	159.147	2.7059
	52.28	37.83					
	52.29	37.84					
	52.29	37.87					
	52.33	37.89					
3	52.42	37.82	52.43	37.81	58.83	158.968	2.70176
	52.43	37.83					
	52.43	37.8					
	52.42	37.79					
	52.45	37.81					
4	52.31	37.79	52.308	37.812	58.7079	159.376	2.7147
	52.28	37.81					
	52.27	37.81					
	52.3	37.82					
	52.38	37.83					
5	52.53	37.71	52.55	37.748	58.78	158.501	2.6965
	52.54	37.72					
	52.54	37.76					
	52.57	37.77					
	52.57	37.78					
6	51.21	37.72	51.24	37.77	57.381	154.874	2.699
	51.22	37.75					
	51.23	37.79					
	51.26	37.79					
	51.28	37.8					
7	45.87	37.81	45.858	37.814	51.474	137.949	2.67997
	45.84	37.81					
	45.84	37.81					
	45.85	37.82					
	45.89	37.82					
8	51.2	37.69	51.21	37.746	57.275	158.366	2.765
	52.2	37.72					
	52.21	37.77					
	52.22	37.77					
	52.22	37.78					

Table 4.2: Pre-test values for acoustic measurements (continued)

Plug No.	Length (mm)	Diameter (mm)	Average Length (mm)	Average Diameter (mm)	Volume (cc)	Weight (gms)	Density (gms/cc)
9	52.27	37.77	52.288	37.8	58.648	158.3	2.6991
	52.28	37.8					
	52.28	37.81					
	52.3	37.81					
	52.31	37.81					
10	51.72	37.66	51.732	37.738	57.834	156.403	2.7043
	51.72	37.71					
	51.73	37.77					
	51.74	37.77					
	51.75	37.78					
11	50.62	37.81	50.66	37.83	56.912	152.543	2.6803
	50.63	37.82					
	50.66	37.83					
	50.69	37.84					
	50.7	37.85					
12	50.38	37.77	50.396	37.79	56.496	151.029	2.673
	50.39	37.77					
	50.4	37.78					
	50.4	37.81					
	50.41	37.82					
13	50.96	37.75	50.988	37.784	57.141	153.035	2.6781
	50.98	37.77					
	51.02	37.77					
	51	37.81					
	50.98	37.82					
14	51.13	37.75	51.124	37.752	57.197	154.7	2.7046
	51.16	37.68					
	51.07	37.72					
	51.11	37.8					
	51.15	37.81					

4.4.1 Qusaiba Shale

Acoustic measurements were performed on 14 samples at different confining pressures i.e. 2000, 3000, 4000, 5000, and 6000 psi. The results exhibit the direct relation between P and S wave velocities and confining pressure. The results derived from acoustic measurements on Plug 1 are shown below. For complete results, please refer to Appendix-G.

Table 4.3: P and S waves velocities with confining pressures (Plug no. 1)

Test Number	Formation	Confining Pressure (MPa)	P-wave Velocity (m/s)	S_1 Velocity (m/s)	S_2 Velocity (m/s)
0	Qusaiba Shale	13.8283	5558	3047	3118
1	Qusaiba Shale	20.7112	5603	3062	3110
2	Qusaiba Shale	27.6183	5610	3085	3115
3	Qusaiba Shale	34.5173	5626	3105	3121
4	Qusaiba Shale	41.4164	5648	3108	3127
5	Qusaiba Shale	34.5173	5626	3100	3124
6	Qusaiba Shale	27.6585	5618	3083	3121
7	Qusaiba Shale	20.7112	5610	3067	3118
8	Qusaiba Shale	13.8684	5595	3056	3116

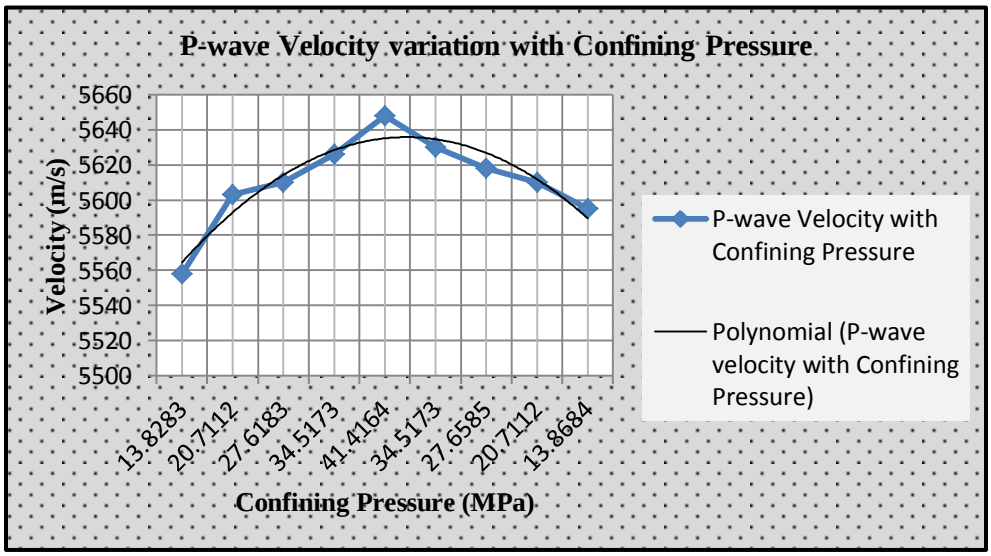

Figure 4.4: P-wave velocity variation with confining pressure

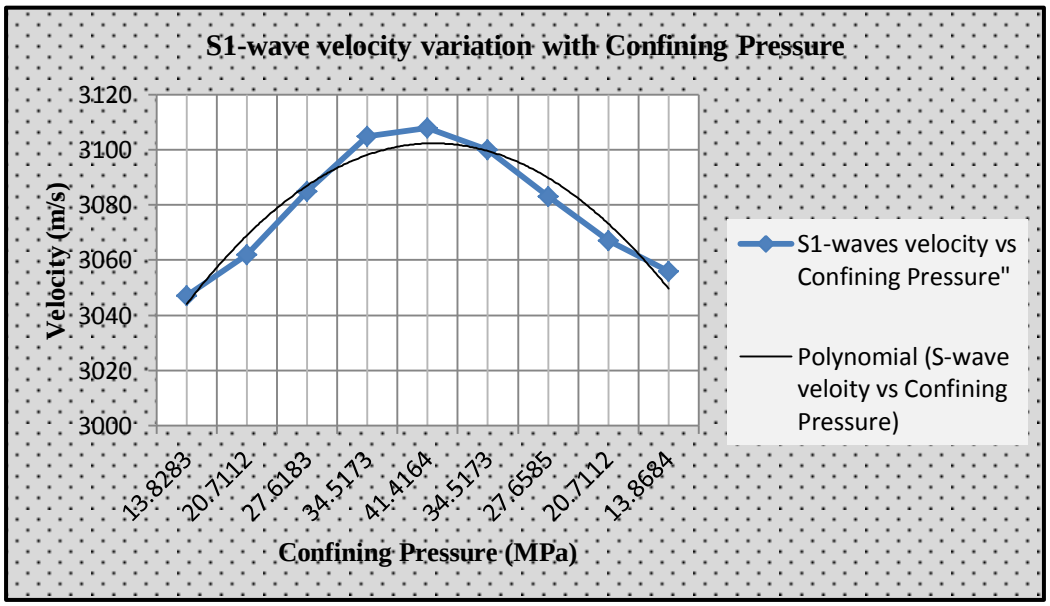

Figure 4.5: S_1-wave velocity variation with confining pressure

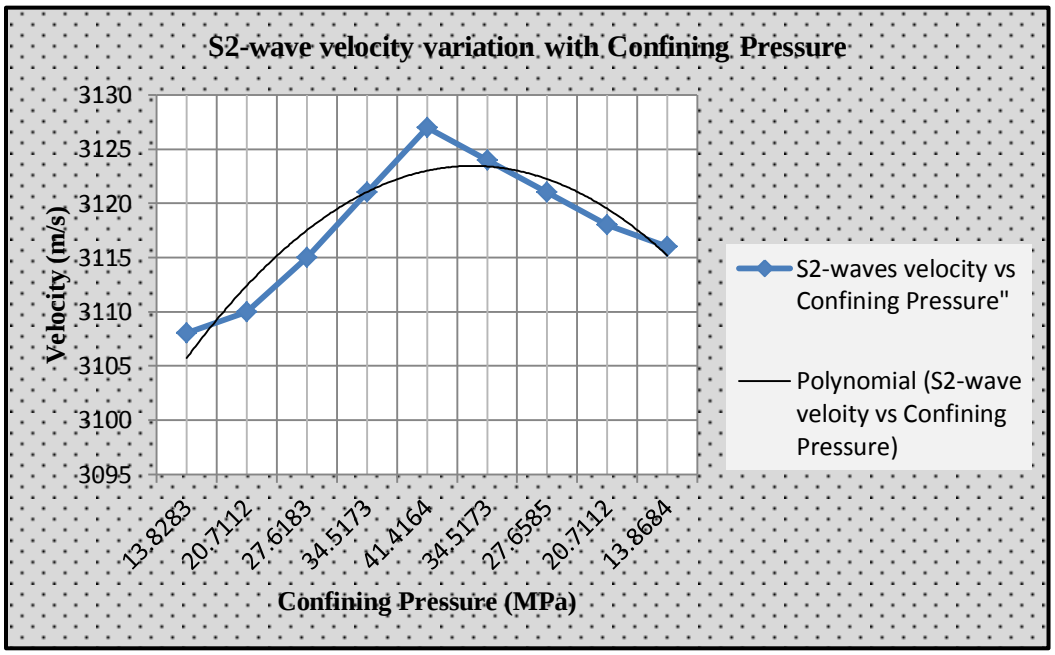

Figure 4.6: S_2-wave velocity variation with confining pressure

4.5 Uniaxial Compression Test (UCS)

The uniaxial compression tests were performed on 13 Qusaiba Shale samples (both vertical and horizontal) following the ASTM D 2938. Static elastic parameters i.e. Young's modulus and Poisson's ratio were derived from measured stress and strain values. The results of uniaxial compressive strength tests are shown below (Table 4.4). The stress versus axial strain and lateral strain relationships for the Plug '1' are illustrated in Figure 4.7. Stress strain plots are presented in the Appendix-G.

Table 4.4: Summary of Uniaxial Compressive Strength Test Results

Lithofacies	Plug No.	Young's Modulus (GPa)	Poisson's Ratio	UCS (MPa)	UCS (psi)	Cohesion (MPa)	Angle of friction (degree)
III	2	33.22	0.25	103.334	14983.43	30.952	22.977
	4	34.82	0.29	81.347	11795.315	31.639	22.817
	6	28.7	0.246	106.114	15386.53	24.069	21.896
	9	30.5	0.25	86.978	12611.81	23.381	22.312
	Average	32	0.25	94.4	13694	27	23
II	1	27.9	0.33	45.059	6533.555	26.822	22.177
	7	32.79	0.319	30.462	4416.99	23.381	21.975
	11	31.76	0.305	128.833	18680.785	27.51	22.614
	Average	31	0.32	68	9877	26	22
I	3	35.27	0.372	46.044	6676.38	27.51	22.614
	14	26.48	0.331	105.711	15328.095	33.016	23.908
	15	18.2	0.312	78.576	11393.52	24.069	22.177
	Average	26	0.34	77	11132	28	23

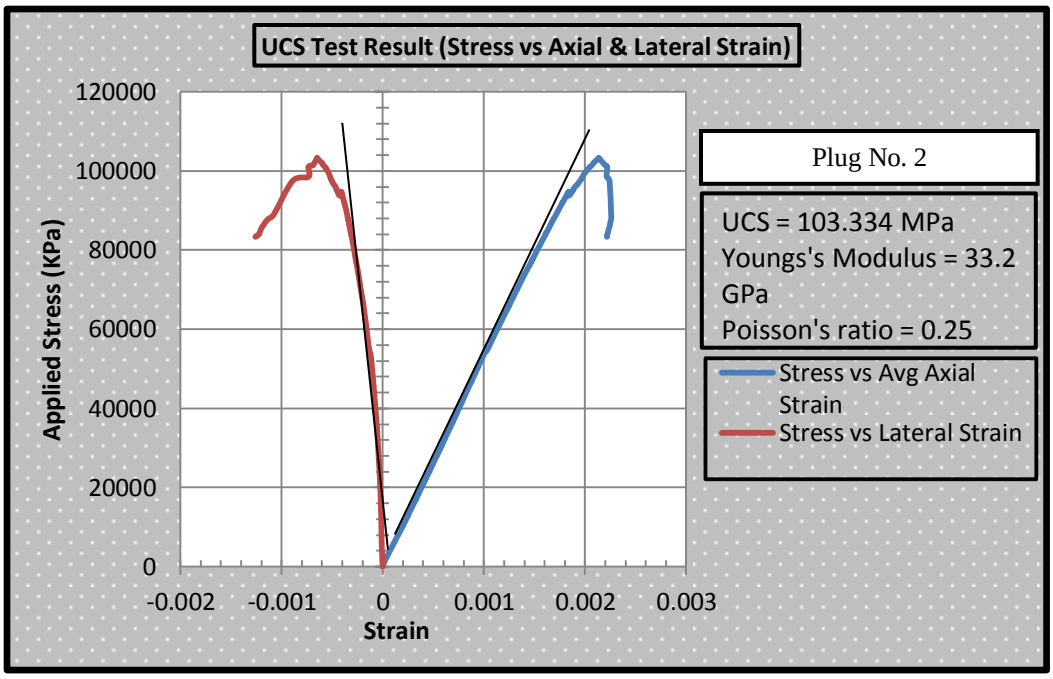

Figure 4.7: Stress vs Axial strain and Lateral strain

4.6 Correlations between Mechanical and Physical Parameters

The elastic and strength parameters of materials are closely related to their physical properties. On the basis of experimental and calibrated log values of elastic and strength parameters determined in this study, various relationships have been developed for the Qusaiba Shale. The parameters used for the correlations are density (ρ), P-wave and S-wave velocities (V_P and V_S), porosity (Φ), Dynamic Young's modulus (E_{dyn}), Dynamic Poisson's ratio (υ_{dyn}), Static Young's modulus (E_{stat}), Static Poisson's ratio (υ_{stat}), cohesion (c), frictional angle (ø), clay content, quartz feldspar mica (QFM) content, and UCS. These relationships will be useful for the further geomechanical studies of Qusaiba Shale and contribute to the understanding of the behavior of shale under stresses. The complete list of derived relationships are given in Table 4.5.

Table 4.5: Correlations between Mechanical and Physical parameters

Sr. No	Parameters	Correlations
1	E_{dyn} *and* E_{stat}	$E_{stat} = 0.9416*(E_{dyn})^{0.9501}$
2	υ_{stat} *and* υ_{dyn}	$\upsilon_{stat} = 0.405*(\upsilon_{dyn})^{0.2502}$
3	*UCS and* E_{dyn}	$UCS = 12.862*(E_{dyn})^{0.4539}$
4	*UCS and* E_{dyn}	$UCS = 1.4191*(E_{dyn})^{1.0354}$
5	E_{dyn} *and Density*	$E_{dyn} = 77.895*(\rho)^{-0.766}$
6	E_{stat} *and Density*	$E_{stat} = 350.76*(\rho)^{-2.543}$
7	*UCS and Density*	$UCS = 1782.7*(\rho)^{-3.235}$
8	E_{dyn} *and Porosity*	$E_{dyn} = 31.144*(\Phi)^{-0.053}$
9	*UCS and Cohesion*	$UCS = 21.055 \exp^{0.0464*(c)}$
10	E_{stat} *and Cohesion*	$E_{stat} = 1.201*(c)^{0.9648}$
11	E_{dyn} *and Cohesion*	$E_{dyn} = 3.2531*(c)^{0.7353}$
12	E_{stat} *and Frictional Angle*	$E_{stat} = 6e\text{-}05*(\text{ø})^{4.1866}$
13	E_{dyn} *and Frictional Angle*	$E_{dyn} = 6E\text{-}05*(\text{ø})^{4.3039}$
14	*UCS and Frictional Angle*	$UCS = 0.0435 \exp^{0.3302*(\text{ø})}$
15	E_{stat} *and Clay Content*	$E_{stat} = 18.441*((W/W)_{CLAY})^{-0.663}$
16	E_{dyn} *and Clay Content*	$E_{dyn} = 28.099*((W/W)_{CLAY})^{-0.396}$
17	*UCS and Clay Content*	$UCS = 185.3 \exp^{-1.753*((W/W)_{CLAY}}$
18	E_{stat} *and QFM Content*	$E_{stat} = 49.4*((W/W)_{QFM})^{0.6739}$
19	E_{dyn} *and QFM Content*	$E_{dyn} = 49.896*((W/W)_{QFM})^{0.3849}$
20	*UCS and QFM Content*	$UCS = 32.186 \exp^{1.8119*((W/W)_{QFM})}$
21	E_{stat} *and P-wave velocity*	$E_{stat} = 0.9316*(V_P)^{2.3674}$
22	E_{dyn} *and P-wave velocity*	$E_{dyn} = 1.0292*(V_P)^{2.464}$
23	*UCS and P-wave velocity*	$UCS = 1.1302 \exp^{0.9806*(V_P)}$

These correlations can be used for estimating the elastic mechanical and failure parameters from physical properties in case of missing data. The graphical representations of these relationships are illustrated in figures 4.8 to 4.28. The mechanical parameters exhibit relationships, either increasing or decreasing trends, with physical and other mechanical parameters. However, some correlations (Figure 4.9, 4.12, 4.13, 4.14, 4.16, 4.23, and 4.26) are poor indicating variability in experimental results. High variability may be due to the small scale heterogeneity in shale or due to errors in measurements (instrumental or human).

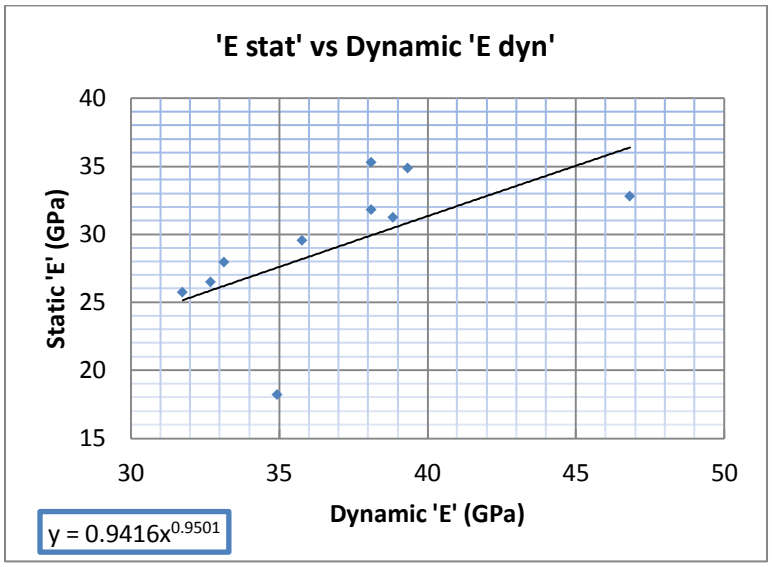

Figure 4.8: Static vs Dynamic Young's Modulus

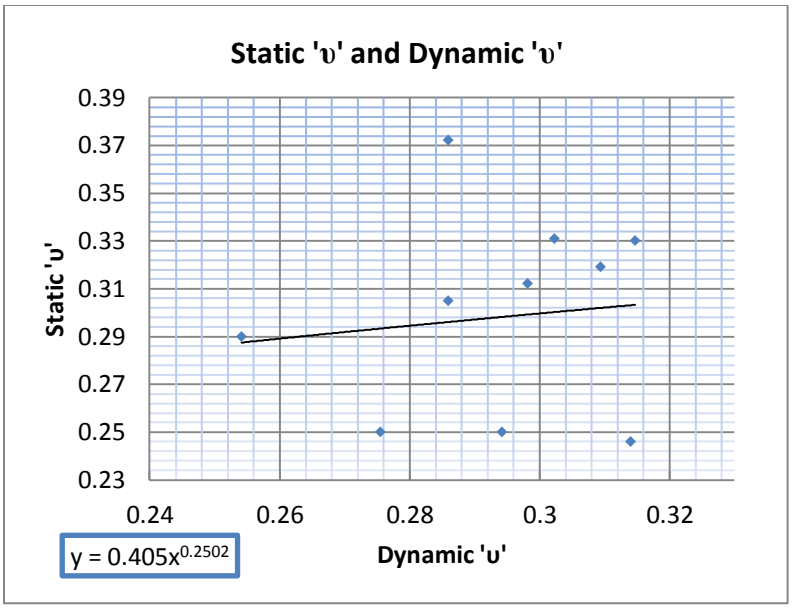

Figure 4.9: Static vs Dynamic Poisson's ratio

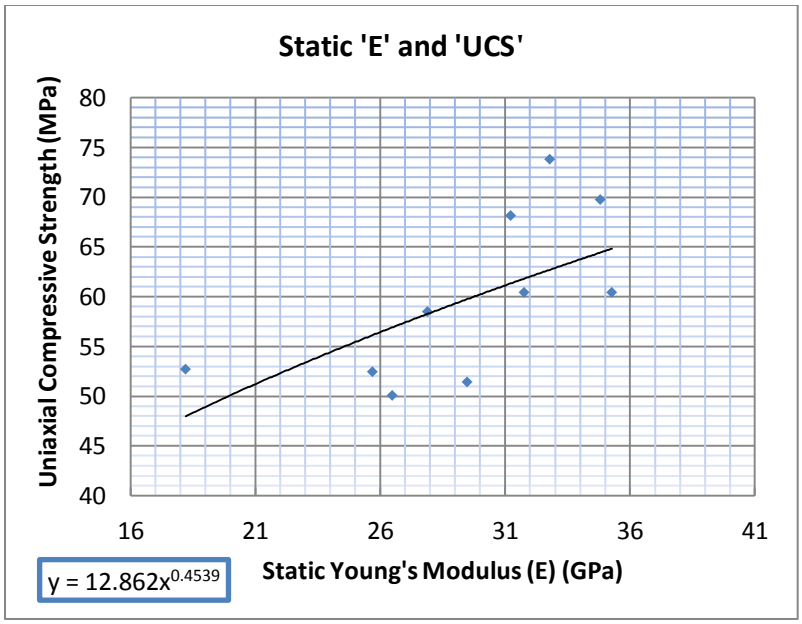

Figure 4.10: Uniaxial Compressive Strength (UCS) vs Static Young's Modulus

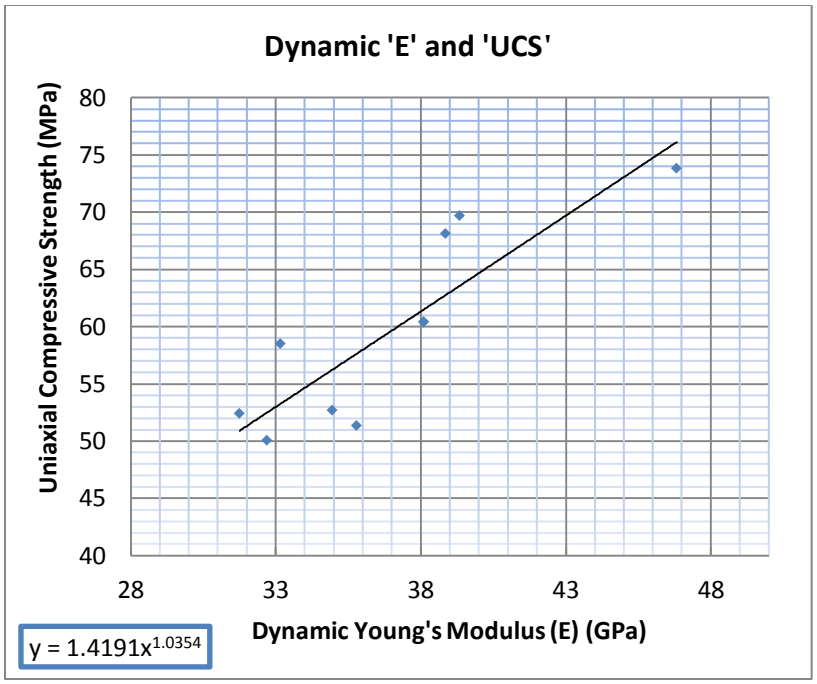

Figure 4.11: Uniaxial Compressive Strength (UCS) vs Dynamic Young's Modulus

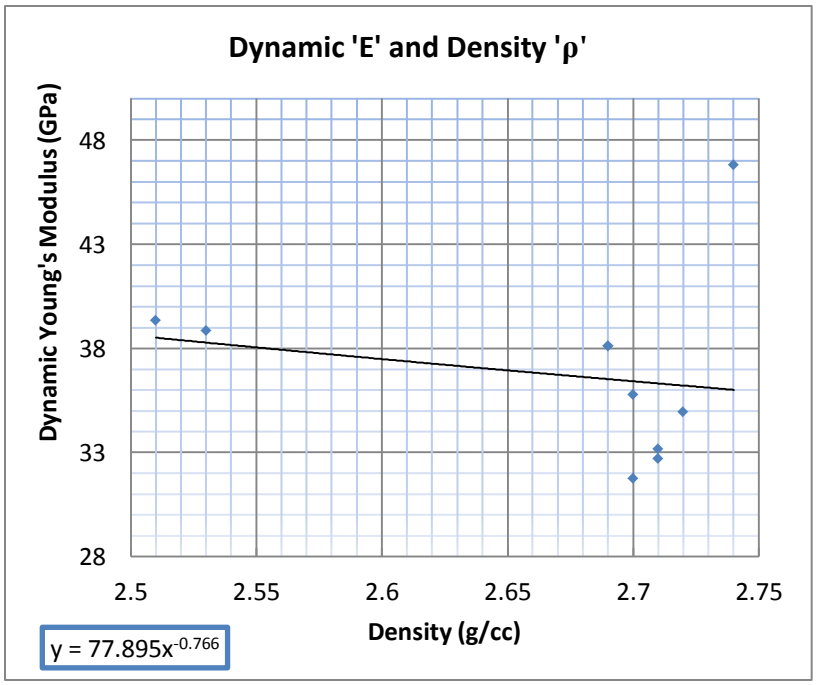

Figure 4.12: Dynamic Young's Modulus vs Density

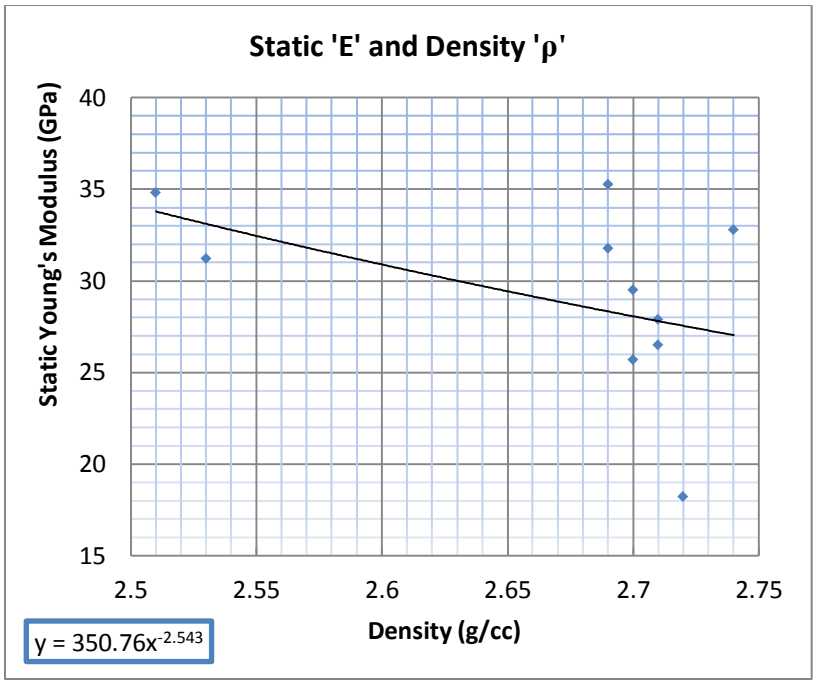

Figure 4.13: Static Young's Modulus vs Density

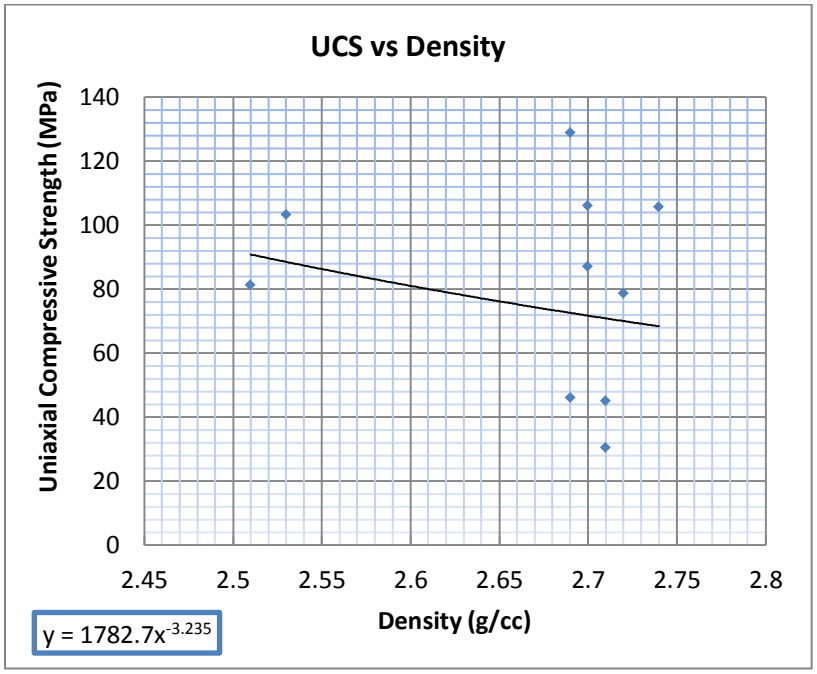

Figure 4.14: Uniaxial Compressive Strength vs Density

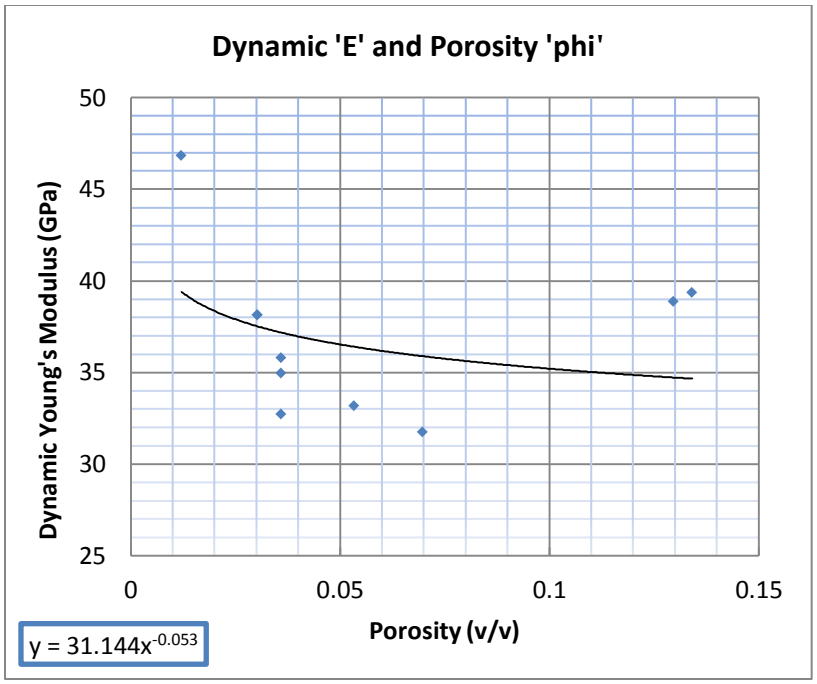

Figure 4.15: Dynamic Young's Modulus vs Porosity

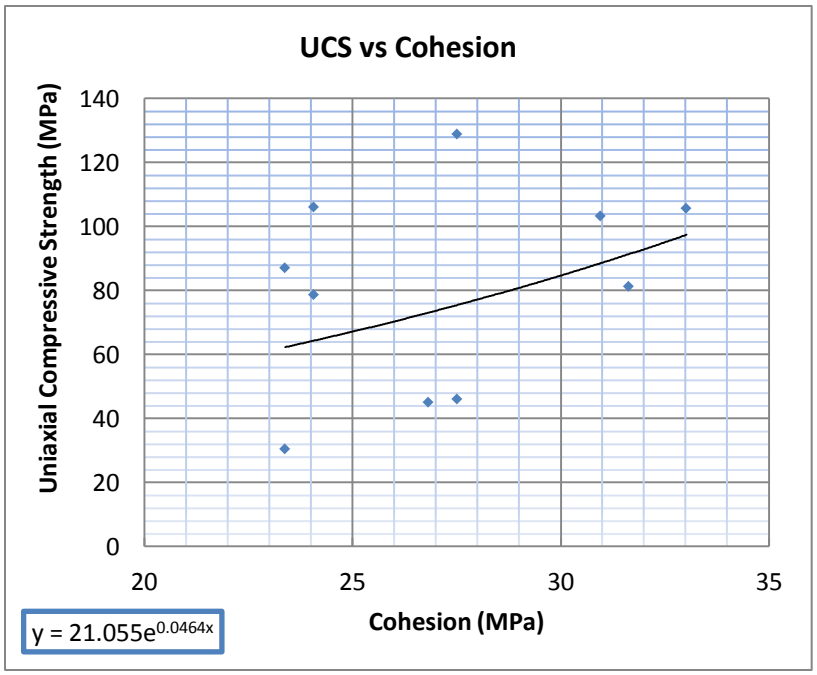

Figure 4.16: Unaxial Compressive Strength vs Cohesion

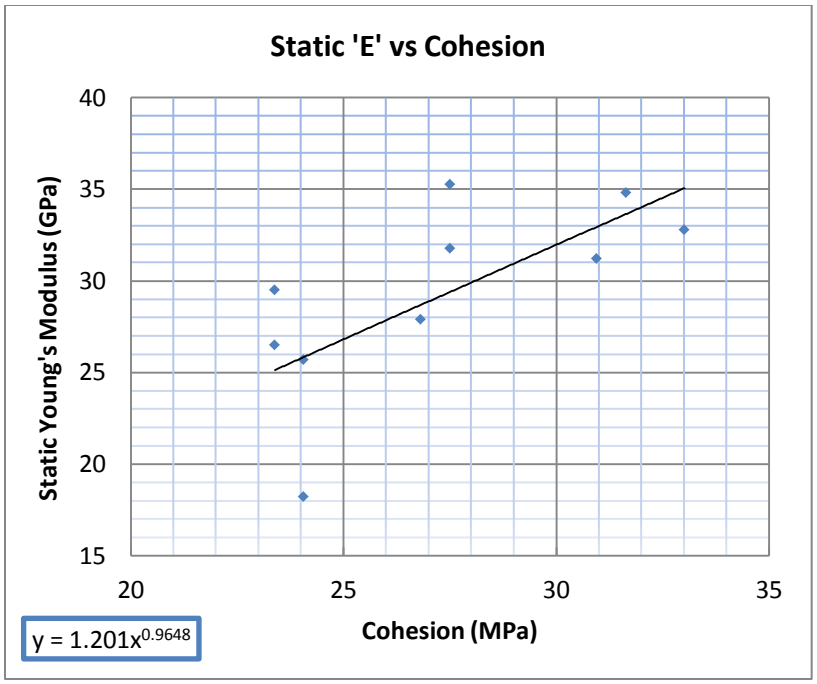

Figure 4.17: Static Young's Modulus vs Cohesion

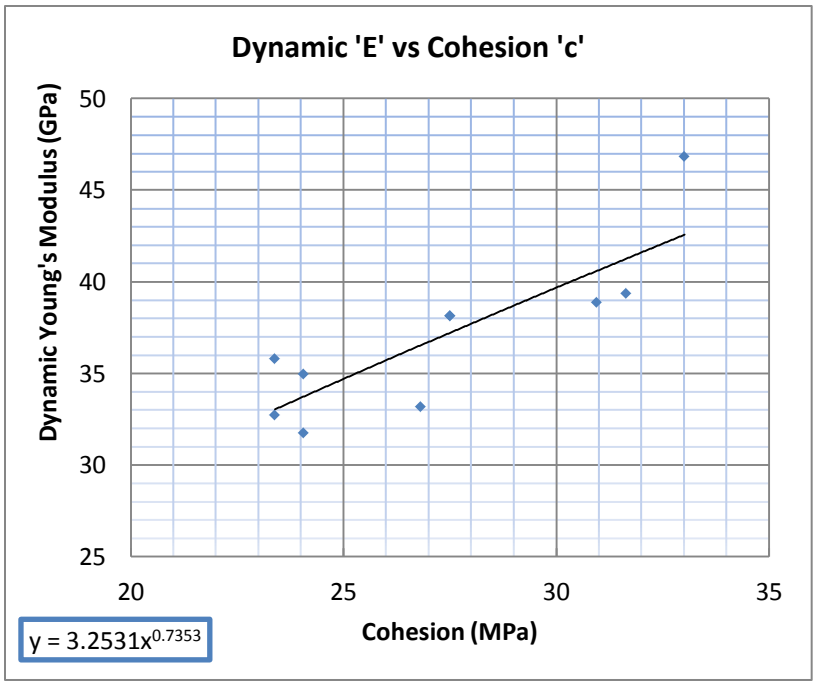

Figure 4.18: Dynamic Young's Modulus vs Cohesion

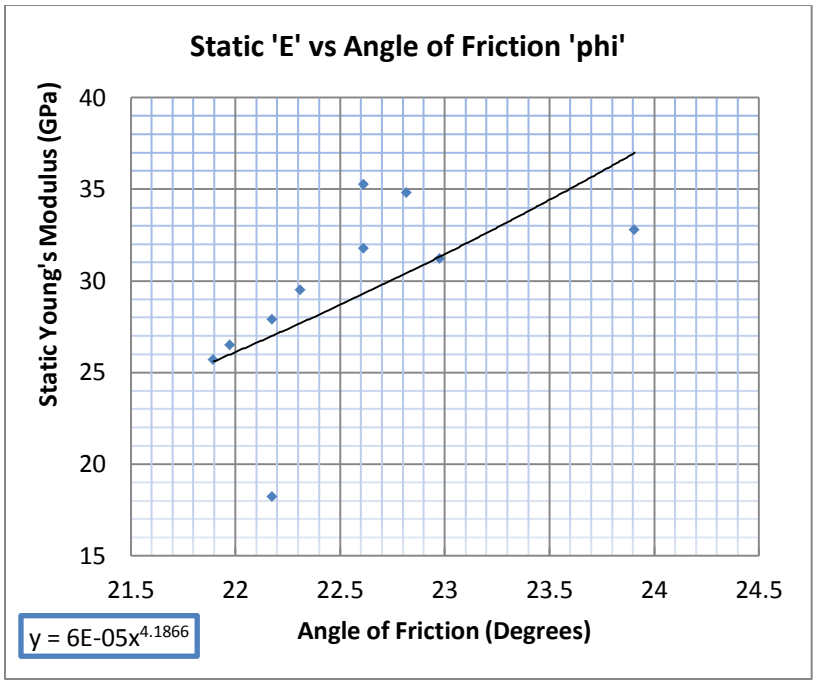

Figure 4.19: Static Young's Modulus vs Angle of Friction

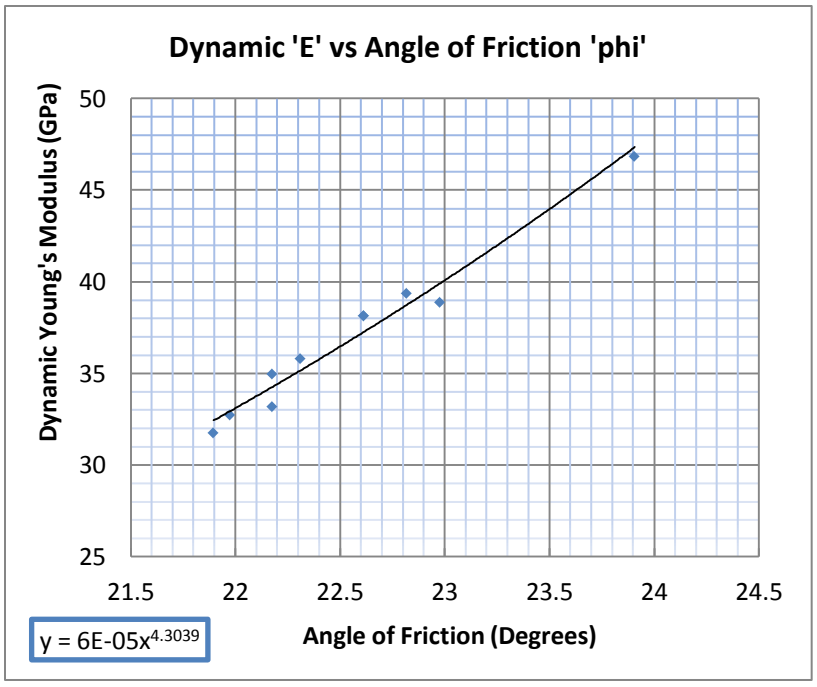

Figure 4.20: Dynamic Young's Modulus vs Angle of Friction

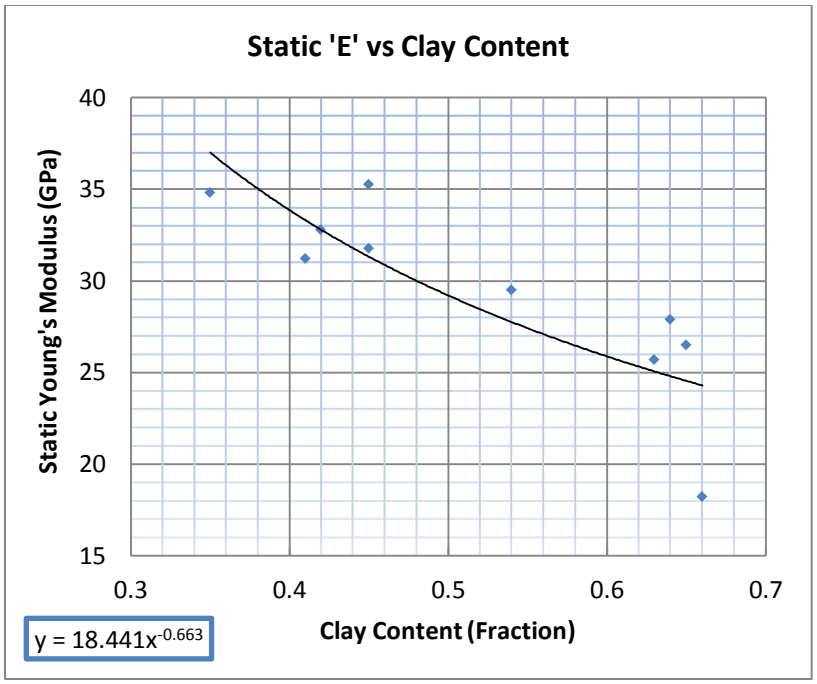

Figure 4.21: Static Young's Modulus vs Clay Content

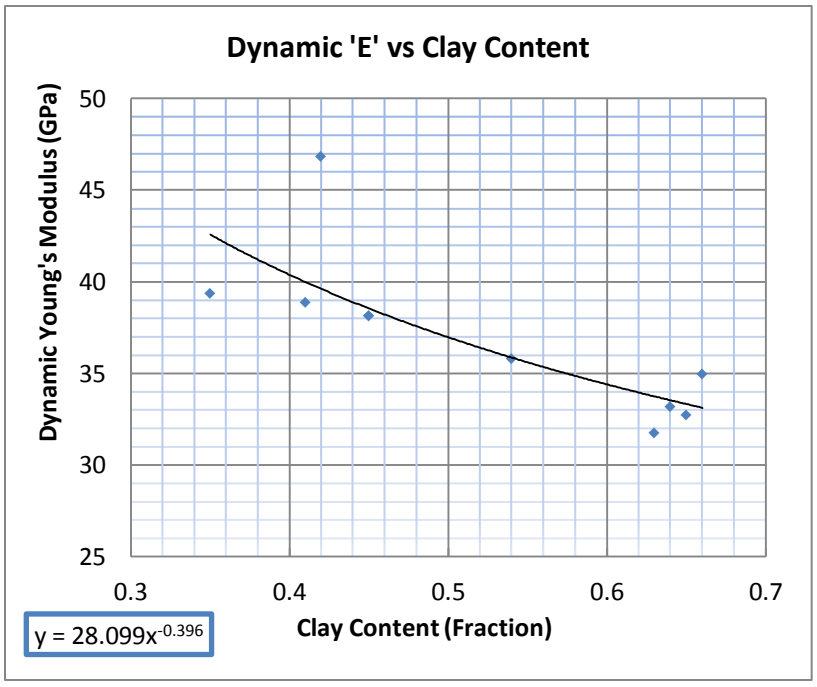

Figure 4.22: Dynamic Young's Modulus vs Clay Content

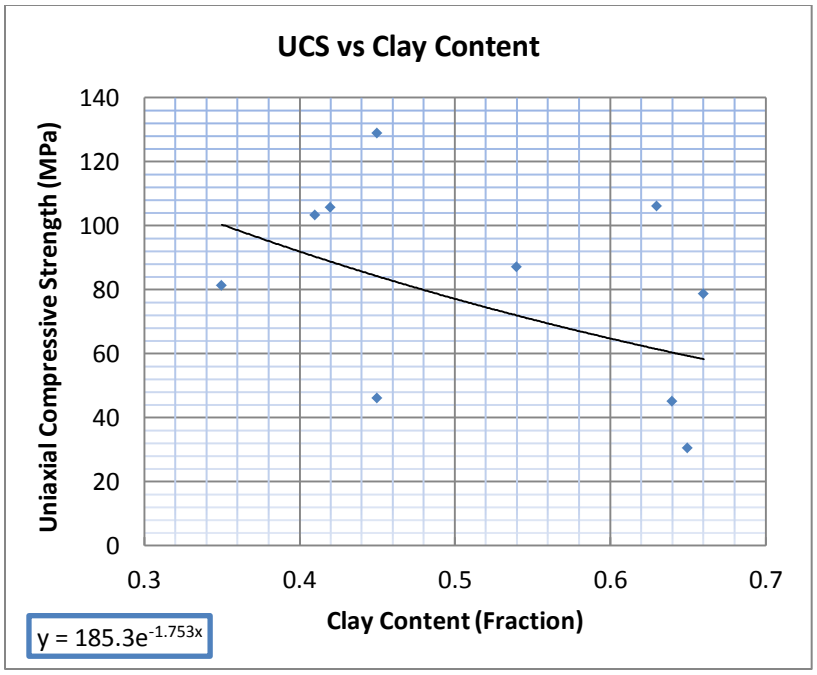

Figure 4.23: Uniaxial Compressive Strength vs Clay Content

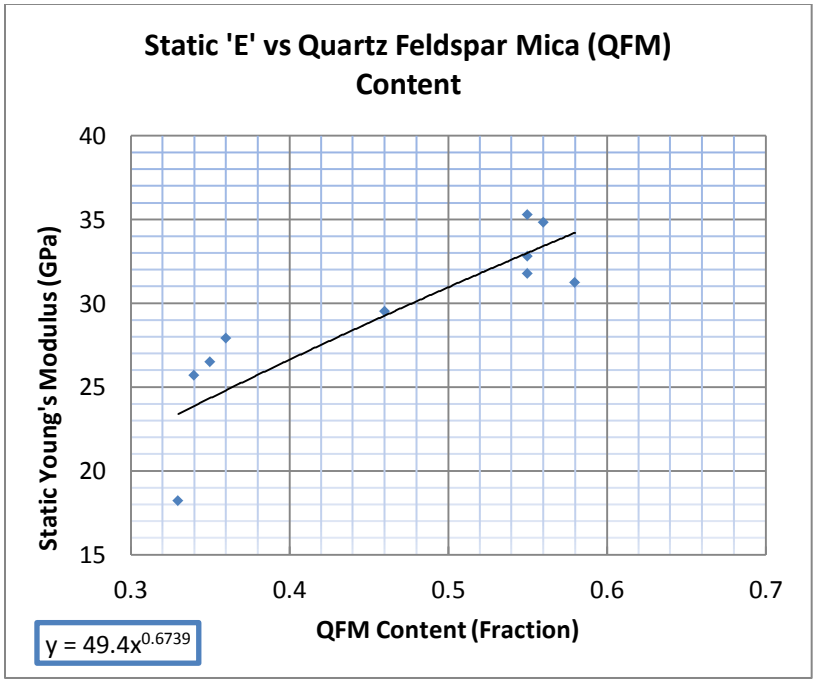

Figure 4.24: Static Young's Modulus vs Quartz Feldspar Mica Content

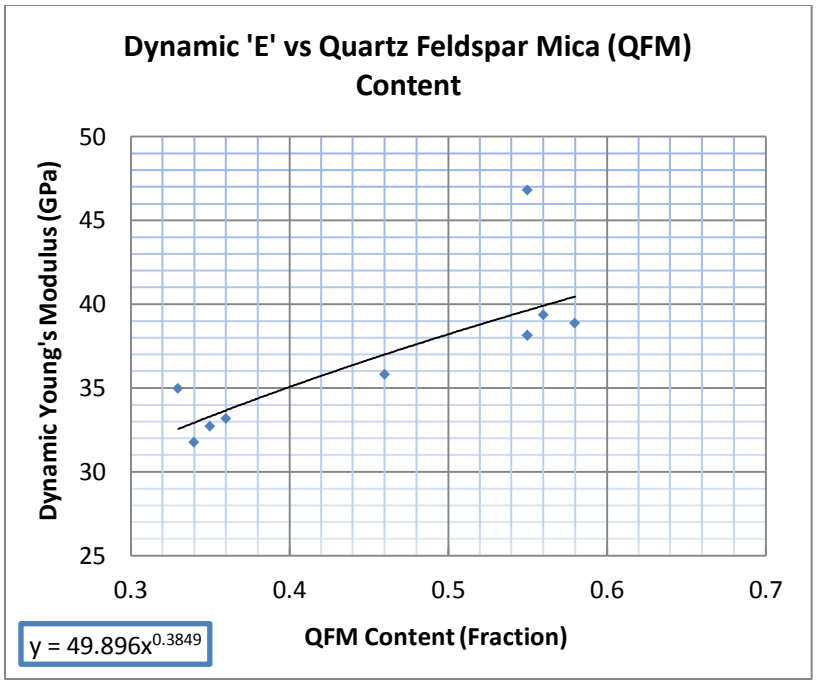

Figure 4.25: Dynamic Young's Modulus vs Quartz Feldspar Mica Content

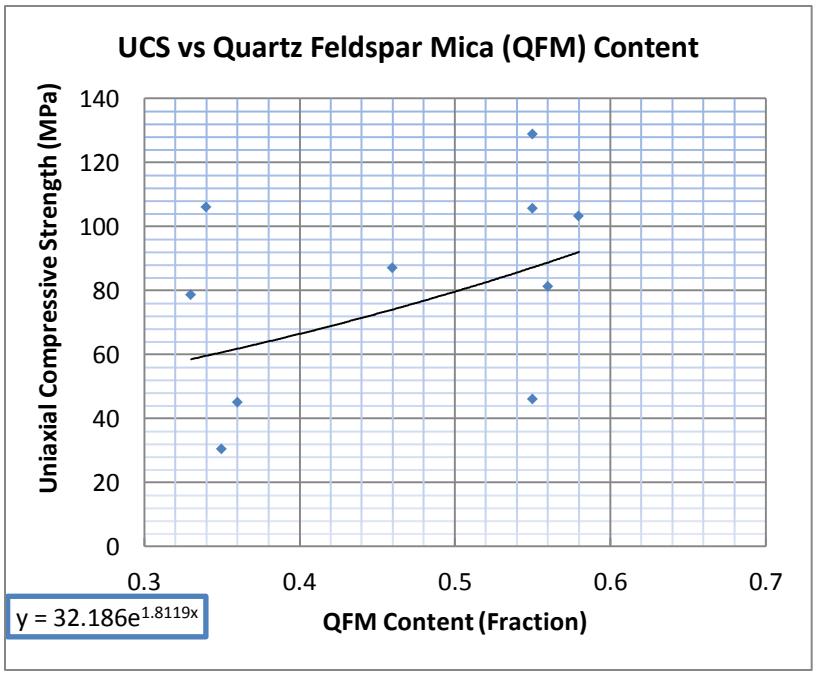

Figure 4.26: Uniaxial Compressive Strength vs Quartz Feldspar Mica Content

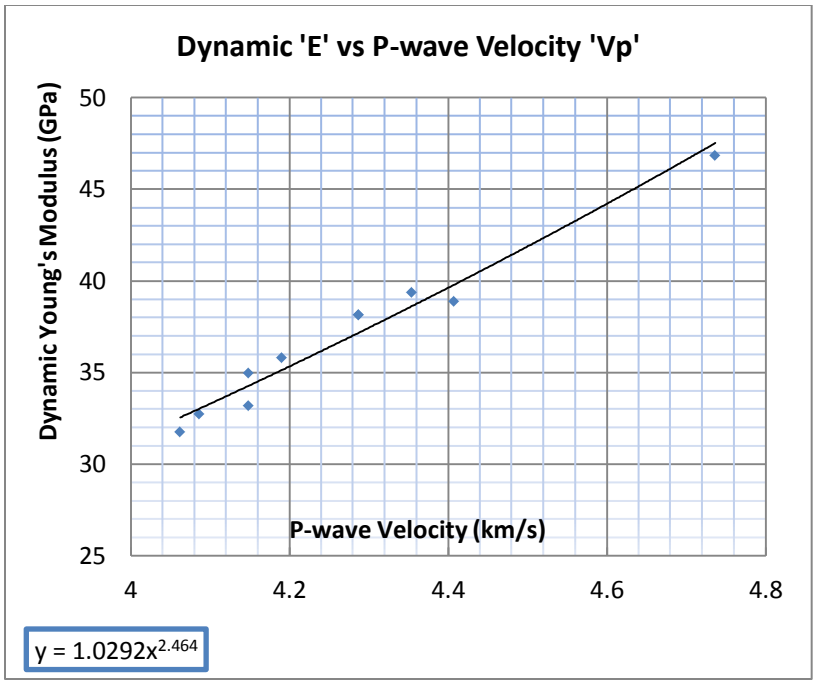

Figure 4.27: Dynamic Young's Modulus vs P-wave Velocity

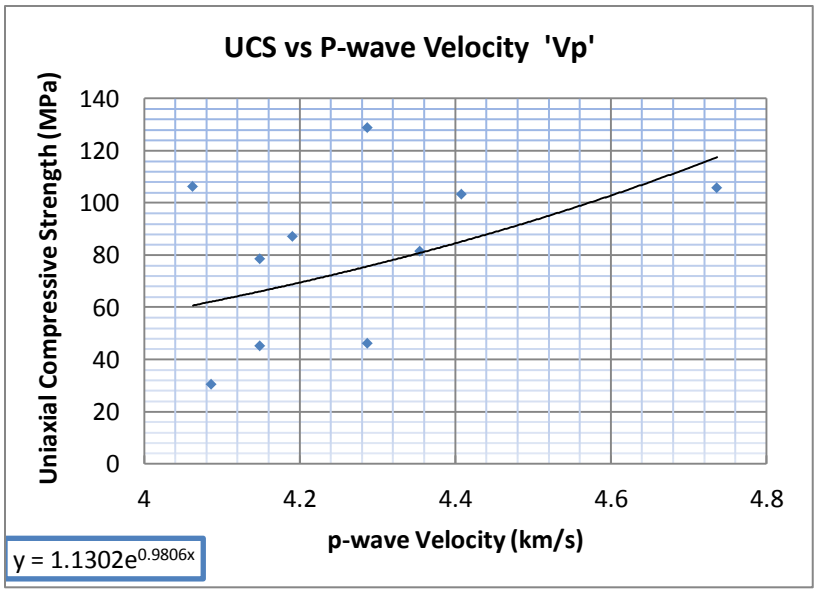

Figure 4.28: Uniaxial Compressive Strength vs P-wave Velocity

4.7 1-D Mechanical Earth Model (1-D MEM)

The mechanical earth model (MEM) is a set of data about the formation. It is used to make rock mechanical predictions. It should be noted that this model related to the earth, not to the trajectory of a well. It can be 1D, 2D, 3D, or 4D and its complexity is determined by: (1) available data, (2) purpose (3) complexity of structure and properties. The MEM needs to be complex enough to provide a useful representation of the geomechanics in the field, but simple enough to populate easily and access quickly.

Mechanical earth model is used to provide the economical and efficient solution for various problems such as wellbore instability, sand production and hydraulic fracture stimulation.

The steps involved in preparing the mechanical earth model are illustrated in sequence below.

Step 1: Data Auditing, Sample Preparation, and Depth Correction

First of all, samples were collected and prepare for the tests. The sample preparation process has already been discussed in the Section 4.3.

After sample preparation, log depths corrections were performed as illustrated in Appendix-F. As our borehole is vertical, so correction can be done by simple shift as given in Eq. (4.1).

$$D_{corrected} = D_{actual} + 2.17 \quad (4.1)$$

Step 2: Static to Dynamic Elastic Parameters Calibration

After depth corrections, samples were tested in laboratory in order to determine the static elastic parameters and failure parameters. After testing, laboratory results (static elastic parameters) were correlated with log data (dynamic elastic parameters, Young's modulus and Poisson's ratio) for core-log calibration. The calibrated results were used to determine the further geomechanics parameters. The calibrated values are given below in Figure 4.29 and Figure 4.30.

Note: Dynamic elastic parameters were calculated from sonic log (P and S-waves velocity) and density log data using equation (4.2) and (4.3) (Fjaer et al., 2008).

$$\nu_{dyn} = \frac{\left[\left\{2-\left(\frac{\Delta Ts}{\Delta Tp}\right)\right\}\right]}{\left[\left\{2-2\left(\frac{\Delta Ts}{\Delta Tp}\right)2\right\}\right]} \tag{4.2}$$

$$E_{dyn} = 2\left[1+\nu_{dyn}\right].\left[\rho_b.1000\right].\left(\frac{0.3048}{\Delta Ts}\right)^2.1000 \tag{4.3}$$

Static mechanical parameters were determined using the graphs obtained after performing uniaxial compressive strength tests.

Step 3: Failure Parameters Determination

The failure parameters (Cohesion 'c' and angle of friction 'Φ') were obtained from the established relation given by Lal and Amoco, (1999) specifically for shale formation using sonic log data.

$$Angle\ of\ friction = \text{'}\Phi\text{'} = Sin^{-1}\left[\frac{(Vp-1)}{(Vp+1)}\right] \tag{4.4}$$

$$Cohesion = c = \left[UCS * \frac{(1-Sin\,\Phi)}{2Cos\,\Phi}\right] \quad (4.5)$$

Where angle of friction 'Φ' is in degrees and cohesions 'c' and UCS in MPa, V_P in km/s. The cohesion has been calculated using laboratory data (UCS and angle of friction). The cohesion values were then calibrated with porosity data in order to attain values for entire log run as shown below in Figure 4.31. For the entire well log depth, uniaxial compressive strength (UCS) was determined using the following geometrical relation.

$$\text{UCS } (C_O) = \frac{2c}{[Cos\Phi - (1-Sin\Phi)tan\Phi]} \quad (4.6)$$

The geometrically determined UCS was then calibrated with experimental values of UCS by plotting the graph between UCS of same depths. A relationship was obtained from the correlation of UCS values.

$$UCS_{measured} = 0.706UCS_{Calculated} + 2.1343 \quad (4.7)$$

The calibrated values were then plotted with depth as shown in Figure 4.32. The tensile strength was determined by dividing uniaxial compressive strength by 8 (Fjaer et al., 2008). The graphs showing variations of failure parameters (cohesion, friction, UCS, and tensile strength) with depth are given below (Figures 4.32-4.34).

Step 4: In-Situ Stress Determination

The vertical overburden stress was calculated by integrating density logs.

$$\sigma_z = \int \rho\,(z).g.dz \quad (4.8)$$

Where σ_z is overburden stress, ρ is formation density, and g is the gravitational acceleration. Vertical stress profile is shown in Figure 4.35.

Pore pressure is very important in MEM preparation and needed for determining the horizontal stresses and effective vertical stresses. Sonic log data were used to estimate the pore pressures in shale formation.

Most commonly used Eaton approach (Mouchet and Mitchell, 1989) was applied to estimate the pore pressure using sonic data as illustrated in Figure 4.38. Trendline was drawn using sonic log values for particular depth values (XX750 to XX150). Pore pressure profile is illustrated in Figure 4.38.

Eaton Equation for Pore pressure determination is given as:

$$P = \sigma_v - \left(\sigma_v - P_{hyd}\right)\left(\frac{\Delta T_n}{\Delta T_{log}}\right)^{3.0} \quad (4.9)$$

Where; P = Pore pressure, σ_v = Overburden, ΔT_n = Sonic transit time (μs/ft), ΔT_{log} = Sonic log observed values, P_{hyd} = Normal hydrostatic pressure

On the basis of the hydraulic fracturing and extended leak-off tests data, the reverse stress regime has been reported for Qusaiba Shale in the study area (Al-Jalal et al. 2011). The fracturing gradient is 1.08 psi/ft. The minimum horizontal and maximum horizontal stress gradients have been used according to reverse stress regime i.e. 1.12 and 1.18 psi/ft, respectively.

$$\sigma_h = 1.12\ psi/ft \quad (4.10)$$

$$\sigma_H = 1.18\ psi/ft \quad (4.11)$$

In-situ stresses magnitude and directions are essential in order to assess the hydraulic fractures orientation. Stresses profiles are illustrated in figures 4.35 to 4.37.

Step 5: Determination of Stable Drilling Direction

After stress determination, most stable drilling direction was determined for wellbore on the basis of stress concentration around the wellbore. Tangential stresses were determined for all three possible wellbore directions i.e. vertical, as well as minimum and maximum horizontal stress directions. Tangential stress exhibited lowest stress concentration around the wellbore in case of wellbore along maximum horizontal stress direction. For this direction, lesser drilling stability problems will be encountered.

Tangential stress along vertical = $\sigma_\theta = 3\sigma_H - \sigma_h$

Tangential stress along minimum horizontal stress = $\sigma_\theta = 3\sigma_H - \sigma_V$

Tangential stress along maximum horizontal stress = $\sigma_\theta = 3\sigma_V - \sigma_H$

The most stable direction for drilling, based on tangential stresses, was found to be vertical indicating minimum problems during drilling operations in this direction.

Step 6: Safe Mud Weight Window

One of the most important applications of the MEM is to define the safe mud weight to avoid any serious problem during drilling. Keeping in mind the four limits (two upper and two lower) for safe drilling operation, safe mud weight windows were determined (Figure 4.39). Four limits for mud weight (Fjaer et al., 2008) are defined as:

1) 1st Upper limit to avoid borehole collapse. Mud weight should be less than this limit to avoid shear failure or collapse that cause stuck pipe, tight hole etc. problems.

$$P_w \leq \frac{1}{tan^2\beta+1}\left[(3\sigma_h - \sigma_H)tan^2\beta - \alpha P_f(tan^2\beta - 1) + C_o\right] \quad (4.12)$$

2) 2nd Upper limit to avoid induced fractures. Mud weight should be less than this limit to avoid fractures that cause loss circulation.

$$P_w \leq 3\sigma_h - \sigma_H - T_o + P_p \quad (4.13)$$

3) 1st Lower limit to avoid borehole collapse. Mud weight should be higher than this limit to avoid shear failure or collapse that cause stuck pipe, tight hole etc. problems.

$$P_w \geq \frac{1}{tan^2\beta+1}\left[(3\sigma_H - \sigma_h) + \alpha P_f(tan^2\beta - 1) - C_o\right] \quad (4.14)$$

4) 2nd Lower limit is formation pressure. Mud weight should be higher than formation pressure in order to avoid kick or blowout problems.

Note: In addition to above mentioned limits, our mud weight should also less than fracture gradient to avoid the reopening of already existing natural fractures. Fracture gradient is normally taken as equal to minimum horizontal stress.

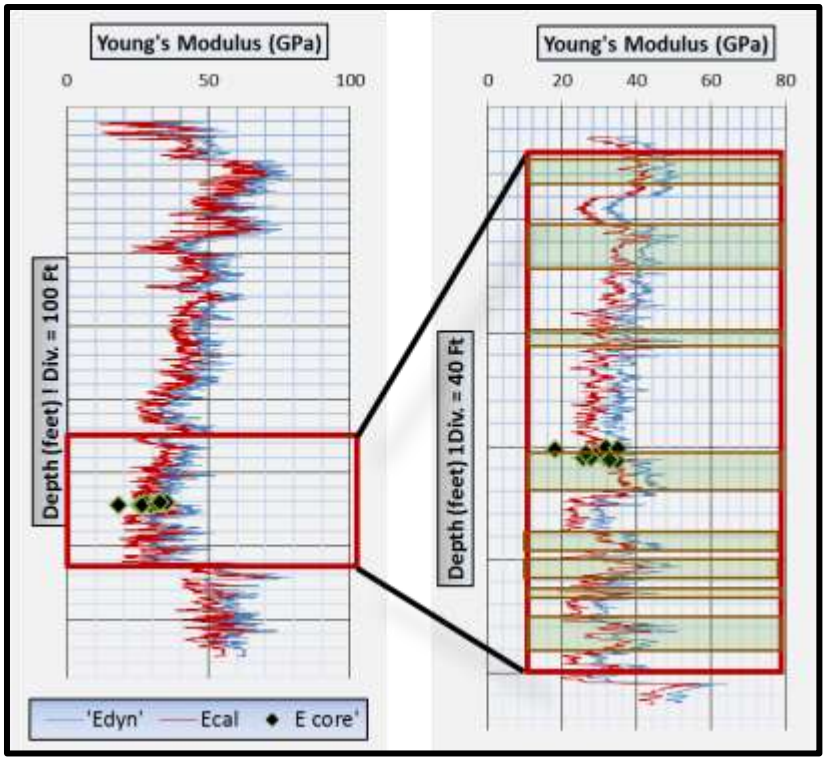

Figure 4.29: Young's Modulus profile

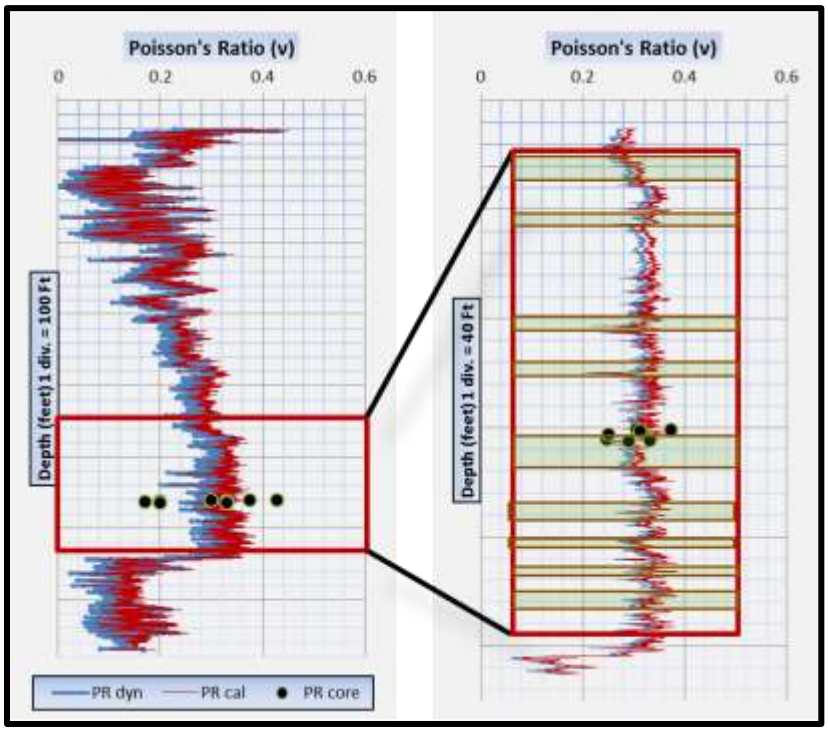

Figure 4.30: Poisson's ratio profile

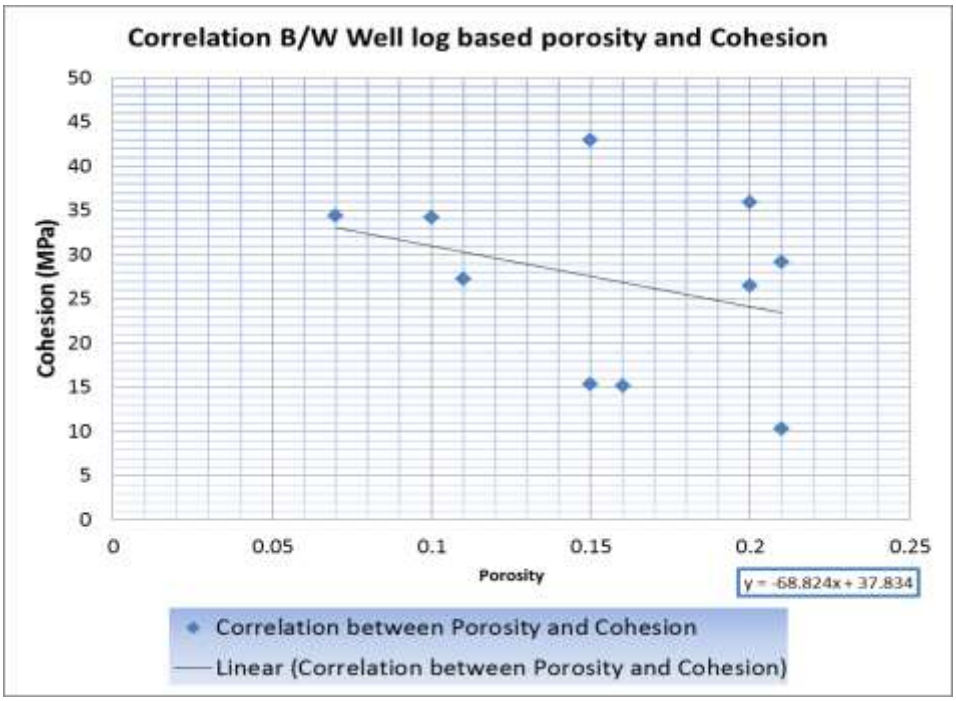

Figure 4.31: Correlation between well log based porosity and Cohesion

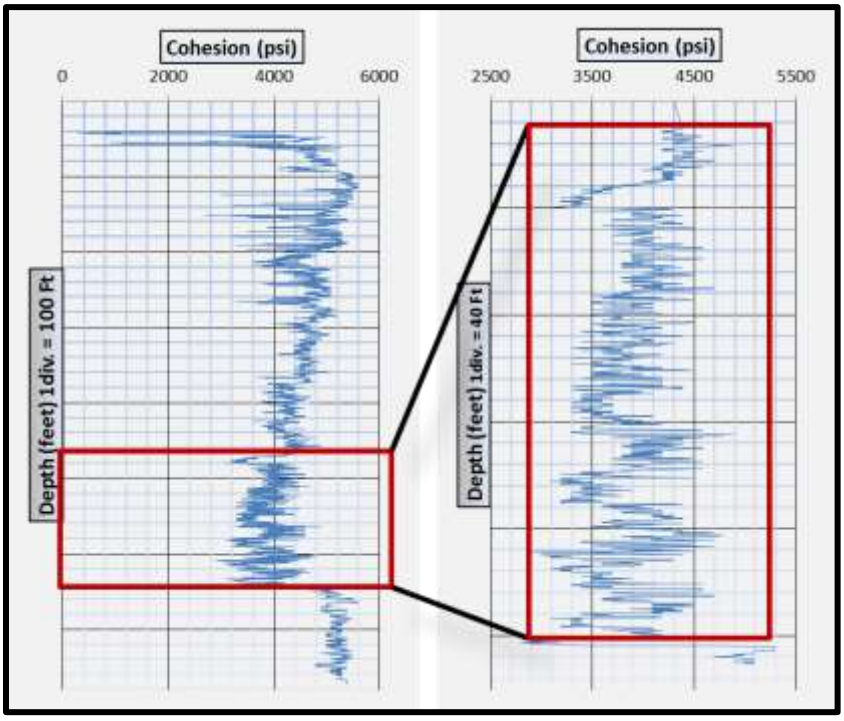

Figure 4.32: Cohesion Profile

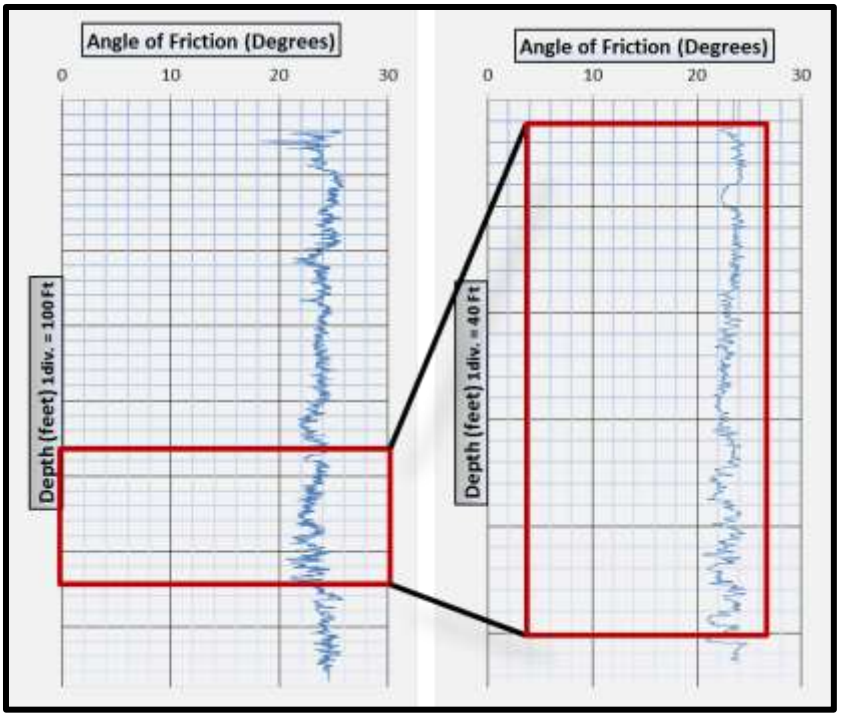

Figure 4.33: Angle of Friction profile

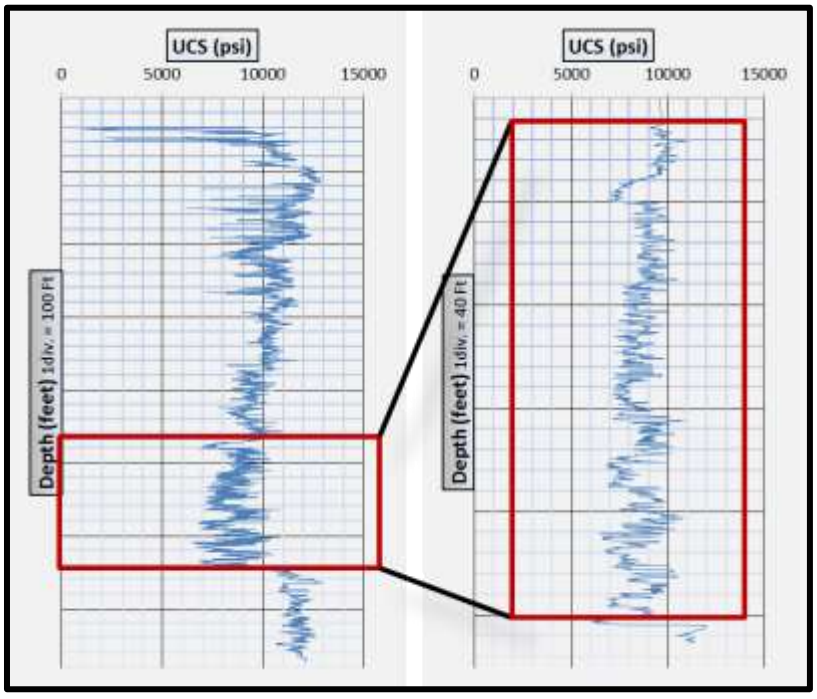

Figure 4.34: Uniaxial Compressive Strength profile

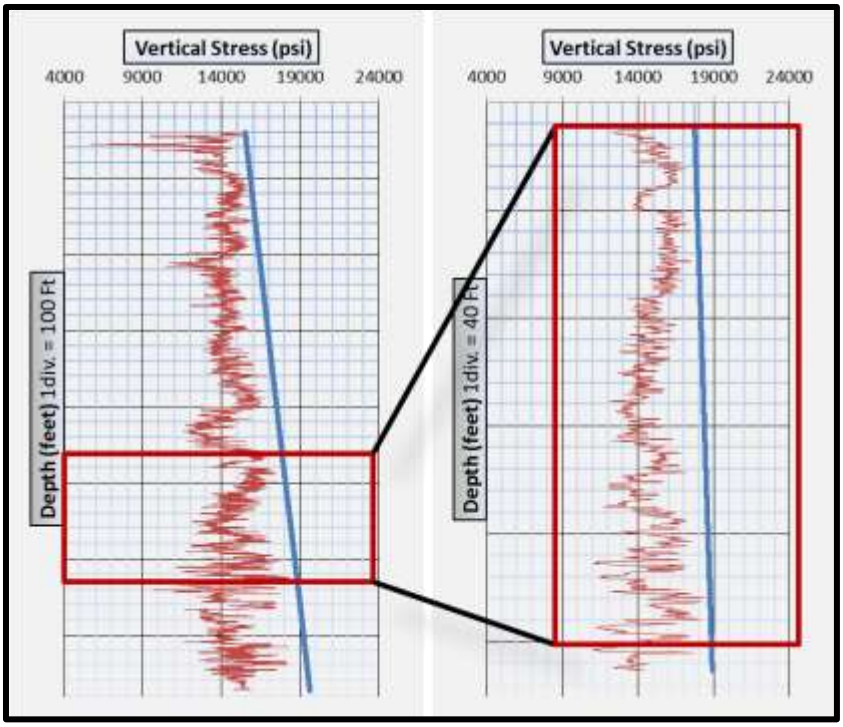

Figure 4.35: Total and effective vertical stress profiles

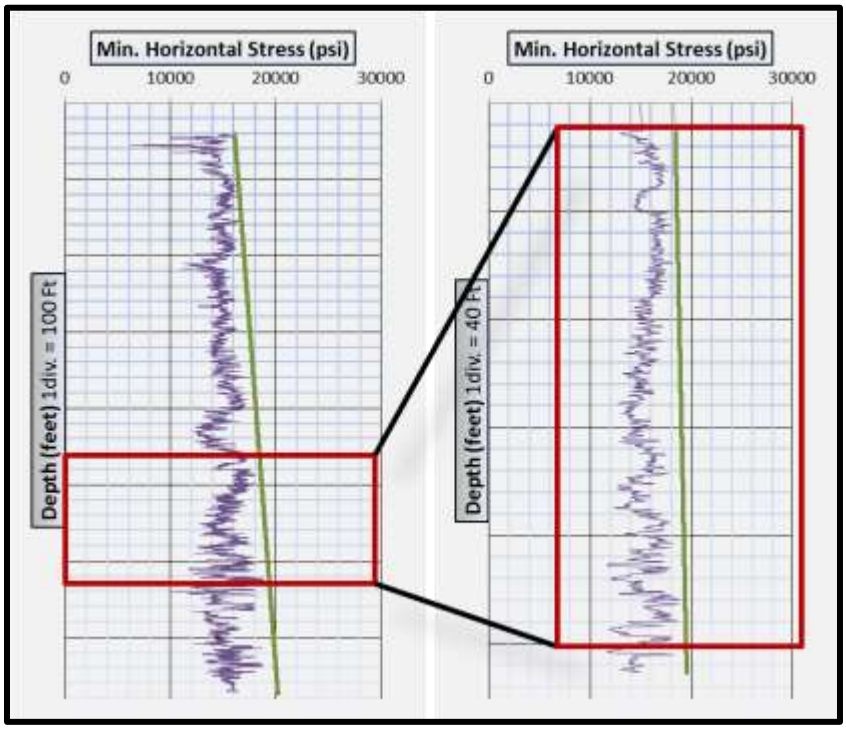

Figure 4.36: Total and effective minimum horizontal stress

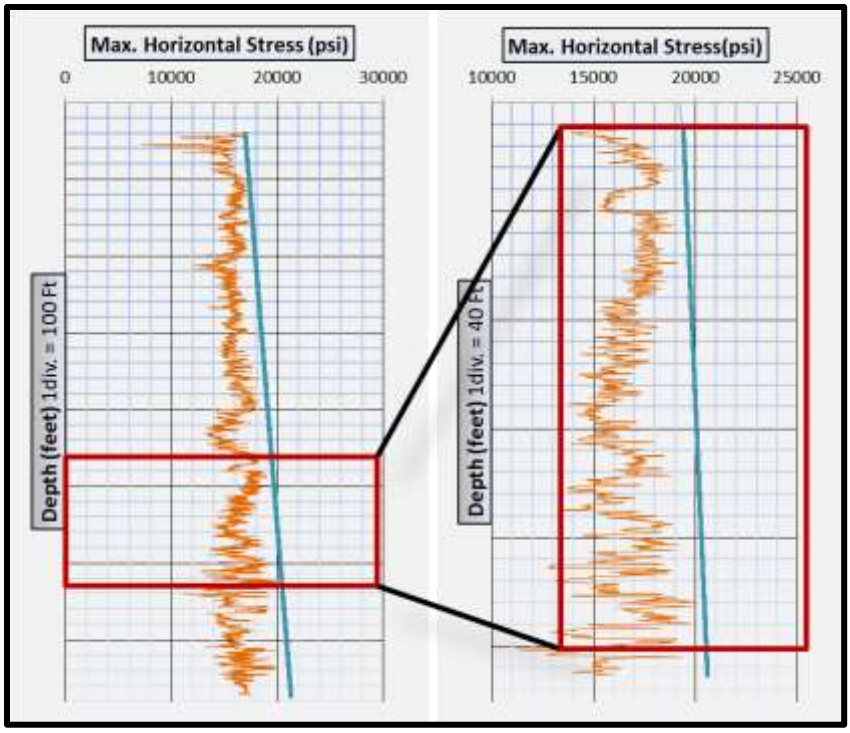

Figure 4.37: Total and effective maximum horizontal stress profile

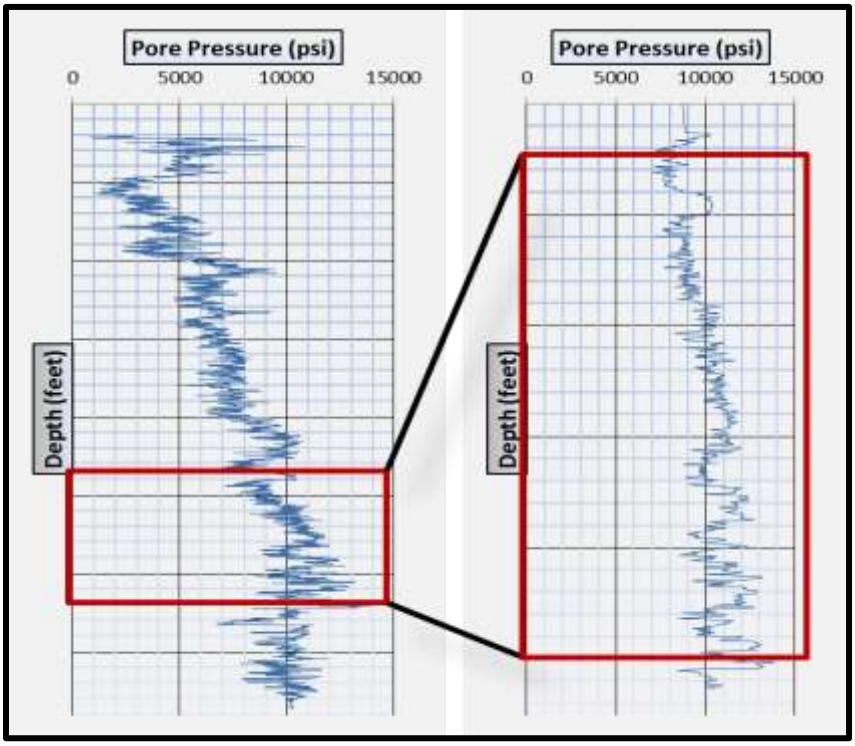

Figure 4.38: Pore pressure profile

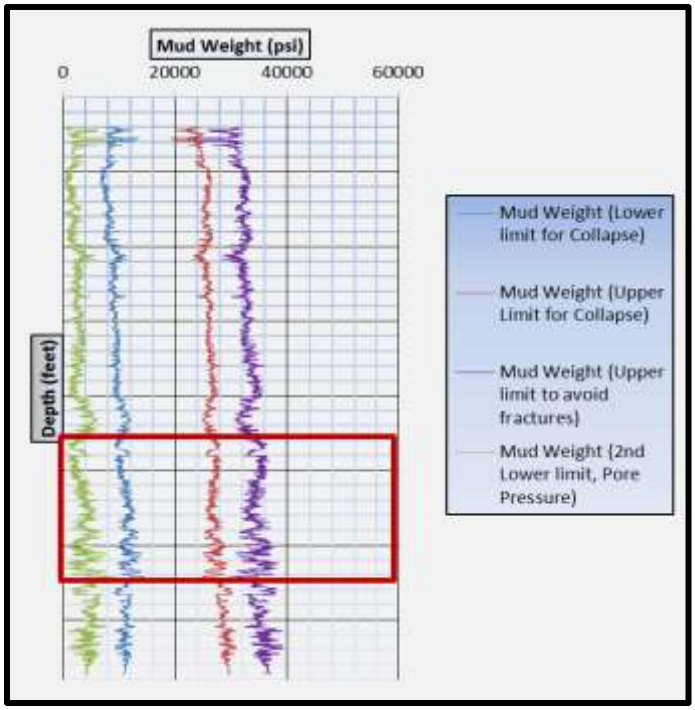

Figure 4.39: Mud weight window for safe drilling operations

4.8 Brittleness Determination

Brittleness is mainly controlled by the mineralogy. Brittleness in shales can be estimated on the basis of mineralogy (clay and quartz contents) (Wang, 2008). In this thesis, a new approach proposed by Rickman et al., (2008), has been implemented for brittleness estimation. This approach is based on elastic mechanical parameters i.e. Young's modulus and Poisson's ratio. Higher values of Young's modulus and lower values of Poisson's ratio reflect the brittle behavior of rock as illustrated for the Barnett Shale in Figure 4.40 (Rickman et al., 2008).

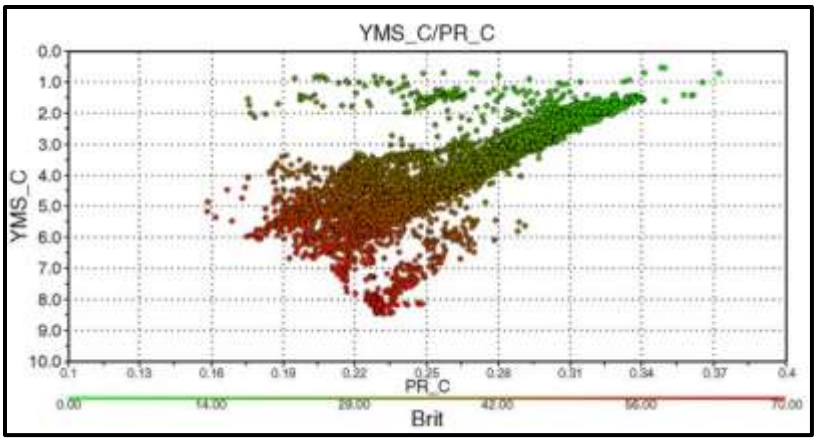

Figure 4.40: Brittleness estimation for Barnett Shale using Young's Moduli and Poisson's ratios (Rickman et al., 2008)

This study used calibrated log (with core results) values of Young's modulus and Poisson's ratio for about 950 ft shale interval for brittleness determination. The cross plot of Young's Modulus and Poisson's ratio for Qusaiba Shale is illustrated in Figure 4.41.

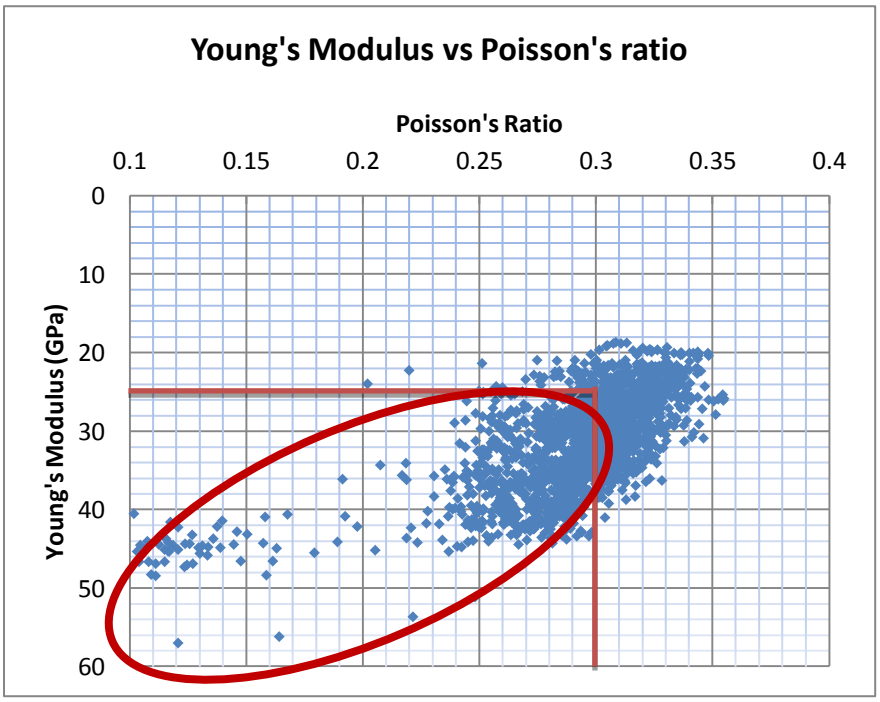

Figure 4.41: Young's Modulus and Poisson's ratio cross plot (Red line indicates cut-off values for brittleness)

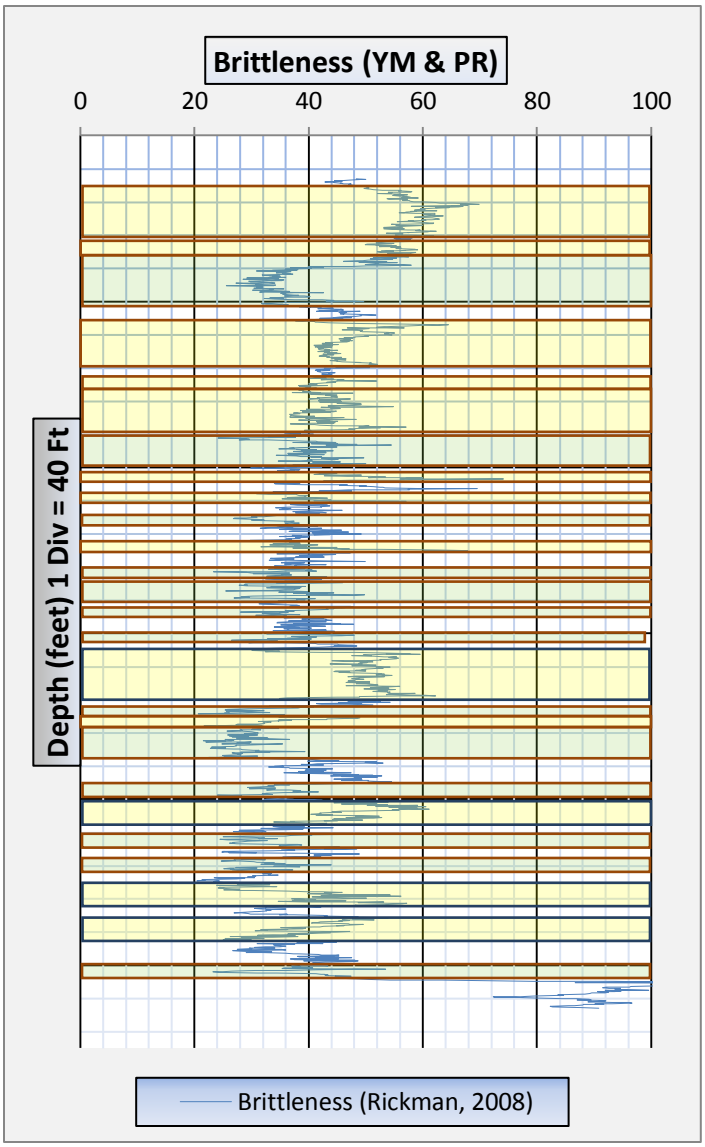

Figure 4.42: Brittleness percentage for Qusaiba Shale interval (Elastic parameter approach)

Figure 4.41 shows that as the Young's modulus increases the Poisson's ratio decreases. The cut-off values of Young's Modulus (YM > or = 25 GPa) and Poisson's ratio (PR < or = 0.3) for the Qusaiba Shale were selected on the basis of the thresholds Rickman et al., (2008) used for the Barnett Shale. The cut-off values (Rickmen et al., 2008) were applied to distinguish between brittle and ductile shale. It is clear from the cross plot

(Figure 4.41) that the points cloud for ductile shale lie in northeastern part (Young's Modulus < 25 GPa and high Poisson's ratio > 3.0) and the brittle points on the southwestern part (Young's Modulus > 25 GPa and high Poisson's ratio < 3.0). Brittle layers within shale interval are targeted for hydraulic fracture treatment. However, ductile shale layers are very important as they provide the fracture barrier for hydraulic fracture stimulation (Rickman et al., 2008). Shale gas plays with good production potential have Young's modulus > 20 GPa and Poisson's ratio less <0.25 (Burnaman et al., 2009).

Rickman et al., (2008) used the following relations (4.15-4.17) to estimate the brittleness percentage.

$$Britt\_YM\ (\%) = \frac{(E-10)}{(60-10)} * 100 \tag{4.15}$$

$$Britt\_PR\ (\%) = \frac{(\upsilon-0.4)}{(0.1-0.4)} * 100 \tag{4.16}$$

$$Brittleness\ (\%) = (Britt_{YM} + Britt_{PR})/2 \tag{4.17}$$

It has been observed in this study that, with these equations, the brittleness for the Young's modulus values higher than 25 GPa (red line in Fig. 4.42) is 40% or more. Similarly, for the Poisson's ratios lower than 0.3 (indicated by red line in Fig. 4.42), brittleness is almost 50% or higher. By averaging the brittleness percentages from Young's Modulus and Poisson's ratio, the brittleness percentage is 43% or higher within these aforementioned bounds.

Another approach, based on mineralogical composition of shale (Jarvie et al., 2007), has been applied to determine the brittleness. This approach determines the brittleness index

(BI) on the basis of quartz mineral percentage in shale. Higher quartz content indicate higher brittleness index of shale (Jarvie et al., 2007).

$$Brittleness\ Index\ (BI) = \frac{Quartz}{Clay+Quartz+Calcite} \quad (4.18)$$

According to the equation (4.18), higher the quartz content, greater the brittleness index of shale. Perez and Marfurt, (2013), applied mineralogy approach to determine brittleness in Barnett Shale and found alternate brittle (quartz rich) and ductile (low quartz content) layers (Figure 4.43).

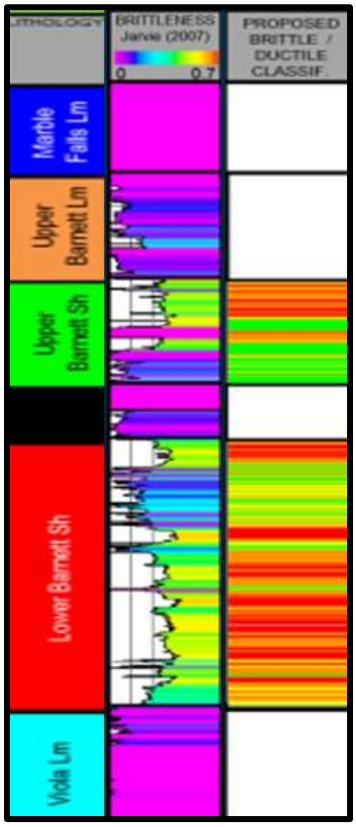

Figure 4.43: Brittleness index (Mineralogy Approach) for Barnett Shale (red color indicate brittle layers and green, ductile layers) (Perez and Marfurt, 2013)

The same mineralogy approach has been applied for Qusaiba Shale in this study. Brittleness index for the whole Qusaiba interval is shown in Figure 4.44.

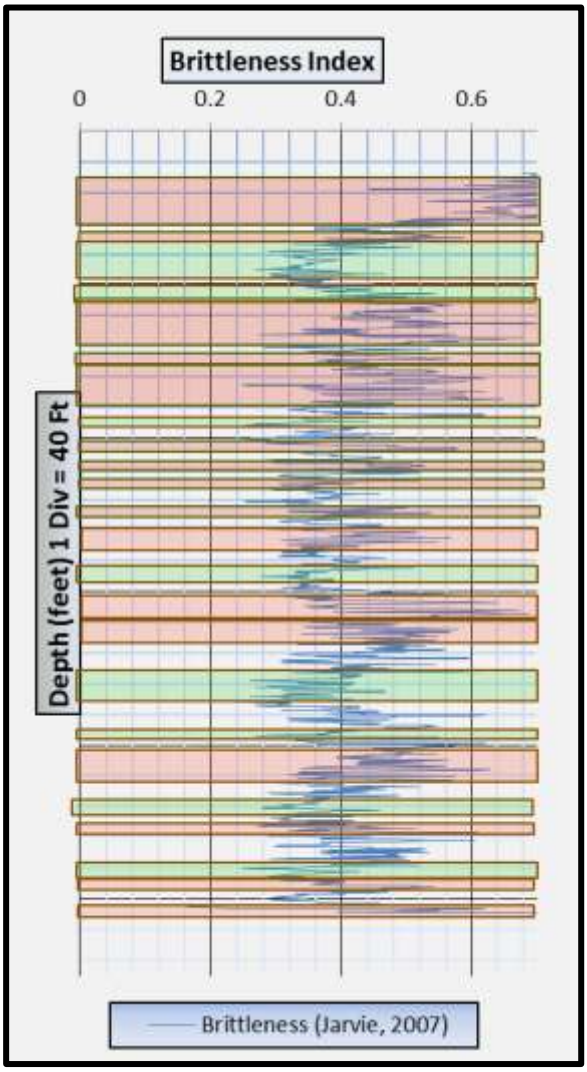

Figure 4.44: Brittleness Index (Jarvie at al., 2007). Red shaded bands indicate brittle layers and green bands indicate ductile layers

The brittleness index profile for the whole Qusaiba Shale interval exhibits alternate brittle (red shades) and ductile (green shades) layers. Brittle layers are the potential targets for hydraulic fracture treatment. These brittle layers can be referred as sweet spots in terms of brittleness.

Comparison of the results of these two approaches indicates that they are in good agreement (Figure 4.45).

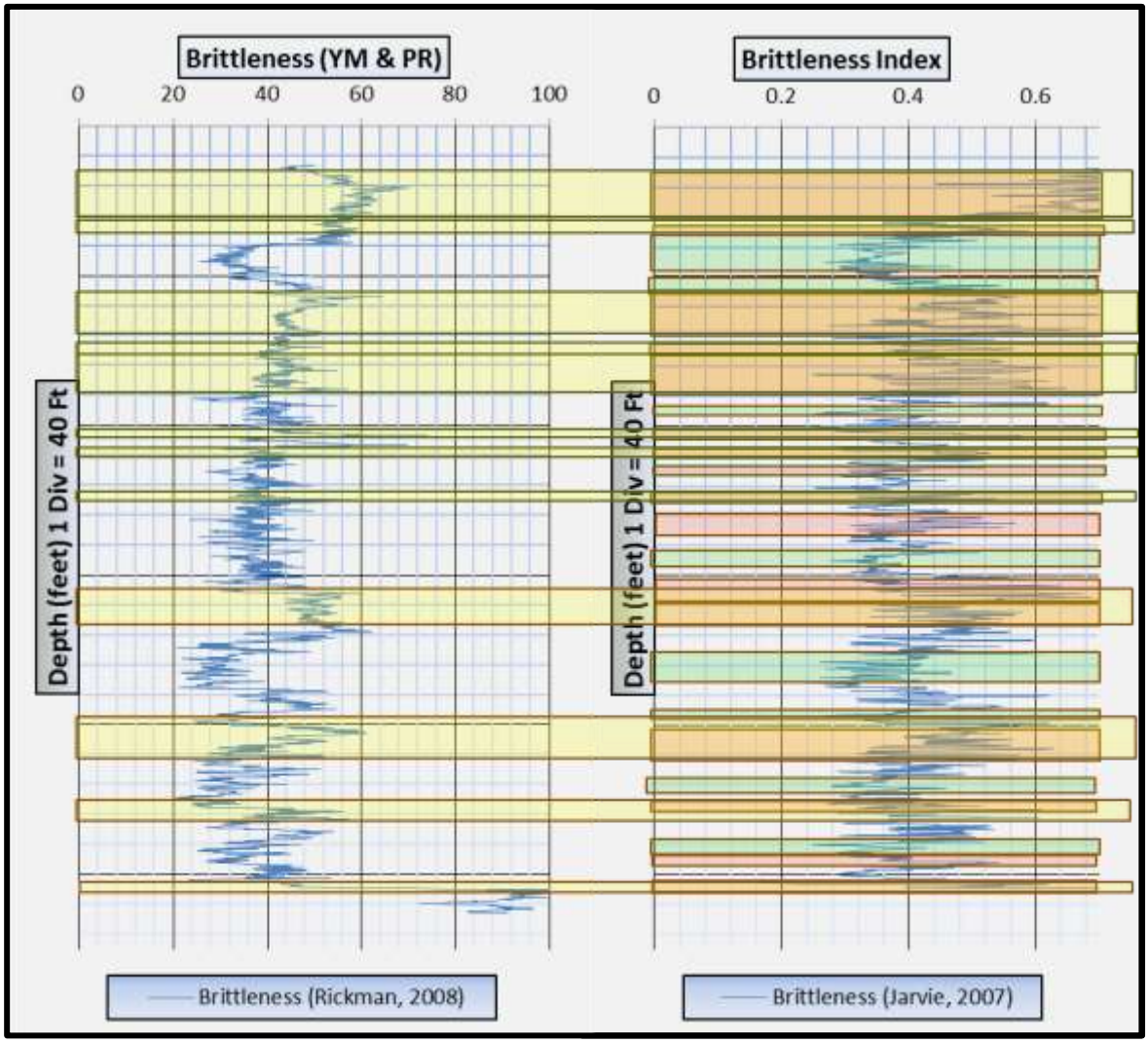

Figure 4.45: Comparison of Brittleness Indices using elastic parameters and mineralogy

By comparing the brittleness of Qusaiba Shale with that of the Barnett Shale (Figures 4.40, 4.41, 4.43, and 4.44), it can be concluded that the brittle behavior of Barnett Shale is similar to that of the Qusaiba Shale. This conclusion can further be supported by comparing their mineralogy (which has remarkable influence on elastic behavior of rocks as discussed earlier). Both shales have high quartz content with variable amount of clay. Moreover, both shales have low carbonate content. The comparison of mineralogy between Barnett and Qusaiba Shale is illustrated in Figure 4.46.

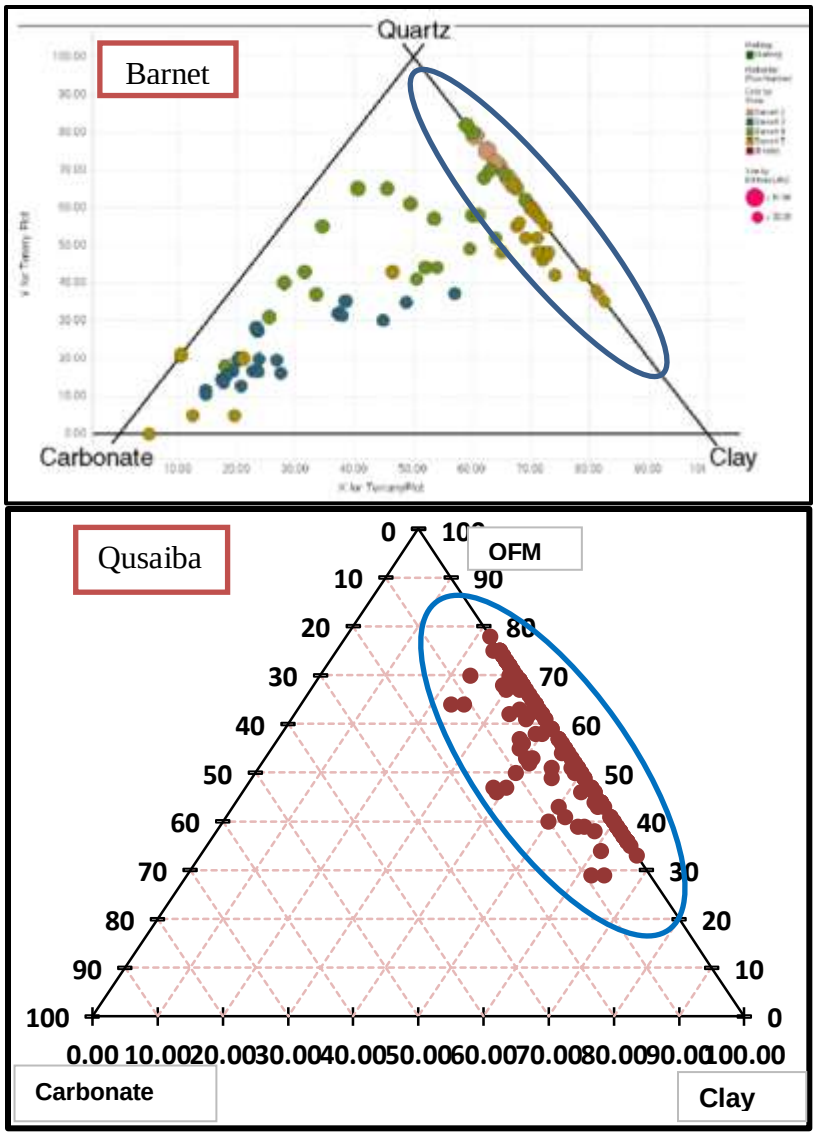

Figure 4.46: Mineralogy (clay, quartz and carbonate) comparison between Qusaiba and Barnett (Rickman et al., 2008) Shale

4.9 Anisotropy Analysis

If the elastic response of a material changes with the orientation of the material in the stress field, we call the material anisotropic. In other words, the elastic moduli will be different in different directions.

The general anisotropy is defined by 81 elastic constants in the completely anisotropic case (Fjaer et al., 2008).

$$\sigma_{ij} = \sum_{kl} C_{ijkl}\ \varepsilon_{kl} \tag{4.19}$$

where, C_{ijkl} are the elastic constants and can be represented in matrix form, σ_{ij} is stress, and ε_{kl} is strain. The values for indices i, j, k can be 1, 2 and 3.

However, with some simplification, the most general anisotropy reduces to orthorhombic symmetry with 9 independent elastic constants.

Shale has anisotropic nature with a weak plane of bedding. It is considered to have an intrinsic anisotropic behavior due to the microlayers of clay minerals. For the best representation of the anisotropy in horizontally layered sedimentary rocks, special type of anisotropy is introduced namely transversely isotropy. It exhibits rotational symmetry around the axis perpendicular to plane of symmetry (bedding plane). Elastic properties are considered same all around the axis within the plane of symmetry (bedding plane) and different outside the plane. In transversely isotropic materials with a plane of symmetry, the number of independent elastic constants reduces from nine (orthorhombic symmetry) to five. Transverse isotropy thus can be represented by the matrix in the equation given below (Fjaer et al., 2008).

Sedimentary rocks with horizontal symmetry plane are vertically transverse isotropic (TIV) and materials with vertical plane of weakness are referred to as horizontally transversely isotropic (TIH) (Schoenberg et al., 1996). To elaborate the anisotropy in transversely isotropic materials like shales, Schoenberg et al., (1996) proposed a simple three parameter anisotropy velocity model. This is known as the ANNIE model.

Anisotropy analysis of Qusaiba Shale was conducted in this study on the basis of this model.

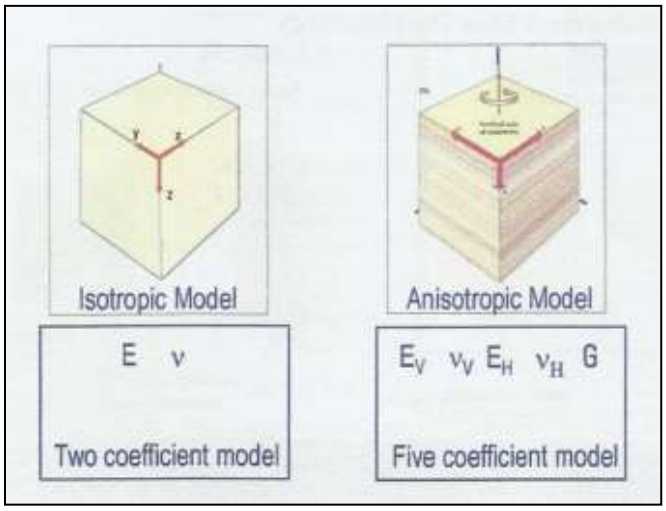

Figure 4.47: Anisotropic model for Shale with five independent elastic constants (Schlumberger, 2014)

TIV Properties

$$C = \begin{bmatrix} C_{11} & C_{12} & C_{13} & 0 & 0 & 0 \\ C_{21} & C_{22} & C_{23} & 0 & 0 & 0 \\ C_{31} & C_{32} & C_{33} & 0 & 0 & 0 \\ 0 & 0 & 0 & C_{44} & 0 & 0 \\ 0 & 0 & 0 & 0 & C_{55} & 0 \\ 0 & 0 & 0 & 0 & 0 & C_{66} \end{bmatrix} \quad (4.20)$$

The matrix contains 12 non-zero elements, where,

C_{11} = Horizontal compressional wave velocity (X-direction)

C_{22} = Horizontal compressional wave velocity (Y-direction)

C_{33} = Vertical compressional wave velocity (Z-direction)

C_{44} = Vertical Shear wave velocity (polarized 'Y')

C_{55} = Vertical Shear wave velocity (polarized 'X')

C_{66} = Horizontal Shear wave velocity (polarized 'Z')

To determine these elastic stiffness coefficients, relationships are given as:

Measure C_{33}, C_{44}, C_{66}

$C_{11} = C_{33} - 2C_{44} + 2C_{66}$

$C_{12} = C_{11} - 2C_{66}$

$C_{13} = C_{33} - 2C_{44}$

$C_{11} = C_{22}$

$C_{12} = C_{21}$

$C_{13} = C_{23} = C_{32}$

$C_{44} = C_{55}$

These equations can be used to calculate the elastic stiffness coefficients using sonic data. It is also possible to use engineering stiffness coefficients to determine the elastic stiffness coefficients. The following relationships are used:

$C_{33} = \rho*(V_P)^2 = 63.10$ (4.21)

$C_{44} = \rho*(V_{\text{Fast Shear}})^2 = 22.73$ (4.22)

$C_{55} = \rho*(V_{\text{Slow Shear}})^2 = 22.73$ (4.23)

$C_{66} = \rho*(V_{\text{Shear from Stonely}})^2 = 5.66$ (4.24)

$$C_{11} = \frac{E_h\left(1-\frac{E_h(\upsilon_v^2)}{E_v}\right)}{Denom} = 80.71 \quad (4.25)$$

$$C_{12} = \frac{E_h\left(\frac{E_h(\upsilon_v^2)}{E_v}+\upsilon_h\right)}{Denom} = 35.15 \quad (4.26)$$

$$C_{13} = \frac{E_h\upsilon_v(\upsilon_h+1)}{Denom} = 31.86 \quad (4.27)$$

$$C_{33} = \frac{E_v(1-(v_h)^2)}{Denom} = 57.99 \quad (4.28)$$

$$Denom = (1 + v_h)\left\{1 - 2\frac{E_h}{E_v}(v_v)^2 - v_h\right\} \quad (4.29)$$

To determine the acoustic stiffness coefficient, we have used acoustic laboratory measurements. P and S wave velocities were measured in both vertical and horizontal direction and Stoneley wave velocity was used from sonic log data.

The matrix of stiffness coefficients was found as:

$$C = \begin{bmatrix} 80.71 & 35.15 & 31.86 & 0 & 0 & 0 \\ 35.15 & 80.71 & 31.86 & 0 & 0 & 0 \\ 31.86 & 31.86 & 63.10 & 0 & 0 & 0 \\ 0 & 0 & 0 & 22.73 & 0 & 0 \\ 0 & 0 & 0 & 0 & 22.73 & 0 \\ 0 & 0 & 0 & 0 & 0 & 5.66 \end{bmatrix}$$

The anisotropy analysis indicates strong anisotropy based on variability of acoustic stiffness coefficients along and perpendicular to symmetry plane.

To elaborate the anisotropy in terms of parameters of elastic constants, Thomsen, (1986) developed three dimensionless parameters for enhanced understanding of anisotropic materials. These parameters are known as Thomsen anisotropy parameters given as:

$$\varepsilon = \frac{C_{11}-C_{33}}{2C_{33}} \quad (4.30)$$

$$\gamma = \frac{C_{66}-C_{55}}{2C_{55}} \quad (4.31)$$

$$\delta = \frac{(C_{13}+C_{55})^2-(C_{33}-C_{55})^2}{2C_{33}((C_{33}-C_{55})} \quad (4.32)$$

The parameters ‘ε’ (epsilon) indicates degree of P-wave anisotropy and stands for fractional difference of vertical and horizontal P-wave velocities. Gamma ‘γ’ is the fractional difference between vertically and horizontally polarized S-wave velocities and indicate the degree of S-wave anisotropy. Third parameter ‘δ’ is a combination of elastic constants.

The values of these above mentioned parameters are zero for isotropic material. If their values are less than 0.1, then the material is considered as weakly anisotropic. For the values larger than 0.1, the material reflects relatively strong anisotropy (Jin et al., 2014). For Qusaiba Shale, these parameters are shown below:

$$\varepsilon = \frac{C_{11} - C_{33}}{2C_{33}} = 0.196$$

$$\gamma = \frac{C_{66} - C_{55}}{2C_{55}} = 0.38$$

$$\delta = \frac{(C_{13} + C_{55})^2 - (C_{33} - C_{55})^2}{2C_{33}((C_{33} - C_{55})} = 0.27$$

These parameters reflect strong transversely isotropic nature of the Qusaiba Shale especially for S-wave anisotropy which is 38 percent.

CHAPTER 5

CONCLUSIONS AND RECOMMENDATIONS

5.1 Introduction

The study characterizes the Qusaiba Shale and Mid-Qusaiba Sandstone in terms of their geological and geomechanical parameters. Various techniques were applied in order to identify the lithofacies. After the detailed analysis on subsurface cores, thin sections, micro-imaging, mineralogy and elemental analysis, three lithofacies have been identified in Qusaiba Shale and two in Mid-Qusaiba Sandstone. The three lithofacies of Qusaiba Shale are (1) Micaceous laminated organic-rich mudstone facies (2) Laminated Clay-rich mudstone facies (3) Massive siliceous mudstone facies. The Mid-Qusaiba Sandstone revealed two lithofacies including (1) Quartz Arenite and (2) Quartz Wacke. Each lithofacies has its own geological and geomechanical characteristics which will be further discussed in the following sections.

5.1.1 Qusaiba Shale Lithofacies

5.1.1.1 Micaceous laminated organic-rich mudstone facies (Lithofacies-I)

This lithofacies is rich in organic matter (about 12-15%) and clay with detrital mineral grains (quartz and mica). Clay minerals are present as groundmass and have visual porosity less than 1 percent (< 1%). Organic matter and mica minerals are present along laminations. The main minerals identified by the XRD in this lithofacies are quartz, kaolinite, muscovite, albite. quartz percentage is relatively low (about 39.9%). The SEM

images indicated high organic matter content and the occurrence of these minerals is also confirmed by elemental composition analysis for elements Al, Si, K, O and Na (Ch 2, Figure 2.3).

The intensity of macro-scale fractures is low in Lithofacies-I which contains relatively smaller amount of quartz (39%). However, micro-scale bedding fractures (parallel to lamination planes) have been observed that are filled with organic matter and have relatively higher intensity in Lithofacies-I and II.

Importantly, the elastic mechanical parameters (Young's Modulus and Poisson's ratio) and failure parameters (cohesion and angle of friction) reflect relatively low stiffness and brittleness of this lithofacies. By laboratory measurements, Young's Modulus and Poisson's ratio have been found ranging from 18.2 GPa to 35.27 GPa (with average of 26 GPa) and 0.312 to 0.372 (average 0.34), respectively. Cohesion of the lithofacies varies between 3490 and 4787 psi, and frictional angle between 22 and 23.91 degrees. The laboratory measured uniaxial compressive strength (UCS) varies between 6676.38 psi and 15328 psi.

5.1.1.2 Laminated clay-rich mudstone facies (Lithofacies-II)

Lithofacies-II is composed mainly of clay minerals (groundmass) embedded with detrital mineral grains (quartz and micas). High silica mudstone is present alternately. Interparticle porosity is very low (< 1%). The organic matter represents about 1-5 % of the total lithofacies volume. The major minerals are quartz, feldspar (albite), kaolinite and muscovite. Quartz and feldspar concentrations are 49.3% and 28.7% respectively. The elemental composition showed Al, Si, K, O and Na as major elements. The

geomechanical characteristics including elastic and failure parameters are different from the Lithofacies-I. The Young's modulus ranges from 27.9 GPa to 32.7 GPa (average 31 GPa) and Poisson's ratio from 0.31 to 0.33 (average 0.32) indicating relatively higher stiffness as compared to Lithofacies-I. Higher variability in uniaxial compressive strength (UCS) has been found with values ranging from 4417 psi to 186801 psi indicating more heterogeneous nature of this lithofacies.

Macro-scale fracture intensity is relatively higher than Lithofacies-I (contain relatively higher silica content of about 45-55%). Fractures are also observed at the sharp contacts between Lithofacies-I and II. Micro-scale bedding fractures have also been observed in this lithofacies.

Brittleness of shale is mainly controlled by the mineralogy and can be estimated on the basis of clay and quartz concentrations. High concentration of quartz attributes brittleness to shale with low cohesion and higher angle of friction (Wang, 2008). So, the calculated cohesion (3390.25- 3889.2 psi) and angle of friction (21.98 to 22.61 degrees) for this lithofacies are due to relatively higher quartz and lower clay concentration as compared to Lithofacies-I.

5.1.1.3 Massive siliceous mudstone facies (Lithofacies-III)

This is mainly composed of detrital mineral grains (quartz, micas) with high silica contents embedded in clay groundmass. Interparticle porosity is very low (< 1%). The organic matter is about 1- 3 % of the total volume. The mineralogy of lithofacies-III comprises quartz, illite, feldspar (albite), and chlorite. This lithofacies tends to be more

brittle due to high quartz (78.1%) which is detected by elemental composition (Wang 2008). The major elements are Si, Al, O, K, Na, Mg, and Fe.

The intensity of macro-scale fractures (Mode-I and Mode-II) is highest in Lithofacies-III with highest quartz content (60-78%). Due to the massive nature of this lithofacies, no prominent micro-scale bedding fractures have been observed.

As far as mechanical characteristics are concerned, Young's modulus ranges between 28.7 and 34.8 GPa (average 32 GPa) and Poisson's ratio between 0.246 and 0.29 (average 0.25). Cohesion of the massive siliceous mudstone facies varies between 3390.3 and 4587.7 psi, and frictional angle lies between 21.9 and 23 degrees. The laboratory measurements of UCS varied between 11795.3 psi and 15386.5 psi indicating medium to high strength.

5.1.2 Mid-Qusaiba Sandstone Lithofacies

5.1.2.1 Quartz Arenite facies (Lithofacies-IV)

The quartz arenite facies is mainly composed of fine to medium quartz grain with monocrystalline and polycrystalline internal pattern. The quartz content varies from 75 to 90 percent with some clay coating on the grains. Most of the quartz is monocrystalline (93 to 97%). Many grains have sutured grain contacts resulting from local partial dissolution of silica due to high compaction between grains. Micro fractures and fractured grains are also observed that enhances the porosity and permeability of the lithofacies. The major minerals found are quartz, illite and microcline. The elemental composition revealed Si, O and C as major elements along with Al, K, Mg and Fe indicating presence of clay and quartz (fine) matrix.

Quartz Arenite is intensely fractured on macro-scale with both open and filled types. Most of the filled fractures are oriented at 20^0 to 40^0 degrees. Most of the observed fractures are of extensional fractures (Mode-I), however, few of them as shear fractures (Mode-II). Randomly oriented micro-scale fractures were observed under thin sections. The elastic parameters tend to show its brittle nature with low values of Poisson's ratio and high values of Young's modulus. Young's modulus was recorded up to 45.5 GPa with lowest Poisson's ratio value being 0.2. The UCS ranges between 5843.5 and 8303.7 psi. Crack or fracture closure effect has also been observed in uniaxial compressive strength tests as reported in Appendix-F (Figure F78 and Figure F85).

5.1.2.2 Quartz Wacke facies (Lithofacies-V)

The quartz wacke facies has bimodal grains with poorly to moderately sorted and generally sub-rounded to rounded grains. The facies is mainly composed of quartz ranging from 65 to 80%, (90 to 95% being monocrystalline). Quartz grains are coated with clay minerals with vacuoles on their surfaces. High compaction is indicated by the observed sutured grain contacts and micro-fractures. The visually estimated porosity of quartz wacke is 5%. The major elements include Si, O, Al, K, Mg, Fe, indicating quartz mineral with clay matrix.

Macro-scale fracture intensely is high with both open and filled types. Most of them are extensional type. Thin sections also revealed micro-scale fractures in this lithofacies that reflects the brittle nature of sandstone.

The mechanical parameters of both sandstone facies are more or less the same. One of the possible reasons is the high percentage of quartz in both lithofacies resulting in stiffness.

Measurements of elastic parameters gave a Young's modulus 30 GPa and Poisson's ratio 0.245. The UCS of quartz wacke was measured as 5843.5 psi.

5.2 Conclusions

5.2.1 Geological Characteristics

The main conclusions are as follows:

- The Qusaiba Shale shows lamination pattern of grey and black shales with variable thickness. Grey shale has high silica content whereas, black shale is rich in clay.
- Various sedimentary features including lamination, bioturbation, soft sediment deformation, concretion and natural fractures (open and filled) were observed.
- Natural fractures in Qusaiba Shale and Mid-Qusaiba Sandstone cores indicated their brittle behavior.
- Qusaiba Shale is predominantly composed of three lithofacies including (1) Micaceous laminated organic-rich mudstone facies, (2) Laminated clay-rich mudstone facies, (3) Massive siliceous mudstone facies.
- Micro-fractures are mostly oriented along lamination as observed in thin sections due to the deposition of clay minerals in preferred direction.
- Qusaiba Shale has high production potential due to its observed high organic content.
- Two lithofacies were found in Mid-Qusaiba Sandstone: (1) Quartz Arenite (2) Quartz Wacke.

- Quartz Arenite lithofacies revealed greater porosity (about 15 percent) as compared to Quartz Wacke. In addition, fractures observed also attributed to porosity of sandstone.
- Major minerals found in Qusaiba Shale using the XRD include quartz, illite, kaolinite, muscovite, albite. All three lithofacies have variable amount of quartz ranging from 40% to 78 %.
- High quartz content indicates brittle nature of Qusaiba Shale which is beneficial for fracking.
- The presence of nano-pores within organic matter of shale, observed on the SEM images, indicates maturity of hydrocarbon in Qusaiba Shale.

5.2.2 Geomechanics Characteristics

- Qusaiba Shale mineralogy indicated brittle layers present within ductile layers in shale interval.
- Young's Modulus and Poisson's ratio are the two main controlling factors of brittleness. Brittleness percentage for Qusaiba Shale is found to be greater than or equal to 43% when Young's Modulus > 25 GPa and Poisson's ratio < 0.25.
- Mechanical properties show strong dependence on intrinsic properties of shale. Massive siliceous mudstone facies with high quartz content reflected highest stiffness, in comparison with other lithofacies, with Young's modulus ranging from 25.7 to 34.8 GPa and Poisson's ratio from 0.25 to 0.29.
- P-wave and S-wave velocities are relatively higher along lamination (horizontal direction) than the direction perpendicular to lamination (vertical direction) indicating transversely isotropic behavior.

- The relatively higher velocity along lamination planes also accounts for stress anisotropy as the study area is in reverse stress regime.
- The stiffness of Qusaiba Shale is higher in horizontal direction (along lamination) as compared to vertical direction (perpendicular to lamination) as indicated by relatively higher values of Young's modulus and lower Poisson's ratio in that direction.
- The reverse stress regime exists at the study area with maximum stress gradient of 1.18 psi/ft and minimum stress gradient of 1.08 psi/ft.
- The required mud weight for safe drilling operation ranges from 14476 psi to 24840 psi at 17403 ft. depth which is the narrowest mud weight window for the safe drilling and completion operations. Special care is needed in the narrowest mud weight window to avoid risk of hazard (blowout, loss circulation, or kick etc).
- A low stress concentration has been observed along maximum horizontal stress direction which may considered as the preferred inclination for borehole. So, this direction possesses the minimum stability risk for drilling operations. On the other hand, maximum drilling risks are associated with vertical borehole direction.

5.3 Recommendations

Main recommendations arising from this study are listed below.

- For the complete reservoir characterization, geochemical analysis should be conducted, to supplement lithofacies analysis and geomechanical characterization. This will lead to accurately identify the sweet spot locations and to optimize the hydraulic fracturing stimulation.

- Reservoir simulations should be run for optimum design of the hydraulic fracture treatment. This will help in assessing fracture compatibility, containment, and complexity with Qusaiba Shale.
- Implement Real Time Geomechanics monitoring to update the MEM in real time.
- To increase the accuracy of interpretation, more data from scattered wells should be used to get 3-D MEM for better delineation of mechanical properties variation.
- Field test data such as extended leak-off tests would enhance the reliability of the mechanical earth model.
- For better interpretation of natural fractures, borehole images should be studied.
- Tri-axial compression test should be included as part of geomechanical testing in order to get more accurate values for failure parameters (c and Φ).

NOMENCLATURE

υ_{dyn}	Dynamic Poisson's ratio	α	Biot's pore pressure coefficient
E_{dyn}	Dynamic Young's Modulus, GPa	Φ	Porosity, fraction
υ_{stat}	Static Poisson's ratio	c	Cohesion, MPa
E_{stat}	Static Young's Modulus, GPa	C_o	Uniaxial Compressive Strength, MPa
ε_{kl}	Strain Matrix	$\emptyset$	Angle of Internal Friction, Degree
σ_{ij}	Stress Tensor	g	Gravitational Acceleration, ms^{-2}
C_{ijkl}	Stiffness Coefficient Matrix, GPa	V_P	P-wave Velocity, ms-1
P_p	Pore Pressure, psi	Vs	S-wave Velocity, ms^{-1}
σ_z	Vertical overburden stress, psi	P_f	Formation Pressure, psi
σ_θ	Stress Concentration around Wellbore, psi	E_{cal}	Calibrated Young's Modulus, GPa
σ_h	Minimum Horizontal Stress, psi	υ_{cal}	Calibrated Poisson's ratio
σ_H	Maximum Horizontal Stress, psi	P_w	Mud Weight, psi
P_{hyd}	Normal Hydrostatic Pressure, psi	ε	Fractional P-wave Anisotropy
T_o	Tensile Strength, MPa	γ	Fractional S-wave Anisotropy
ΔT_{log}	Sonic log observed data, µs/ft	δ	Complex Combination of P and S waves effects
ΔT_n	Sonic transit time, µs/ft	$V_{Stonely}$	Stonely-waves Velocity, ms^{-1}

REFERENCES

Abu-Ali, M. A., U.A. Franz, J. Shen, F. Monnier, M.D. Memoud and T.M. Chambers. "Hydrocarbon Generation and Migration in the Paleozoic Sequence of Saudi Arabia." *SPE Middle East Oil Show, Bahrain,* Society of Petroleum Engineers, SPE 21376: 1-12, 1991.

Abouelresh, M.O. and R.M. Slatt. "Shale Depositional Processes: Example from the Paleozoic Barnett Shale, Fort Worth Basin, Texas, USA". *Central European Journal of Geosciences* 3(4):398–409. 2011.

Abousleiman, Y., M. Tran and S. Hoang. Geomechanics Field and Laboratory Characterization of Woodford Shale : The Next Gas Play." *SPE Annual technical Conference and Exhibition,Anaheim, California, USA.* Society of Petroleum Engineers, SPE 110120: 1-14, 2007.

Al-jalal, Z., L. Ramsey, N. Gurmen and D. Kalinin. "Evolution of Tight-Gas Fracturing Methodology in the Lower Paleozoic Sandstone Formations of Saudi Arabia." *SPE Middle East Oil and Gas Show and Conference, Manama, Bahrain:* Society of Petroleum Engineers, SPE 141813: 1-21, 2011.

Barclay, A. "Thin section petrography of selected samples from the Bowen Basin, Queensland, Australia. (Appendix 10.6.2 of report no. RPT05-0225)." *Cooperative Research Centre for Greenhouse Gas Technologies, Canberra. CO2CRC. Report Number RPT06-0073*. Available Online, 2006.

Bowker, K.A. "Barnett Shale Gas Production, Fort Worth Basin: Issues and Discussion." *American Association of Petroleum Geologists (AAPG) Bulletin* 91(4): 523–33, 2007.

Britt, L.K. and J. Schoeffler. "The Geomechanics Of A Shale Play : What Makes A Shale Prospective!" *SPE Eastern Regional Meeting,* Society of Petroleum Engineers, SPE 125525: 1-9, 2009

Bryant, W.R.. "Environmental Processes: A Continuum-Overview". *Chapter 11, Book title:* "Microstructure of Fine Grained Sediments: From Mud to Shale." Richard H. B., W. R. Bryant, M. H. Hulbert (Editors), *Springer Verlag. New York:* 1- 590, 1990.

Burnaman, M., W. Xia and J. Shelton. Shale Gas Play Screening and Evaluation Criteria." *China Petroleum Exploration*, Issue 3: 51-64. 2009.

Cole, G.A. "Graptolite-Chitinozoan Reflectance and Its Relationship to Other Geochemical Maturity Indicators in the Silurian Qusaiba Shale, Saudi Arabia." *Energy and Fuels, American Chemical Society,* (21): 1443–59, 1994.

Crain, E.R. "Crain's Petrophysical Handbook." Crain's Petrophysical Pocket Pal, 2010. Available online at "www.spec2000.net/00-orders.htm" (Retrieved on Octobet 14, 2014).

Davies, D. K., W. R. Bryant, R. K. Vessel, and P. J. Burkett. "Porosities, Permeabilities, and Microfabrics of Devonian Shale." Chapter 10, Book title: "Microstructure of Fine Grained Sediments: From Mud to Shale." Richard H. B., W. R. Bryant, M. H. Hulbert (Editors), *Springer Verlag. New York:* 1- 590, 1990.

Ding, W., D. Zhu, J. Cai, M. Gong and F. Chen.. "Analysis of the Developmental Characteristics and Major Regulating Factors of Fractures in Marine–continental Transitional Shale-Gas Reservoirs: A Case Study of the Carboniferous–Permian Strata in the Southeastern Ordos Basin, Central China." *Marine and Petroleum Geology* 45: 121–33, 2013.

Energy Information Administration (EIA), Annual Energy Outlook, U.S, 2014.

Eseme, E., J.L. Urai, B.M. Krooss and R. Littke. "Review Of Mechanical Properties Of Oil Shales: Implications For Exploitation and Basin Modelling." *Oil Shale* 24 (2): 159–74, 2007.

Faraj, B. and M. Brown. "Key Attributes of Canadian and U.S. Productive Shales: Scale and Variability." *American Association of Petroleum Geologists (AAPG) Annual Convention and Exhibition, New Orleans, USA.* Presentation, 2010.

Fjaer, E., R.M. Holt, A. Raeen, R. Risnes and P. Horsud. "Petroleum Related Rock Mechanics." *Elsevier*: 1-491, 2008.

Fertl, J. W. "Evaluation of Oil Shales Using Geophysical Well-Logging Techniques." Chapter 10, Book title: "Oil Shale." T. F. Yen, G. V. Chilingar (Editors), *Elsevier, New York:* 1-291, 1976.

Gale, J., S. Laubach, J. Oslon, P. Eichhubi and F. Andras. "Natural Fractures in Shale: A Review and New Observations." *American Association of Petroleum Geologists (AAPG),* 11(11): 2165–2216. 2014.

Gao, J., N. Blair, C. Queena and M. Uno. "Systematic Geomechanical Application For Unconventional Resource Development." *Integration Geoconvention,* Presentation, 2013.

Grunewald, W. and K. Pingel. "Analysis of Oil Shale as an Alternative Source of Energy." *Science Lab*. Article, 2014.

He, Z.J., B.J. Liu, and P. Wang. "Genesis of Bedding Fracture and Its influences on Reservoirs in Jurassic, Yongjin Area, Junggar Basin." *Petroleum Geology and Recovery Efficiency* 18(1): 15–17, 2011.

Higgins, S., S. Goodwin, A. Donald, T. Bratton and G. Tracy. "Anisotropy Stress Models Improve Completion Design in Baxter Shale." *Society of Petroleum Engineers (SPE), Annual Technical Conference and Exhibition, 21-24 September, Denver, Colorado, USA,* SPE 115736: 1-10, 2008

Holditch, S.A. "The Increasing Role of Uncoventional Reservoirs in the Future of the Oil and Gas Business." *Journal of Petroleum Technology JPT,* 55(11): 34-37. 2003

Holditch, S.A. Tight Gas Sands, *Journal of Petroleum Technology JPT,*58(6): 86-94. 2006

Huang, F., T. Yang, and W. Yan. "Geologic Factors of Formation of Tight Oil and Its Resource Potential in China." *AAPG Annual Convention and Exhibition, Pitsburgh, Pennsylvania,* Article # 80306. May 2013.

Hulsey, K. M. "Lithofacies Charcterization and Sequence Stratigraphy Framework for Some Gas-Bearing Shales within the Horn River Basin, Northeastern, British Columbia." *MS Thesis, University of Oklahoma, USA*. 2011.

Jacobi, D.J., J.J. Breig, M. Kopal, G. Hursan, F.E. Mendez, S. Bliven and J. Longe. "Effective Geomechanical and Geochemical Characterisation of Shale Gas Reservoirs from the Wellbore Environment: Caney and the Woodford Shales." *Society of Petroleum Engineers (SPE) Annual Technical Conference and Exhibition, 4-7 October, New Orleans, Louisiana*. SPE 124231: 1-20, 2008.

Jarvie, D.M., R.J. Hill, T.E. Ruble and R.M. Pollastro. "Unconventional shale-gas systems: The Mississippian Barnett Shale of north-central Texas as one model for thermogenic shale-gas assessment." *American Association of Petroleum Geologists (AAPG) Bulletin* 91, 475–499.

Jiang, P. and B.A. Cheadle. "Depositional and Burial Domain Influences on Microporosity Modalities in Carbonaceous Mudstones of the Upper Cretaceous Colorado Group , Western Canada Foreland Basin." *AAPG Annual Convention and Exhibition, Pitsburgh, Pennsylvania,* Article # 50802. 2013.

Jin, G., H.G. Perez, G. Agrawal, A.Z. Ali and M.R. Khodja. "Elastic Anisotropy of Unconventional Shale at Reservoir Conditions - New , Faster Laboratory Characterization Technique." *Society of Petroleum Engineers (SPE) Annual Technical Conference and Exhibition, Amsterdam, Netherland*. SPE 170839: 1-14, 2014.

Jones, P.J. and T.E. Stump. "Depositional and Tectonic Setting of the Lower Silurian Hydrocarbon Source Rock Facies , Central Saudi Arabia." American Association of Petroleum Geologists (AAPG) Bulletin, V. 83, No. 2: 314–332. 1999.

Josh, M., L. Esteban, C.D. Piane, J. Sarout, D.N. Dewhurst and M.B. Clennell. "Laboratory Characterisation of Shale Properties." *Journal of Petroleum Science and Engineering* 88-89: 107–24. 2012.

Kawata, Y., and K. Fujita. "Some Prediction of Possible Unconventional Hydrocarbon Availability until 2100." *Society of Petroleum Engineers (SPE) Asia Pacific Oil and Gas Conference, Jakarta*. SPE 68755: 1-10, 2001.

KFUPM/RI "Core and Fluid Analyses for FRAS-0001 (Volume 1)." submitted to *Sino Saudi Gas Limited, Dhahran,* (Confidential, Unpublished CPM Report), May 2008.

KFUPM/RI "Core and Fluid Analysis, Phase Behavior, and Rock Mechanics for ATNB-0002 (Volume 1)." submitted to *Sino-Saudi Gas Limited, Dhahran,* (Confidential, Unpublished CPM Report), May 2008.

KFUPM/RI "Petrography and Geological Core Description for FRAS-0001 (Volume 2)." submitted to *Sino-Saudi Gas Limited, Dhahran,* October 2009 (Confidential, Unpublished CPM Report), May 2008.

KFUPM/RI "Geology, Petrography and Core Description for ATNB-0002 (Volume 2)." submitted to *Sino-Saudi Gas Limited, Dhahran,* December 2009 (Confidential, Unpublished CPM Report), May 2008.

Khan, S. "Introduction to Geomechanics and Hydraulic Fracturing in Unconventional Resources." *A short course Presentation, Schlumberger,* 2014.

Kleineidam, S., H. Rügner, B. Ligouis and P. Grathwohl. 1999. "Organic Matter Facies and Equilibrium Sorption of Phenanthrene." *Environmental Science & Technology* 33(10):1637–44. 1999.

Konert, G., A.M. Afifi, S. Al-Hajri and H.J. Droste. 2001. "Paleozoic Stratigraphy and Hydrocarbon Habitat of the Arabian Plate." *GeoArabia* 6(3): 407–42. 2001.

Lal, S. M. and B. Amoco. "Shale Stability: Drilling Fluid Interaction and Shale Strength." *Society of Petroleum Engineers (SPE) Asia Pacific Oil and Gas Conference and Exhibition,* SPE 54356: 1-10, 1999.

Laongsakul, P. and H. Dürrast. "Characterization of Reservoir Fractures Using Conventional Geophysical Logging." *Songklanakarin Journal of Science and Technology* 33(2): 237–46. 2011.

Le Heron, D. P. and J. Craig. 2008. "First Order Reconstruction of a Late Ordovician Saharan Ice Sheet." *Journal of the geological Society, London* 165: 19–29. 2008.

Luning, S., J. Craig, D.K. Loydell, P. Storch and B. Fitches. “Lower Silurian ‘ Hot Shales’ in North Africa and Arabia: Regional Distribution and Depositional Model.” *Earth Science Reviews* 49, 121-200, *Elsevier*. 2000.

Mahmoud, M. D., D. Vaslet and M.I. Husseini. "The Lower Silurian Qaibah Formation of Saudi Arabia: An Important Hydrocarbon Source Rock." *American Association of Petroleum Geologists (AAPG),* Vol. 76. No. 10: 1491-1506. 1992.

Milner, M., R. Mclin and J. Petriello. “Imaging Texture and Porosity in Mudstones and Shales: Comparison of Secondary and Ion-Milled Backscatter SEM Methods.” *Canadian Unconventional Resources and International Petroleum Conference, Calgary, Alberta,* CSUG/SPE 138975, 1–10. 2010.

Montgomery, S. L., D.M. Jarvie, K.A. Bowker and R.M. Pollastro. “Mississippian Barnett Shale, Fort Worth Basin, North-Central Texas: Gas-Shale Play with Multi-Trillion Cubic Foot Potential.” *AAPG Bulletin Vol.* 89 No. 2: 155–75. 2005.

Mouchet, J.P. and A. Mitchell. "Abnormal Pressures While Drilling: Origins, Prediction, Detection, Evaluation." Fundamental of Exploration and Production, *Editions Technip:*1-255, 1989.

Mustafa, A., A. Sahin and M.O. Abouelresh. "Geological Characteristics of The Lower Silurian Qusaiba Shale, Rub Al-Khali Basin, Saudi Arabia." (Extended Abstract) *2nd EAGE/SPE/AAPG Shale Gas Workshop, Dubai, UAE:* 1-4, 2014.

Ouenes, A. “Distribution of Well Performances in Shale Reservoirs and Their Predictions Using the Concept of Shale Capacity.” *AAPG Search and Discovery Article* # 41139. 2013.

Ozkaya, S.I., H.J. Lewandoswki and S.B. Coskun. “Fracture Study of a Horizontal Well in a Tight Reservoir - Kuwait.” *Journal of Petroleum Science and Engineering* 55(1-2): 6–17. 2007.

Perez, R. and K. Marfurt. "Calibration of Brittleness to Elastic Rock Properties via Mineralogy Logs in Unconventonal Reservoirs." *AAPG International Conference and Exhibition, Catagena, Columbia,* Article # 41237. 2013

Rickman, R., M. Mullen, E. Petre, B. Grieser and D. Kudert. "A Practical Use of Shale Petrophysics for Stimulation Design Optimization: All Shale Plays Are Not Clones of the Barnett Shale.” *Society of Petroleum Engineers (SPE), Annual Technical Conference and Exhibition, Denver, Colorado, USA.* SPE 115258: 1-11, 2008.

Sahin, A. “Unconventional Natural Gas Potential in Saudi Arabia.” *Society of Petroleum Engineers (SPE) Middle East Oil and Gas Show and Conference, Manama, Bahrain*. SPE 164364: 1-9, 2013.

Sahin, A. and M.O. Abouelresh. "Spectral Gamma Ray Signatures for Qusaiba Shale." (Extended Abstract) *2nd EAGE/SPE/AAPG Shale Gas Workshop, Dubai, UAE:* 1-4, 2014.

Schmoker, J.W. "Resource-Assessment Perspectives for Unconventional Gas Systems." *American Association of Petroleum Geologists (AAPG) Bulletin* 86(11): 1993-99, 2002.

Schoenberg, M., F. Muir and Sayer. "Introducing ANNIE: A Simple Three Parameter Anisotropy Velocity Model for Shales." *Journal of Seismic Exploration* 5: 35–49. 1996.

Senalp, M. and A. Al-Duaiji. "Qasim Formation: Ordovician Storm- and Tide-Dominated Shallow-Marine Siliciclastic Sequences, Central Saudi Arabia." *GeoArabia* 6(2). 2001.

Slatt, R.M., P. Singh, R.P. Philp, K.J. Marfurt, Y.N. Abousleiman and N.R. Brien. "Workflow for Stratigraphic Characterization of Unconventional Gas Shales." *Society of Petroleum Engineers (SPE) Shale Gas Production Conference, Fort Worth, Texas, USA*. SPE 119891: 1-17, 2008.

Terry, R.D. and G.V. Chilingar. "Summary of Concerning Some Additional Aids in Studying Sedimentary Formations." *Journal of Sedimentary Petrology* 25: 229-234, 1955.

Thomsen, L. "Weak Elastic Anisotropy." *SEG, Geophysics* 51(10): 1954–66. 1986.

Tucker, M.E. "Sedimentary Petrology: An Introduction to the Origin of Sedimentary Rocks." Third Edition, *Blackwell, USA*. 2001.

Wang, F. "Production Fairway: Speed rails in Gas Shale?" *7th Annual Gas Shales Summit, Dallas, Texas.* 2008.

Wang, B., C. Yong, and T. Wong. "A Discrete Element Model for the Development of Compaction Localization in Granular Rock." *Journal of Geophysical Research: Solid Earth,* Volume 113(Issue B3), American Geophysical Union. 2008.

Warlick, D. "Gas Shale and CBM Development in North America." *Oil Gas Financial Journal* 3(11). 2006.

Williams, P. "The Barnett Shale." *Oil and Gas Investor* 22(3): 34–45. 2002.

Young, C., B.C. Trent, N.C. Patti, K.P. Chong and J.W. Smith. "Stratigraphic Variations in Fracture Properties." *Mechanics of oil shale*, Elsevier: 291–335, 1984.

VITAE

Name	:	Ayyaz Mustafa
Nationality	:	Pakistani
Date of Birth	:	14-Oct-1987
Email	:	engineerayyaz@gmail.com g201202380@kfupm.edu.sa
Address	:	House No. 21, Khawar Street No. 31, National Town, Sanda road, Lahore, Pakistan.
Academic background	:	M.S. in Geology, 2014, King Fahd University of Petroleum & Minerals. B.S. in Geological Engineering, 2009, University of Engineering & Technology, Lahore, Pakistan.
Research papers	:	Brittleness Estimation and Anisotropy Analysis of Lower Silurian Qusaiba Shale, Saudi Arabia. 77th EAGE Conference and Exhibition, Madrid, Spain. (Under review) Multi-Scale Geological Characterization of the Lower Silurian Qusaiba Shale, Rub' Al-Khali Basin, Saudi Arabia. AAPG-SEG International Conference, Melbourne, Australia, Sep, 2015. (Under Review)